IMPLICIT FINITE-DIFFERENCE ANALYSIS OF COMPRESSIBLE LAMINAR, TRANSITIONAL, AND TURBULENT BOUNDARY LAYERS ALONG THE WINDWARD STREAMLINE OF A SHARP CONE AT INCIDENCE

John C. Adams, Jr.
ARO, Inc.

December 1971

VON KÁRMÁN GAS DYNAMICS FACILITY
ARNOLD ENGINEERING DEVELOPMENT CENTER
AIR FORCE SYSTEMS COMMAND
ARNOLD AIR FORCE STATION, TENNESSEE

NOTICES

When U. S. Government drawings specifications, or other data are used for any purpose other than a definitely related Government procurement operation, the Government thereby incurs no responsibility nor any obligation whatsoever, and the fact that the Government may have formulated, furnished, or in any way supplied the said drawings, specifications, or other data, is not to be regarded by implication or otherwise, or in any manner licensing the holder or any other person or corporation, or conveying any rights or permission to manufacture, use, or sell any patented invention that may in any way be related thereto.

Qualified users may obtain copies of this report from the Defense Documentation Center.

References to named commercial products in this report are not to be considered in any sense as an endorsement of the product by the United States Air Force or the Government.

IMPLICIT FINITE-DIFFERENCE ANALYSIS OF COMPRESSIBLE LAMINAR, TRANSITIONAL, AND TURBULENT BOUNDARY LAYERS ALONG THE WINDWARD STREAMLINE OF A SHARP CONE AT INCIDENCE

John C. Adams, Jr.
ARO, Inc.

FOREWORD

The work reported herein was sponsored by Headquarters, Arnold Engineering Development Center (AEDC), Air Force Systems Command (AFSC), under Program Element 64719F.

The results of research presented were obtained by ARO, Inc. (a subsidiary of Sverdrup & Parcel and Associates, Inc.), contract operator of AEDC, AFSC, Arnold Air Force Station, Tennessee, under Contract F40600-72-C-0003. The research was conducted from July 1970 until June 1971 under ARO Project No. VW5106, and the manuscript was submitted for publication on August 4, 1971.

Appreciation and acknowledgement is extended Mr. E. O. Marchand, ARO, Inc., for performing the inviscid calculations reported herein.

This technical report has been reviewed and is approved.

Maurice A. Clermont
Captain, CF
Research and Development Division
Directorate of Technology

Robert O. Dietz
Acting Director
Directorate of Technology

ABSTRACT

Formulation and application of a windward plane of symmetry laminar, transitional, and turbulent boundary-layer analysis is presented for sharp cones at incidence in a supersonic or hypersonic flow. The governing boundary-layer equations in the plane of symmetry are numerically integrated on a digital computer using a marching implicit finite-difference technique. A so-called invariant model of turbulence is used in a two-layer eddy viscosity-mixing length approach for calculation of the turbulent boundary layer in conjunction with an intermittency factor treatment of the transition zone. Comparison of the present theory with experimental data (surface heat transfer, boundary-layer parameters such as displacement thickness, and boundary-layer profiles) under supersonic and hypersonic flow conditions over sharp cones at incidence reveals good agreement. In general, smaller crossflow (outflow) effects on the windward plane of symmetry boundary layer can be expected for turbulent layers as compared with laminar layers subject to the same boundary conditions.

CONTENTS

APPENDIXES

Figure Page

NOMENCLATURE

A_*	van Driest damping constant, 26.0
A_n, B_n, C_n	Coefficients in finite-difference Eq. (III-34)
C_{f_∞}	Local skin-friction coefficient, $2\tau_w/\rho_\infty U_\infty^2$
C_p	Constant pressure specific heat, 6006 $ft^2/sec^2\text{-}°R$
D_1, D_2	Coefficients for finite-difference derivatives defined by Eqs. (III-30) and (III-31)
E_n	Coefficient in finite-difference Eq. (III-39)
e_n	Coefficient in finite-difference Eq. (III-39)
$\bar{\bar{e}}$	Inviscid flow swallowing parameter defined by Eq. (61)
f	Transformed streamwise stream function defined by Eq. (49)

f'	Streamwise velocity ratio, $\bar{u}/U_e$
f''	Streamwise velocity gradient, $\partial(u/U_e)/\partial\eta$
G	Geometry parameter defined by Eq. (62)
$\overline{G}$	Scalar velocity function
g	Transformed crossflow stream function defined by Eq. (50)
g'	Crossflow velocity ratio, $\overline{w}_\phi/U_e$
g'_e	Outer edge boundary condition for crossflow momentum equation
H'	Fluctuating total enthalpy
$\overline{H}$	Mean total enthalpy
h'	Fluctuating static enthalpy
$\bar{h}$	Mean static enthalpy
I_f	Intermittency factor
K	Variable grid parameter defined by Eq. (III-32)
k	Thermal conductivity
k_*	Inner law mixing length constant, 0.435
L	Slant height of sharp cone
ℓ	Density-viscosity product ratio, $\rho\mu/\rho_e\mu_e$
ℓ_*	Mixing length
ℓ^*	Modified density-viscosity product ratio for use in momentum equation defined by Eq. (79)
ℓ^{**}	Modified density-viscosity product ratio for use in energy equation defined by Eq. (80)
M	Streamwise Mach number
M_e	Local edge streamwise Mach number, $U_e/\sqrt{\gamma RT_e}$
M_∞	Free-stream Mach number, $U_\infty/\sqrt{\gamma RT_\infty}$
$\overline{M}$	Mean streamwise Mach number, $\bar{u}/\sqrt{\gamma R\overline{T}}$

N	Total number of grid points
Pr	Laminar Prandtl number, 0.71
Pr_t	Turbulent Prandtl number, 0.90
$\overline{p}$	Static pressure
p_t	Pitot pressure in boundary layer
p_o'	Free-stream pitot pressure
$p_{o,\infty}$	Reservoir stagnation pressure
$\dot{q}_w$	Wall heat flux
R	Specific gas constant, 1716 $ft^2/sec^2\text{-}^\circ R$
Re_{e,X_T}	Local Reynolds number at inception of fully turbulent flow, $\rho_e U_e X_T/\mu_e$
Re_{e,X_t}	Local Reynolds number at onset to transition, $\rho_e U_e X_t/\mu_e$
$Re_{e,x}$	Local Reynolds number, $\rho_e U_e x/\mu_e$
$Re_{\infty,x}$	Free-stream Reynolds number, $\rho_\infty U_\infty x/\mu_\infty$
R_n	Coefficient in finite-difference Eq. (III-34)
r	Body radius
r_f	Recovery factor
$St_{e,aw}$	Local Stanton number based on adiabatic wall conditions, $-\dot{q}_w/\rho_e U_e C_p (T_{aw}-T_w)$
$St_{\infty,aw}$	Free-stream Stanton number based on adiabatic wall conditions, $-\dot{q}_w/\rho_\infty U_\infty C_p (T_{aw}-T_w)$
$\overline{T}$	Mean static temperature
T_{aw}	Adiabatic wall temperature
T_e	Static temperature at outer edge of boundary layer
$\overline{T_o}$	Mean stagnation temperature
$T_{o,\infty}$	Reservoir stagnation temperature

T_w	Wall temperature
T_∞	Free-stream static temperature
U_e	Streamwise velocity component at outer edge of boundary layer
U_∞	Free-stream velocity
u'	Fluctuating streamwise velocity component
$\bar{u}$	Mean streamwise velocity component
V	Combined normal velocity components according to Eq. (6)
v'	Fluctuating normal velocity component
$\bar{v}$	Mean normal velocity component
W	Dependent variable in finite-difference Eq. (III-14)
W_e	Crossflow velocity component at outer edge of boundary layer
w'	Fluctuating crossflow velocity component
$\bar{w}$	Mean crossflow velocity component
$\bar{w}_\phi$	Partial derivative of $\bar{w}$ with respect to ϕ
X_T	Surface distance from apex to beginning of fully turbulent flow
X_t	Surface distance from apex to onset of transition location
x	Coordinate along body surface
y	Coordinate normal to body surface
y_ℓ	Characteristic thickness of boundary layer in Eq. (30)
α	Angle of attack
a_1, a_2 a_3, a_4	"Standard" form coefficients for parabolic partial differential equation following Eq. (III-14)
β	Velocity gradient parameter defined by Eq. (59)
γ	Specific heat ratio, 1.40

Δ^*	Three-dimensional displacement thickness defined by Eq. (90)
δ	Boundary-layer thickness (y-distance where $f' = 0.995$)
δ^*	Displacement thickness
δ_v	Cone half-angle
ϵ	Eddy viscosity
ϵ_i	Eddy viscosity in inner region
ϵ_o	Eddy viscosity in outer region
θ	Static temperature ratio, $\overline{T}/T_e$
θ'	Static temperature gradient, $\partial(\overline{T}/T_e)/\partial\eta$
κ	Eddy thermal conductivity
λ	Outer law mixing length constant, 0.090
μ	Laminar (molecular) viscosity
ξ,η	Transformed coordinates defined by Eqs. (42) and (43)
ρ'	Fluctuating mass density
$\overline{\rho}$	Mean mass density
ρ_e	Mass density at outer edge of boundary layer
ρ_∞	Free-stream mass density
τ	Shear stress
τ_w	Wall shear stress
Φ	Intermittency factor constant, 0.412
ϕ	Circumferential coordinate
χ	Crossflow pressure gradient parameter defined by Eq. (60)
$\overline{\chi}$	Characteristic extent of transition zone defined by Eq. (72)
Ψ	Streamwise stream function

ψ	Crossflow stream function
Ω	Initial η step-size increment defined by Eq. (III-33)

SUBSCRIPTS

2-D	Two-dimensional
aw	Adiabatic wall
e	Outer edge of boundary layer
I	Initial approximation
o	Stagnation or total
o,∞	Reservoir
ref	Reference value
turb	Turbulent
w	Wall
x	x-direction
ϕ	ϕ-direction
∞	Free-stream

SUPERSCRIPTS

$'$	Fluctuating quantity or partial derivative with respect to η depending on usage
$-$	Averaged quantity with respect to time

SECTION I
INTRODUCTION

The laminar, transitional, and turbulent boundary layer along the windward ray of a sharp cone at incidence is of practical importance in many aeronautical applications. An excellent example is the compression inlet for high-performance engines on supersonic and hypersonic air-breathing vehicles at angle of attack. Three-dimensional effects on boundary-layer behavior are also of interest relative to maneuverable reentry bodies and lifting surfaces (such as delta wings) at incidence. All of these flows involve pressure gradients in the plane of symmetry, either favorable or adverse, and crossflow pressure gradients that may cause either inflow toward or outflow from the plane of symmetry. An excellent collection of current topics in three-dimensional inviscid and viscous analysis techniques for such flows as discussed above may be found in Ref. 1.

The present report concentrates on formulation of a windward plane of symmetry laminar, transitional, and turbulent boundary-layer analysis for sharp cones at incidence in a supersonic or hypersonic flow and comparison of results with those from experiments. The governing boundary-layer equations in the plane of symmetry have been numerically integrated on a digital computer using a marching implicit finite-difference technique, with a two-layer eddy viscosity-mixing length approach based on a so-called invariant model of three-dimensional turbulence used for calculation of the turbulent boundary layer. The transition region is treated through an intermittency factor approach coupled to the eddy viscosity model mentioned above. In order to help understand the basis for the current analysis, a short review of applicable boundary-layer technology relative to analysis of fully turbulent two-dimensional flows (utilizing accurate numerical integration techniques in conjunction with eddy viscosity models of turbulence) as well as laminar and turbulent plane of symmetry applications is given below. Also included is a summary of very recent analytical work involving numerical calculation of transitional boundary layers.

1.1 REVIEW OF BOUNDARY-LAYER TECHNOLOGY APPLICABLE TO LAMINAR, TRANSITIONAL, AND TURBULENT PLANE OF SYMMETRY FLOWS

Calculation techniques for the two-dimensional, nonsimilar, fully turbulent, supersonic and hypersonic boundary layer utilizing large digital computer codes have become available during the past few years, e.g., Smith and Cebeci (Ref. 2), Patankar and Spalding (Ref. 3), Bushnell and Beckwith (Ref. 4), Herring and Mellor (Ref. 5), Martellucci, Rie, and Sontowski (Ref. 6), Mayne and Dyer (Ref. 7), Cebeci (Ref. 8), and Pletcher (Ref. 9). Comparison of results from the above analyses with experimental data has shown good agreement for fully turbulent supersonic and hypersonic (up to $M_\infty \approx 10$) boundary layers on sharp and slightly blunted cones, as well as sharp flat plates. These results suggest that the eddy viscosity model employing the Prandtl mixing length is indeed adequate for prediction of hypersonic turbulent boundary-layer flows over simple bodies under cold wall conditions (and may be used with some confidence).

With regard to calculations for transitional boundary-layer flows, little has been accomplished. Most of the above-listed references employ an instantaneous step transition from fully laminar to fully turbulent flow at either a specified body location or local

Reynolds number along the boundary-layer edge. In order to provide a suitable progressive transition model for the transition region, Harris (Ref. 10) and Adams (Ref. 11) have applied an intermittency-factor, phenomenological description of the transition region based on the experimentally observed fact that transition in a boundary layer is characterized by the intermittent appearance of turbulent spots which grow and move downstream with the fluid. The basis behind this approach may be found in the work of Masaki and Yakura (Ref. 12). In general, the analyses by Harris and Adams indicate that the intermittency factor treatment of the transition region yields a reasonably accurate description of transitional heating on sharp plates and cones under supersonic and hypersonic conditions.

The mathematical theory of the three-dimensional laminar boundary layer as formulated by Moore (Ref. 13) and Hayes (Ref. 14) has been available for about twenty years. Both Moore and Hayes showed that the laminar boundary-layer equations for a sharp cone at incidence allow a similarity transformation which reduces the number of independent variables from three to two. Moore (Ref. 15) published a solution to these equations in the limit of very small angle of attack, corresponding to a perturbation solution for the inviscid flow at small angle of attack. Moore expressed the boundary-layer profiles as the sum of a basic flow (satisfying the zero angle-of-attack equations) and correction terms proportional to angle of attack. He reduced the correction terms to universal functions; however, his results were valid only for the adiabatic wall case. In 1952, Moore (Ref. 16) published a study of the conical boundary-layer equations at large angle of attack. In this work, attention was restricted to the symmetry planes where the equations reduce to a set of ordinary differential equations. Again, he considered only the case of zero heat transfer to the surface, although extensions to include heat transfer along the windward plane of symmetry were later published by Reshotko (Ref. 17) and Brunk (Ref. 18). In Ref. 16, Moore obtained numerical solutions to the equations on the windward symmetry plane for all angles of attack and on the leeward symmetry plane for very small angles of attack. A recent report by Bodonyi and Reshotko (Ref. 19) generalizes the small angle-of-attack solutions obtained by Moore (Ref. 15) by removing the restrictions of insulated surfaces and unit Prandtl number.

Recent studies by Libby, et al. (Ref. 20) and Trella and Libby (Ref. 21) have been concerned with similar solutions for the hypersonic laminar boundary layer near a plane of symmetry allowing surface heat transfer. These analyses of similar flows lead to the usual restrictions that arise for similar flows without crossflow and to additional restrictions associated with the three-dimensionality. A linearization procedure in conjunction with an integral method is followed to describe weak three-dimensional effects in Ref. 20; a numerical solution of the full nonlinear system allowing arbitrary favorable and adverse pressure gradients and for inflow and outflow is presented in Ref. 21. The manner of numerical solution has been further refined for the plane of symmetry problem by Libby and Liu (Ref. 22) based on the use of quasilinearization. A recent paper by Libby (Ref. 23) examines the three-dimensional laminar boundary layer near the windward generator of a sharp cone at angle of attack subjected to uniform mass transfer, either suction or injection.

The problem of turbulent boundary-layer flow along a plane of symmetry has received little attention in the literature. The general three-dimensional turbulent boundary-layer

equations have been derived by Vaglio-Laurin (Ref. 24) and Braun (Ref. 25). For the case of incompressible plane of symmetry turbulent boundary layers, Johnston (Ref. 26) applied an integral technique yielding results which agreed well with experiment. Mellor (Ref. 27) reconsidered the same incompressible case using an exact numerical integration of the governing plane of symmetry equations in conjunction with an isotropic model of three-dimensional turbulence through an eddy viscosity approach. Again, good agreement with the data used by Johnston was obtained which supported the assumption that the eddy viscosity was isotropic. Very recently Zakkay and Calarese (Ref. 28) have examined the compressible turbulent boundary layer along a plane of symmetry undergoing both adverse pressure gradient and crossflow effects. The three-dimensional compressible integral equations are written along the symmetry plane and integrated numerically using a power-law assumption for the streamwise velocity profile and a modified Crocco relation for the enthalpy profile. Reasonable results relative to experimental data for boundary-layer thickness, displacement thickness, and momentum thickness were reported for the windward side of the meridian plane along a sharp cone in a supersonic stream.

To the present author's knowledge, the current investigation is the first to consider the plane of symmetry problem allowing for laminar, transitional, and turbulent flow in a single unified analysis based on accurate numerical integration of the governing boundary-layer equations.

SECTION II
ANALYTICAL ANALYSIS

The present analytical investigation employs a three-dimensional windward plane of symmetry laminar, transitional, and turbulent boundary-layer analysis coupled with a three-dimensional inviscid conical flow analysis for a sharp cone at incidence in a supersonic or hypersonic stream. Full development of the boundary-layer analysis will be presented below; the inviscid analysis utilizes a documented digital computer code which will be described briefly.

2.1 GOVERNING BOUNDARY-LAYER EQUATIONS

The present analysis employs the three-dimensional compressible turbulent boundary-layer equations in terms of time-averaged mean flow quantities as derived by Vaglio-Laurin (Ref. 24). The coordinate system is taken to consist of geodesics and geodesic parallels following Moore (Ref. 13). In this coordinate system the body surface is defined by $y = 0$ and a point in space is defined by the distances, x, y, and $r(x)\phi$ where the length $r(x)\phi$ depends implicitly on the distance x and where $r(x)$ has the dimensions of length. This coordinate system is especially useful in the analysis of flow about bodies for which a coordinate x can be defined such that body cross sections are similar for various values of x. The quantity $r(x)$ then gives the variation of scale for these cross sections. For the sharp cone geometry under present consideration, the geodesic coordinates are taken to be the cone generators and the geodesic parallels are the circles swept by the meridianal angle. The corresponding length function $r(x)$ is the local radius of the body. See Fig. 1 for clarification of the sharp cone geometry, nomenclature, and coordinate system. The velocity components are taken to be $\bar{u}$, $\bar{v}$, and $\bar{w}$ in the directions of x, y, and ϕ, respectively. The governing equations of motion are, following Vaglio-Laurin (Ref. 24):

CONTINUITY

$$\frac{\partial}{\partial x}(\bar{\rho}\bar{u}r) + \frac{\partial}{\partial y}(\bar{\rho}Vr) + \frac{\partial}{\partial \phi}(\bar{\rho}\bar{w}) = 0 \tag{1}$$

STREAMWISE (x) MOMENTUM

$$\bar{\rho}\bar{u}\frac{\partial \bar{u}}{\rho x} + \bar{\rho}V\frac{\partial \bar{u}}{\partial y} + \frac{\bar{\rho}\bar{w}}{r}\frac{\partial \bar{u}}{\partial \phi} - \frac{\bar{\rho}(\bar{w})^2}{r}\frac{\partial r}{\partial x} = -\frac{\partial \bar{p}}{\partial x} + \frac{\partial}{\partial y}\left[\mu\frac{\partial \bar{u}}{\partial y} - \bar{\rho}\,\overline{u'v'}\right] \tag{2}$$

CIRCUMFERENTIAL (ϕ) MOMENTUM

$$\bar{\rho}\bar{u}\frac{\partial \bar{w}}{\partial x} + \bar{\rho}V\frac{\partial \bar{w}}{\partial y} + \frac{\bar{\rho}\bar{w}}{r}\frac{\partial \bar{w}}{\partial \phi} + \frac{\bar{\rho}\bar{u}\bar{w}}{r}\frac{\partial r}{\partial x} = \frac{-1}{r}\frac{\partial \bar{p}}{\partial \phi} + \frac{\partial}{\partial y}\left[\mu\frac{\partial \bar{w}}{\partial y} - \bar{\rho}\,\overline{v'w'}\right] \tag{3}$$

NORMAL (y) MOMENTUM

$$\frac{\partial \bar{p}}{\partial y} = 0 \tag{4}$$

ENERGY

$$\bar{\rho}\bar{u}\frac{\partial \bar{H}}{\partial x} + \bar{\rho}V\frac{\partial \bar{H}}{\partial y} + \frac{\bar{\rho}\bar{w}}{r}\frac{\partial \bar{H}}{\partial \phi} = \frac{\partial}{\partial y}\left[\mu\left(\frac{\partial \bar{H}}{\partial y} + \frac{1-Pr}{Pr}\frac{\partial \bar{h}}{\partial y}\right) - \bar{\rho}\,\overline{v'H'}\right] \tag{5}$$

where

$$V = \bar{v} + \frac{\overline{\rho'v'}}{\bar{\rho}} \tag{6}$$

and the usual expressions for the mean and fluctuating parts of the dependent variables are used; e.g.,

$$\rho = \bar{\rho} + \rho' \tag{7}$$

Implicit in Vaglio-Laurin's derivation of the above equations are the following stipulations:

a. The rates of change of the mean flow properties in the x and ϕ directions [$\mathcal{O}(1)$] are smaller than the rates of change in the y direction [$\mathcal{O}(\delta^{-1})$] by an order of magnitude.

b. Mean squares and products of the turbulent fluctuations are $\mathcal{O}(\delta)$; that is, the turbulent level is small. The terms involving mean squares of the velocity fluctuations are taken to be negligible, which is valid for high Reynolds number flows with a zero or favorable pressure gradient.

c. The time average molecular transports are approximated by those pertaining to the mean flow properties; indeed, even the latter are negligible, except very near the wall, compared with terms involving the turbulent transports.

The energy equation (5) is defined in terms of the mean stagnation enthalpy

$$\bar{H} = \bar{h} + \frac{\bar{u}^2 + \bar{w}^2}{2} \tag{8}$$

If the two momentum equations (2) and (3) are multiplied by $\bar{u}$ and $\bar{w}$, respectively, and added, one obtains an equation for $(\bar{u}^2 + \bar{w}^2)/2$ which is simplified by the fact that the curvature terms (those involving $\partial r/\partial x$) vanish. If then this equation is combined with the energy equation (5), one obtains the following energy equation in terms of the mean static enthalpy:

ENERGY

$$\bar{\rho}\bar{u}\frac{\partial \bar{h}}{\partial x} + \bar{\rho}\bar{v}\frac{\partial \bar{h}}{\partial y} + \frac{\bar{\rho}\bar{w}}{r}\frac{\partial \bar{h}}{\partial \phi} = \bar{u}\frac{\partial \bar{p}}{\partial x} + \frac{\bar{w}}{r}\frac{\partial \bar{p}}{\partial \phi} + \mu\left[\left(\frac{\partial \bar{u}}{\partial y}\right)^2 + \left(\frac{\partial \bar{w}}{\partial y}\right)^2\right] - \bar{\rho}\,\overline{u'v'}\frac{\partial \bar{u}}{\partial y} - \bar{\rho}\,\overline{v'w'}\frac{\partial \bar{w}}{\partial y} + \frac{\partial}{\partial y}\left[\frac{\mu}{Pr}\frac{\partial \bar{h}}{\partial y} - \bar{\rho}\,\overline{v'h'}\right] \tag{9}$$

This is the form of the energy equation used in the present analysis.

If subscript w denotes wall and subscript e denotes outer edge of the boundary layer, the associated boundary conditions on the above defined equations are

MOMENTUM

$$\begin{aligned} y = 0 &: \bar{u} = \bar{v} = \bar{w} = \overline{u'v'} = \overline{v'w'} = \overline{\rho'v'} = 0 \\ \lim y \to \infty &: \bar{u} \to U_e,\ \bar{w} \to W_e \\ &\quad \overline{u'v'} \to 0,\ \overline{v'w'} \to 0,\ \overline{\rho'v'} \to 0 \end{aligned} \tag{10}$$

ENERGY

$$\begin{aligned} y = 0 &: \bar{h} = h_w,\ \overline{v'h'} = 0 \\ \lim y \to \infty &: \bar{h} \to h_e,\ \overline{v'h'} \to 0 \end{aligned} \tag{11}$$

which reflect the requirements of no slip or homogeneous mass injection (suction or blowing) at the wall as well as a prescribed wall enthalpy. The normal momentum equation (4) reveals that the static-pressure variation across the boundary layer is negligible, and hence the static pressure, $p(x,\phi)$, is regarded as external input to the boundary-layer analysis from a separate inviscid analysis. The outer edge velocities, U_e and W_e, as well as the outer edge static enthalpy, h_e, must be determined from the inviscid analysis consistent with the imposed static-pressure distribution.

The gas model adopted for the present study is thermally and calorically perfect air having a constant specific heat ratio $\gamma = 1.40$ and obeying the equation of state

$$\bar{p} = \bar{\rho} R \bar{T} \tag{12}$$

where $R = 1716$ ft^2/sec^2-°R. Hence, under this assumption,

$$\bar{h} = C_p \bar{T} \tag{13}$$

where $C_p = 6006$ ft^2/sec^2-°R. The laminar viscosity, μ, is taken to obey Sutherland's law

$$\frac{\mu}{\mu_{ref}} = \frac{T_{ref} + 198.6}{\bar{T} + 198.6} \left(\frac{\bar{T}}{T_{ref}} \right)^{3/2} \tag{14}$$

where $\bar{T}$ must have units of °R and subscript ref denotes a reference condition. The laminar Prandtl number, Pr, is taken to be a constant value of 0.71 across the entire boundary layer.

2.2 TURBULENT TRANSPORT LAWS

Before Eqs. (1), (2), (3), and (9) can be solved, expressions must be supplied for the Reynolds stress or turbulent shear terms in the momentum equations and the turbulent flux of static enthalpy in the energy equation. The approach used in the present analysis is to model these terms as functions of the mean-flow variables following the analysis by Hunt, Bushnell, and Beckwith (Ref. 29).

The concept that the Reynolds stress in turbulent flow is proportional to a momentum exchange coefficient times the mean-flow velocity gradient normal to the surface is well known and commonly used in turbulent boundary-layer analyses. This concept is based on an assumed analogy between the so-called eddy viscosity and the molecular viscosity. The total shear components in the streamwise (x) and circumferential (ϕ) directions are written as

$$\tau_x = \mu \frac{\partial \bar{u}}{\partial y} - \bar{\rho} \overline{u'v'} \approx \mu \frac{\partial \bar{u}}{\partial y} + \epsilon_x \frac{\partial \bar{u}}{\partial y} \tag{15}$$

$$\tau_\phi = \mu \frac{\partial \bar{w}}{\partial y} - \bar{\rho} \overline{v'w'} \approx \mu \frac{\partial \bar{w}}{\partial y} + \epsilon_\phi \frac{\partial \bar{w}}{\partial y} \tag{16}$$

where the eddy viscosities ϵ_x and ϵ_ϕ in the x- and ϕ-directions, respectively, might in general be different. Since the total resultant shear must be a vector quantity, its magnitude is written as

$$\tau = \left[\left(\tau_x \right)^2 + \left(\tau_\phi \right)^2 \right]^{1/2} = \left[\left(\mu + \epsilon_x \right)^2 \left(\frac{\partial \bar{u}}{\partial y} \right)^2 + \left(\mu - \epsilon_\phi \right)^2 \left(\frac{\partial \bar{w}}{\partial y} \right)^2 \right]^{1/2} \tag{17}$$

In a similar manner the total heat flux in the energy equation (9) becomes

$$\dot{q} = \frac{k}{C_p}\frac{\partial \overline{h}}{\partial y} - \overline{\rho}\,\overline{v'h'} \approx \frac{k}{C_p}\frac{\partial \overline{h}}{\partial y} + \frac{\kappa}{C_p}\frac{\partial \overline{h}}{\partial y} \tag{18}$$

where κ is the so-called eddy thermal conductivity.

2.3 EDDY VISCOSITY MODEL

The simplest approach to the formulation of models for the Reynolds stress is based on Prandtl's mixing-length hypothesis. For two-dimensional flow, this hypothesis states that

$$\left.\begin{aligned} u' &\propto -\ell_* \frac{\partial \overline{u}}{\partial y} \\ v' &\propto \ell_* \left|\frac{\partial \overline{u}}{\partial y}\right| \end{aligned}\right\} \tag{19}$$

The turbulent shear and eddy viscosity are then

$$\tau_{turb} \equiv -\overline{\rho}\,\overline{u'v'} = \epsilon\frac{\partial \overline{u}}{\partial y} = \overline{\rho}\ell_*^2\left|\frac{\partial \overline{u}}{\partial y}\right|\frac{\partial \overline{u}}{\partial y} \tag{20}$$

from whence

$$\epsilon = \overline{\rho}\ell_*^2\left|\frac{\partial \overline{u}}{\partial y}\right| \tag{21}$$

The quantity ℓ_* is termed the mixing-length and is some characteristic length related to the size or scales of eddies responsible for the flux of momentum in the y-direction. Although the details of such a transfer mechanism are not well understood, the basic concept gives satisfactory results even at hypersonic Mach numbers in the presence of heat-transfer and pressure gradients as mentioned in the review of turbulent boundary-layer literature given in Section I.

The turbulent boundary-layer studies by Prandtl (Ref. 30) and Glushko (Ref. 31) are based on the concept that the eddy viscosity should depend only on the properties of the turbulence and a local eddy scale. Extending this concept to the three-dimensional case of present interest suggests that the eddy viscosity should be a scalar function independent of the coordinate direction. Accordingly, the components of the Reynolds stress are written as

$$\tau_{turb,\,x} \equiv -\overline{\rho}\,\overline{u'v'} = \overline{\rho}\ell_*^2\frac{\partial \overline{G}}{\partial y}\frac{\partial \overline{u}}{\partial y} \tag{22}$$

$$\tau_{turb,\,\phi} \equiv -\overline{\rho}\,\overline{v'w'} = \overline{\rho}\ell_*^2\frac{\partial \overline{G}}{\partial y}\frac{\partial \overline{w}}{\partial y} \tag{23}$$

so that the eddy viscosity is

$$\epsilon = \epsilon_x = \epsilon_\phi = \bar{\rho}\ell_*^2 \frac{\partial \bar{G}}{\partial y} \tag{24}$$

To determine the scalar function $\bar{G}$, Eq. (24) is substituted into Eq. (17) with the result that the magnitude of the total resultant shear becomes

$$\tau = \left(\mu + \bar{\rho}\ell_*^2 \frac{\partial \bar{G}}{\partial y}\right)\left[\left(\frac{\partial \bar{u}}{\partial y}\right)^2 + \left(\frac{\partial \bar{w}}{\partial y}\right)^2\right]^{1/2} \tag{25}$$

Now, by analogy with Eqs. (20) and (21) where the velocity-gradient function for the turbulent shear component is repeated in the eddy viscosity expression, the relationship for the determination of the $\bar{G}$ function becomes

$$\frac{\partial \bar{G}}{\partial y} = \left[\left(\frac{\partial \bar{u}}{\partial y}\right)^2 + \left(\frac{\partial \bar{w}}{\partial y}\right)^2\right]^{1/2} \tag{26}$$

which results in the final form of the eddy viscosity

$$\epsilon = \bar{\rho}\ell_*^2\left[\left(\frac{\partial \bar{u}}{\partial y}\right)^2 + \left(\frac{\partial \bar{w}}{\partial y}\right)^2\right]^{1/2} \tag{27}$$

Hunt, Bushnell, and Beckwith (Ref. 29) call the above representation of the Reynolds stress the invariant turbulence model. The key assumption in this model is that the eddy viscosity is a scalar function independent of coordinate direction. In a recent analysis of three-dimensional incompressible turbulent boundary-layer flows using the kinetic-energy-of-turbulence approach, Nash (Ref. 32) has advanced arguments that the turbulent shear stress is likely to act in the mean rate of strain direction, defined by the components of the mean velocity gradient vector, so that his closure equation is simply, in the nomenclature of the present analysis,

$$\frac{\tau_{turb,\,x}}{\dfrac{\partial \bar{u}}{\partial y}} = \frac{\tau_{turb,\,\phi}}{\dfrac{\partial \bar{w}}{\partial y}} \tag{28}$$

The same equation results from the scalar eddy viscosity model presented by Eqs. (22) and (23) above. On the other hand, Bradshaw (Ref. 33) has derived a set of differential equations for the two components of the turbulent shear stress based again on the kinetic-energy-of-turbulence approach but permitting the turbulent shear stress vector to deviate from the mean rate of strain direction. However, in the near-wall region, Bradshaw's

turbulent shear stress equation reduces to the form, again in the nomenclature of the present analysis,

$$\tau_{turb} = \bar{\rho}\ell_*^2\left[\left(\frac{\partial\bar{u}}{\partial y}\right)^2 + \left(\frac{\partial\bar{w}}{\partial y}\right)^2\right] \tag{29}$$

which is identical with the results of Eqs. (25) and (26) derived above for the turbulent shear contributions. Arguments for the preference of either variance or invariance of the turbulent shear stress vector relative to the mean rate of strain direction are currently based on slender evidence. The analytical studies by Mellor (Ref. 27) and Cooper (Ref. 34) concerning three-dimensional incompressible turbulent boundary layers indicate that the above-defined invariant model of turbulence results in very acceptable calculated boundary-layer parameters relative to experiment. Much more work, especially carefully controlled experiments involving three-dimensional compressible turbulent boundary layers, remains to be done before the question of variance or invariance can be completely resolved. Until such time, the above invariant turbulence model appears plausible for studying three-dimensional turbulent boundary-layer flow.

2.4 MIXING LENGTH MODEL

The turbulent shear stress in a three-dimensional turbulent boundary layer as governed by Eqs. (25) and (26) is treated herein by the use of a two-layer inner-outer model using Prandtl's mixing length hypothesis and a modification of van Driest's analysis for the near wall region. This results in a continuous distribution of the shear stress from the laminar value at the wall, through the fully turbulent region, reaching zero at the outer edge of the boundary layer. The energy transport in a turbulent boundary layer is treated in this work through the incorporation of the eddy conductivity, κ, into a turbulent Prandtl number, Pr_t. Exactly the same empirical functions are used as in the two-dimensional flow reported by Adams (Ref. 11). This is justified by noting that the scalar properties of a turbulence field are unlikely to be affected by moderate three-dimensionality because turbulence is inherently three-dimensional in nature for even so-called two-dimensional flows.

After Escudier (Ref. 35), Patankar and Spalding (Ref. 3) recommend the following variation of the mixing length, ℓ_*, across the turbulent two-dimensional boundary layer which is adopted for the three-dimensional case per the above discussion:

$$\begin{aligned} \ell_* &= k_* y, \text{ for } 0 < y \leqq \lambda y_\ell / k_* \\ \ell_* &= \lambda y_\ell, \text{ for } \lambda y_\ell / k_* < y \end{aligned} \tag{30}$$

where the values for the various numerical constants are taken to be $k_* = 0.435$ and $\lambda = 0.09$. The value of y at the point where the velocity in the boundary layer is equal to 0.99 of the velocity at the boundary layer outer edge is used to define the distance y_ℓ. The above choices follow Patankar and Spalding and result in good agreement with

the mixing length model proposed by Maise and McDonald (Ref. 36) for compressible two-dimensional turbulent boundary layers.

By analogy with Stokes' solution for an infinite flat plate undergoing simple harmonic motion parallel to itself in an infinite fluid, van Driest (Ref. 37) concluded that in the vicinity of a wall the total shear stress in a turbulent two-dimensional fluid should be of the form

$$\tau = \mu \frac{\partial \bar{u}}{\partial y} + \bar{\rho}\, k_*^2 y^2 \left[1 - \exp\left(\frac{-y\sqrt{\tau_w \bar{\rho}}}{\mu A_*}\right)\right]^2 \left(\frac{\partial \bar{u}}{\partial y}\right)^2 \tag{31}$$

which results in an exponential damping of the turbulent part of the shear stress as the wall is approached and yields exactly the laminar shear stress form, $\tau = \mu(\partial \bar{u}/\partial y)$, at the wall. Although Eq. (31) was originally developed for incompressible flow, it can be applied to compressible flow by application of the suggestion by Patankar and Spalding (Ref. 3) that the local value of shear stress be used instead of the wall value as originally recommended by van Driest (Ref. 37). Hence, by analogy of Eq. (31) with Eqs. (25) and (26), the relationship for the three-dimensional near-wall shear stress as used in the present analysis is

$$\tau = \mu \frac{\partial \bar{G}}{\partial y} + \bar{\rho}\, k_*^2 y^2 \left[1 - \exp\left(\frac{-y\sqrt{\tau \bar{\rho}}}{\mu A_*}\right)\right]^2 \left(\frac{\partial \bar{G}}{\partial y}\right)^2 \tag{32}$$

where the constant A_* is taken to be 26.0 following the original van Driest proposal (Ref. 37). Note that the damping term in Eq. (32) reflects the application of the local total shear stress as opposed to the wall shear stress of Eq. (31) as discussed previously.

Based on Eqs. (26), (27), (30), and (32), the eddy viscosity expression for the inner region is

$$\epsilon_i = \bar{\rho} k_*^2 y^2 \left[1 - \exp\left(\frac{-y\sqrt{\tau \bar{\rho}}}{\mu A_*}\right)\right]^2 \frac{\partial \bar{G}}{\partial \bar{y}} \tag{33}$$

while for the outer region

$$\epsilon_o = \bar{\rho} \lambda^2 y_\ell^2 \frac{\partial \bar{G}}{\partial y} \tag{34}$$

while the constants k_*, A_*, λ, and y_ℓ as defined previously. The constraint used to define the end of the inner region and the beginning of the outer region is the continuity of the eddy viscosity. From the wall outward, the expression for the inner eddy viscosity applies until $\epsilon_i = \epsilon_o$ from which point the outer eddy viscosity is used. A schematic of this variation in terms of the mixing lengths is shown below.

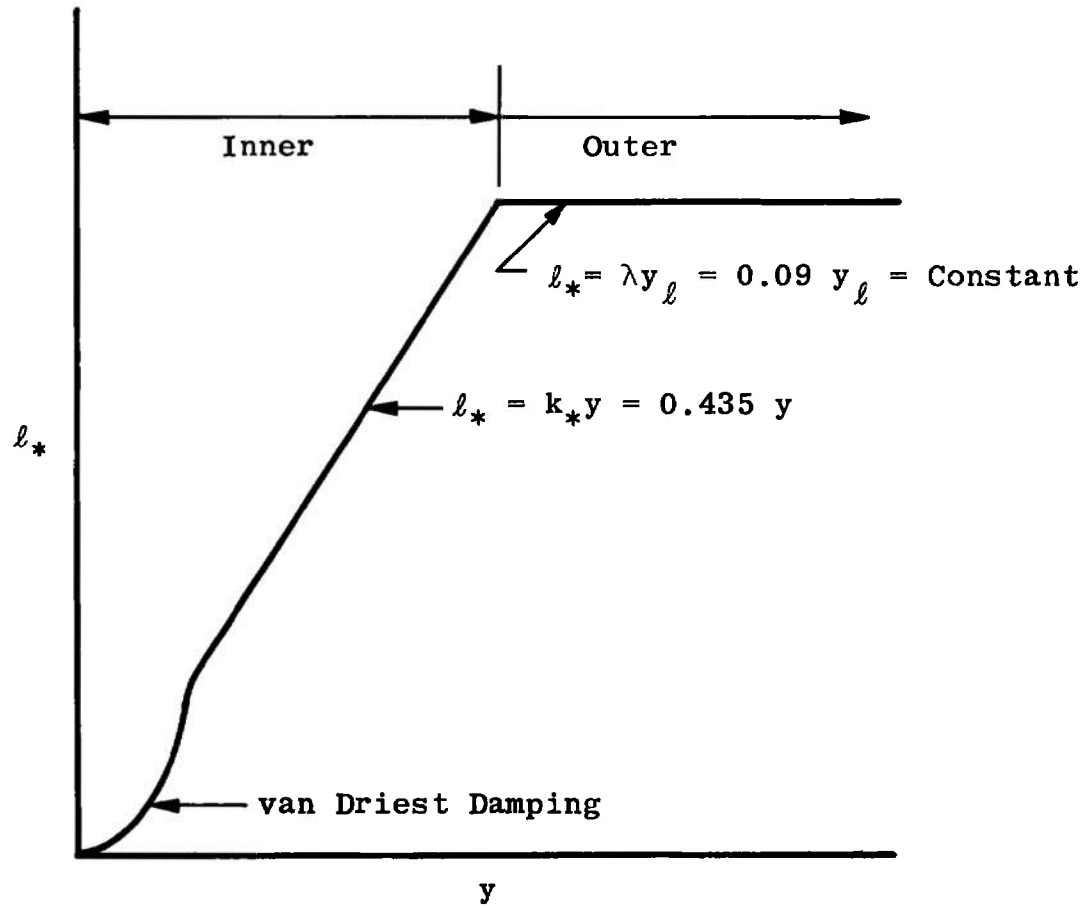

The turbulent Prandtl number defined as

$$Pr_t = \frac{C_p \epsilon}{\kappa} \tag{35}$$

is physically a measure of the ratio of eddy viscosity to eddy conductivity, that is, the ratio of the turbulent transport of momentum to the turbulent transport of heat. Since the flow in the outer region of a turbulent boundary layer shows some similarity to a turbulent wake flow, one may advance arguments that a realistic formulation of turbulent Prandtl number requires a separate expression for the inner and outer region just as in the eddy viscosity formalism. Recent reviews by Rotta (Refs. 38 and 39) and Meier and Rotta (Ref. 40) indicate that the turbulent Prandtl number varies in magnitude from approximately 0.8 near the boundary-layer outer edge to approximately 1.5 near the wall. Much experimental work remains to be done in defining the turbulent Prandtl number distribution as the reviews by Rotta point out. In the present work the turbulent Prandtl number defined by Eq. (35) is taken to remain constant at the value 0.90 across the entire boundary layer as recommended by Patankar and Spalding (Ref. 3) for two-dimensional turbulent boundary layers. This choice of turbulent Prandtl number is consistent with the analyses of Patankar and Spalding (Ref. 3), Martellucci, Rie, and

Sontowski (Ref. 6), Mayne and Dyer (Ref. 7), and Adams (Ref. 11). The early analysis by Smith and Cebeci (Ref. 2) assumed a value of unity, whereas the recent work by Cebeci (Ref. 8) employs a variable turbulent Prandtl number model. Bushnell and Beckwith (Ref. 4), as well as Hunt, Bushnell, and Beckwith (Ref. 29), also use a variable turbulent Prandtl number model.

2.5 GOVERNING BOUNDARY-LAYER EQUATIONS IN PLANE OF SYMMETRY

In order to initiate numerical solution of the complete three-dimensional boundary-layer equations using a marching, implicit finite-difference procedure to integrate the parabolic partial differential equations, initial boundary-layer profiles are required along an initial or starting boundary. For the case of a body of revolution at angle of attack, the initial or starting boundary is the windward plane of symmetry. For the sharp cone geometry of interest in the present work, the windward plane of symmetry corresponds to the most windward ray of the sharp cone; i.e., $\phi = 0$ in Fig. 1. At this symmetry plane, the crossflow velocity component, $\overline{w}$, vanishes due to symmetry. In addition, the crossflow pressure gradient, $\partial\overline{p}/\partial\phi$, also vanishes due to symmetry. Under these restrictions, and under the eddy viscosity model adopted in Section 2.3, every term in the circumferential momentum equation (3) vanishes identically. Noting that under these restrictions the continuity equation (1) still contains the crossflow velocity gradient, $\partial\overline{w}/\partial\phi$, which does not vanish in the plane of symmetry, Moore (Ref. 16) proposed to differentiate the crossflow equation (3) with respect to ϕ first, and only then to neglect the terms which vanish in the plane of symmetry. This procedure applied to Eq. (3) yields the following results, evaluated in the plane of symmetry:

CIRCUMFERENTIAL (ϕ) MOMENTUM

$$\overline{\rho}\,\overline{u}\frac{\partial\overline{w}_\phi}{\partial x} + \overline{\rho}V\frac{\partial\overline{w}_\phi}{\partial y} + \frac{\overline{\rho}}{r}\left(\overline{w}_\phi\right)^2 + \frac{\overline{\rho}\,\overline{u}\,\overline{w}_\phi}{r}\frac{\partial r}{\partial x} = \frac{-1}{r}\frac{\partial^2\overline{p}}{\partial\phi^2} + \frac{\partial}{\partial y}\left[\left(\mu+\epsilon\right)\frac{\partial\overline{w}_\phi}{\partial y}\right] \tag{36}$$

where

$$\overline{w}_\phi = \frac{\partial\overline{w}}{\partial\phi} \tag{37}$$

In the plane of symmetry where $\overline{w} = 0$, the continuity, x-momentum, and energy equations (1), (2), and (9), respectively, reduce to the following form:

CONTINUITY

$$\frac{\partial}{\partial x}\left(\overline{\rho}\,\overline{u}\,r\right) + \frac{\partial}{\partial y}\left(\overline{\rho}Vr\right) + \overline{\rho}\,\overline{w}_\phi = 0 \tag{38}$$

STREAMWISE (x) MOMENTUM

$$\overline{\rho}\,\overline{u}\frac{\partial\overline{u}}{\partial x} + \overline{\rho}V\frac{\partial\overline{u}}{\partial y} = -\frac{\partial\overline{p}}{\partial x} + \frac{\partial}{\partial y}\left[\left(\mu+\epsilon\right)\frac{\partial\overline{u}}{\partial y}\right] \tag{39}$$

ENERGY

$$\bar{\rho}\bar{u}\frac{\partial \bar{h}}{\partial x} + \bar{\rho}V\frac{\partial \bar{h}}{\partial y} = \bar{u}\frac{\partial \bar{p}}{\partial x} + (\mu + \epsilon)\left(\frac{\partial \bar{u}}{\partial y}\right)^2 + \frac{\partial}{\partial y}\left[\left(\frac{\mu}{Pr} + \frac{\epsilon}{Pr_t}\right)\frac{\partial \bar{h}}{\partial y}\right] \tag{40}$$

The eddy viscosity in the above equations is evaluated from Eq. (27) as

$$\epsilon = \bar{\rho}\ell_*^2\left|\frac{\partial \bar{u}}{\partial y}\right| \tag{41}$$

in the plane of symmetry. The absolute magnitude bars on $\partial\bar{u}/\partial y$ in Eq. (41) take into account that the sign on τ_{turb} must change with $\partial\bar{u}/\partial y$ as in Eq. (21) presented previously.

At this point it is well to note that the plane of symmetry restriction has reduced the x-momentum and energy equations to a quasi-two-dimensional form in that they do not explicitly depend on the crossflow velocity gradient, $\bar{w}_\phi$. The continuity equation (38) serves to couple implicitly the streamwise momentum and energy equations with the crossflow momentum equation. The crossflow velocity gradient term, $\bar{\rho}\bar{w}_\phi$, in the continuity equation (38) can be physically considered as a local source (outflow) or local sink (inflow) term with the strength and development history of the source or sink controlled by the crossflow momentum equation (36). This concept is especially helpful in understanding how a quasi-two-dimensional flow reflects three-dimensional influence.

Equation (41) shows that the plane of symmetry restriction has resulted in the eddy viscosity relationship becoming quasi-two-dimensional in form. The crossflow influence is reflected implicitly through the mixing length, ℓ_*, which is, in turn, solely dependent on local boundary-layer conditions. In this respect the application of the local total shear stress in Eq. (33) is especially important.

2.6 COORDINATE TRANSFORMATION

In order to facilitate numerical integration of the governing quasi-two-dimensional plane of symmetry boundary-layer equations (36), (38), (39), and (40), it is convenient to transform them to a coordinate system that removes the singularity at x = 0 and stretches the coordinate normal to the surface, as is usually done in two-dimensional laminar flow. The coordinate transformation used in the present work is the well-known Lees-Dorodnitsyn (Ref. 41, p. 31) transformation. The new independent variables introduced are

$$\xi(x) = \int_0^x \rho_e \mu_e U_e r^2\, dx \tag{42}$$

$$\eta(x,y) = \frac{\rho_e U_e r}{\sqrt{2\xi}}\int_0^y \frac{\bar{\rho}}{\rho_e}\, dy \tag{43}$$

evaluated in the plane of symmetry. The transformed streamwise and normal derivatives hence become

$$\frac{\partial}{\partial x} = \rho_e \mu_e U_e r^2 \frac{\partial}{\partial \xi} + \frac{\partial \eta}{\partial x} \frac{\partial}{\partial \eta} \tag{44}$$

$$\frac{\partial}{\partial y} = \frac{\bar{\rho} U_e r}{\sqrt{2\xi}} \frac{\partial}{\partial \eta} \tag{45}$$

Introducing the two scalar stream functions, $\Psi(x,y)$ and $\psi(x,y)$, in such a manner as to identically satisfy the continuity equation (38) following the approach by Moore (Ref. 13),

$$\bar{\rho} \bar{u} r = \frac{\partial \Psi}{\partial y} \tag{46}$$

$$\bar{\rho} \bar{w}_\phi r = \frac{\partial \psi}{\partial y} \tag{47}$$

$$\bar{\rho} V r = -\frac{\partial \Psi}{\partial x} - \frac{\psi}{r} \tag{48}$$

and defining transformed stream functions $f(\xi,\eta)$ and $g(\xi,\eta)$ such that

$$\Psi(x,y) = \sqrt{2\xi}\, f(\xi,\eta) \tag{49}$$

$$\psi(x,y) = \sqrt{2\xi}\, g(\xi,\eta) \tag{50}$$

the governing plane of symmetry boundary-layer equations (36), (39), and (40) become, in the transformed (ξ,η) plane,

STREAMWISE (x) MOMENTUM

$$(\ell^* f'')' + [f + Gg] f'' + \beta \left[\frac{\theta}{\bar{e}} - (f')^2 \right] = 2\xi \left[f' \frac{\partial f'}{\partial \xi} - f'' \frac{\partial f}{\partial \xi} \right] \tag{51}$$

CIRCUMFERENTIAL (ϕ) MOMENTUM

$$(\ell^* g'')' + [f + Gg] g'' - f' g' \left[\beta + G \frac{dr}{dx} \right] - G[(g')^2 + \chi\theta] = 2\xi \left[f' \frac{\partial g'}{\partial \xi} - g'' \frac{\partial f}{\partial \xi} \right] \tag{52}$$

ENERGY

$$\left(\frac{\ell^{**}}{Pr} \theta' \right)' + [f + Gg] \theta' + (\gamma - 1) M_e^2 \left[\ell^* (f'')^2 - \frac{\beta}{\bar{e}} \theta f' \right] = 2\xi \left[f' \frac{\partial \theta}{\partial \xi} - \theta' \frac{\partial f}{\partial \xi} + \frac{f\theta}{T_e} \frac{dT_e}{d\xi} \right] \tag{53}$$

with the new dependent variables

$$f'(\xi,\eta) = \frac{\bar{u}}{U_e} \tag{54}$$

$$g'(\xi,\eta) = \frac{\bar{w}_\phi}{U_e} \tag{55}$$

$$\theta(\xi,\eta) = \frac{\bar{T}}{T_e} \tag{56}$$

The following definitions apply to the above equations

$$\ell^* = \frac{\bar{\rho}\mu}{\rho_e \mu_e}\left(1 + \frac{\epsilon}{\mu}\right) \tag{57}$$

$$\ell^{**} = \frac{\bar{\rho}\mu}{\rho_e \mu_e}\left(1 + \frac{\epsilon}{\mu}\frac{Pr}{Pr_t}\right) \tag{58}$$

$$\beta = \frac{2\xi}{U_e}\frac{dU_e}{d\xi} \tag{59}$$

$$\chi = \frac{1}{\gamma \bar{p} M_e^2}\frac{\partial^2 \bar{p}}{\partial \phi^2} \tag{60}$$

$$\bar{\bar{e}} = \frac{-\rho_e U_e \dfrac{dU_e}{dx}}{\dfrac{d\bar{p}}{dx}} \tag{61}$$

$$G = \frac{2\xi}{r\dfrac{d\xi}{dx}} \tag{62}$$

$$M_e = \frac{U_e}{\sqrt{\gamma R T_e}} \tag{63}$$

where the inviscid streamwise plane of symmetry momentum equation

$$\frac{d\bar{p}}{dx} + \rho_e U_e \frac{d\bar{U}_e}{dx} = 0 \tag{64}$$

has been used to relate the inviscid velocity, U_e, to the imposed inviscid static pressure. For the classical boundary-layer analysis where the inviscid flow body streamline results are used as the conditions at the outer edge of the boundary layer, the parameter $\bar{\bar{e}} \equiv 1$. For the more general case where swallowing of the inviscid flow into the boundary layer is taken into account, as must be done for blunt-nosed bodies in hypersonic flow, the value of $\bar{\bar{e}}$ must be determined according to Eq. (61). This approach is necessitated because Eq. (64) is only valid along an inviscid streamline. The use of the $\bar{\bar{e}}$ parameter in the above manner follows the approach by Blottner (Ref. 42).

The parameter χ defined by Eq. (60) above may be physically interpreted as a driving potential or forcing function for the plane of symmetry crossflow momentum equation (52). It is controlled solely by the inviscid flow and must be input to the analysis along with the other outer edge conditions for the boundary layer. Furthermore, since χ is directly dependent on the second derivative of the pressure distribution in the ϕ-direction, information concerning the allowable boundary-layer development proceeding away from the plane of symmetry is communicated through this term. In short, χ is the key and controlling parameter in determining the crossflow influence through the crossflow velocity gradient $\overline{w}_\phi$ in a plane of symmetry analysis.

The physical boundary conditions given by Eqs. (10) and (11) become, in terms of the transformed variables in the plane of symmetry,

MOMENTUM

$$\left.\begin{aligned} f(\xi,\eta=0) &= g(\xi,\eta=0) = 0 \\ f'(\xi,\eta=0) &= g'(\xi,\eta=0) = 0 \\ \lim_{\eta\to\infty} \quad f'(\xi,\eta) &= 1 \\ \lim_{\eta\to\infty} \quad g'(\xi,\eta) &= \frac{[\overline{w}_\phi]_e}{U_e} = g'_e \end{aligned}\right\} \tag{65}$$

ENERGY

$$\left.\begin{aligned} \theta(\xi,\eta=0) &= \frac{T_w}{T_e} = \theta_w \\ \lim_{\eta\to\infty} \quad \theta(\xi,\eta) &= 1 \end{aligned}\right\} \tag{66}$$

The outer edge boundary condition, g'_e, for the crossflow momentum equation can be derived as follows. From the asymptotic character of the circumferential momentum equation (52) as the outer edge is approached from below

$$\lim_{\eta\to\infty} \quad g''(\xi,\eta) = 0$$

$$\lim_{\eta\to\infty} \quad g'''(\xi,\eta) = 0$$

and

$$\lim_{\eta\to\infty} \quad g'(\xi,\eta) = g'_e$$

so that, with the use of the boundary conditions (65) and (66), Eq. (52) reduces to the algebraic form

$$G(g'_e)^2 + \left[\beta + G\frac{dr}{dx}\right]g'_e + G\chi = 0 \tag{67}$$

Solving this quadratic equation for g'_e yields

$$g'_e = \frac{-\left(\beta + G\frac{dr}{dx}\right) \pm \sqrt{\left(\beta + G\frac{dr}{dx}\right)^2 - 4G^2\chi}}{2G} \tag{68}$$

The present study is concerned solely with analysis of the windward plane of symmetry along a sharp cone at angle of attack. For this flow condition the appropriate choice of sign in Eq. (68) is positive (+) which can be easily determined by noting that g'_e must be zero for the sharp cone at zero angle of attack where χ is also zero due to the uniform circumferential pressure distribution. Along the windward plane of symmetry for the sharp cone at angle of attack, χ is always a negative quantity so that g'_e is always positive denoting a source (outflow) influence on the governing equations.

2.7 TRANSITION ZONE DESCRIPTION

The distance between transition onset at $x = X_t$ and the beginning of fully turbulent flow further downstream at $x = X_T$ is denoted herein as the transition zone. In the present work, which is restricted solely to analysis of sharp cone windward streamline flows, no attempt is made to predict or correlate a priori the location of transition onset at X_t. Instead, the experimentally indicated beginning of the transition region is used for the onset point X_t based on the particular sharp cone data under examination.

Repeatability of gross characteristics of the transition region such as a nondimensional length has been observed in experimental investigations. Potter and Whitfield (Ref. 43) show that the transition zone local Reynolds number, $Re_{e,\Delta x}$ (where $\Delta x = X_T - X_t$), has a dependence on both transition onset local Reynolds number, Re_{e,X_t}, and the local Mach number, M_e. In the present work, the extent of the transition zone will be represented by a transition zone local Reynolds number ratio, $Re_{e,X_T}/Re_{e,X_t}$, which is related to $Re_{e,\Delta x}$ by

$$\frac{Re_{e,X_T}}{Re_{e,X_t}} = 1 + \frac{Re_{e,\Delta x}}{Re_{e,X_t}} \tag{69}$$

where Re_{e,X_T} is the local Reynolds number at the inception of fully turbulent flow. The onset of transition in the present work is determined from examination of experimental heat-transfer data. The end of transition is taken herein to coincide with the location of experimentally determined maximum heating. A schematic of this nomenclature is shown on the following page.

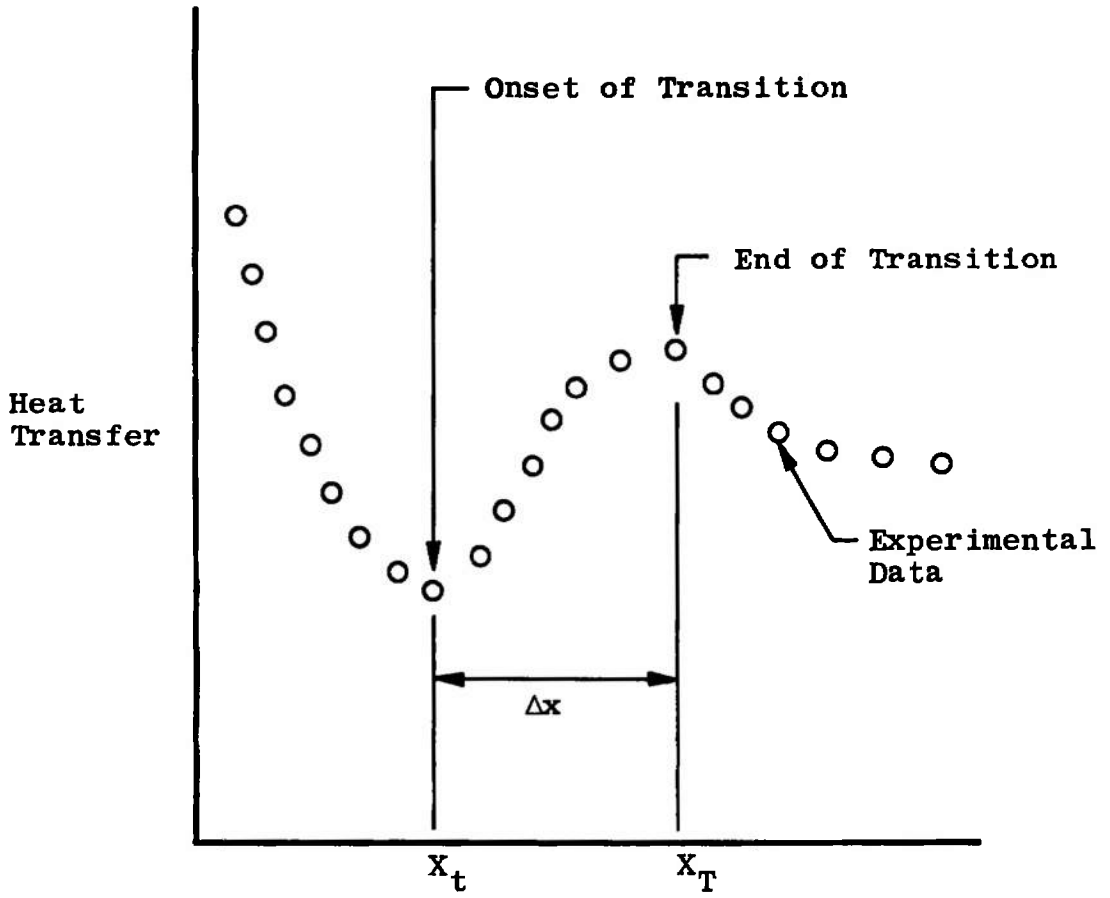

Masaki and Yakura (Ref. 12) present a comprehensive survey of unclassified experimental data showing transition on flat plates and cones over a range of local Mach numbers from 2 to 15. Based on this survey (which is given in Fig. 2 of their paper) they suggest that a value for $Re_{e,x_T}/Re_{e,x_t}$ of approximately two appears reasonable at high supersonic speeds. The value of two is not a universal number, and a great deal of work remains to be done before this boundary-layer characteristic is fully understood. The effects of wall cooling, pressure gradient, and three-dimensional crossflow are moot points at this time. It should be noted, however, that Murphy and Rubesin (Ref. 44) found that $Re_{e,x_T}/Re_{e,x_t} \approx 2$ based on flight test results from the Mark-2 blunt-nosed ballistic reentry vehicle. In addition, the recent experimental data reported by Young, Reda, and Roberge (Ref. 45) taken in a hypersonic wind tunnel (Mach 10) on a lifting entry configuration indicate that the factor of two ratio of transition end-to-onset boundary-layer-edge Reynolds number provides a good description of transition zone extent for even complex geometries at angle of attack. As the transition onset Reynolds number is increased, the ratio of transition end-to-onset boundary-layer-edge Reynolds number appears to slightly decrease below the value of two (see Refs. 12, 45, and 46 for further discussion of this point).

Based on the above discussion, the present investigation utilizes a transition zone description following the criterion

$$\frac{Re_{e,\,X_T}}{Re_{e,\,X_t}} = 2 \tag{70}$$

which is identical to that used previously by Adams (Ref. 11) with success.

2.8 INTERMITTENCY FACTOR TREATMENT OF TRANSITION

In order to provide a suitable progressive transition model as opposed to an instantaneous transition model, the present analysis utilizes the phenomenological theory of the transition zone developed by Emmons (Refs. 47 and 48) which is based upon the experimental observation that transition in a boundary layer is characterized by the intermittent appearance of turbulent spots which grow and move downstream with the fluid. In the transition zone, the intermittent appearance of turbulent spots and their growth as they move downstream produces alterations of laminar and turbulent flow with a gradual increase in the mean turbulence level. At any point in the transition zone, the probability of turbulent flow is prescribed by a model based on the residence times of intermittent turbulent spots. Dhawan and Narasimha (Ref. 49) modified Emmons' original formulation of the probability of turbulent flow to account for a localized region of breakdown about $x = X_t$ in conjunction with a single universal intermittency distribution. The Dhawan and Narasimha model simply expresses the intermittency factor, I_f, which indicates the probability of the flow being turbulent at some point as

$$I_f(x) = 1 - \exp\left[-\Phi\left(\frac{x - X_t}{\overline{X}}\right)^2\right] \tag{71}$$

where Φ is a constant equal to 0.412 and $\overline{X}$ is a measure of the extent of the transition region characterized by

$$\overline{X} = (x)_{I_f = 0.75} - (x)_{I_f = 0.25} \tag{72}$$

The beginning of the transition zone, where $I_f(0) = 0$, was established by Dhawan and Narasimha (Ref. 49) as being located at the transition onset distance $x = X_t$. In order to describe the extent of the transition zone, Masaki and Yakura (Ref. 12) assume that fully turbulent flow is achieved at $x = X_T$ where

$$I_f(X_T) \geqq 0.97 \tag{73}$$

Substituting this assumption into Eq. (71) gives the length of the transition zone as

$$\Delta x = X_T - X_t = 2.96\overline{X} \tag{74}$$

In order to evaluate $\overline{X}$, recall from Eq. (70) that

$$Re_{e,\,X_T} = 2Re_{e,\,X_t} \tag{75}$$

which implies physically that the transition zone length Δx is equal to the transition onset distance X_t. Hence this reveals that

$$\Delta x = X_t \tag{76}$$

so that $\overline{\chi}$ becomes, from Eq. (74),

$$\overline{\chi} = \frac{X_t}{2.96} \tag{77}$$

Under these restrictions the intermittency factor given by Eq. (71) takes the final form

$$I_f(x) = 1 - \exp\left[-0.412\,(2.96)^2\left(\frac{x}{X_t} - 1\right)^2\right] \tag{78}$$

where $x \geqq X_t$.

Although the original derivation of the intermittency factor was based on experiments performed in low speed incompressible flow, Dhawan and Narasimha (Ref. 49) established its validity for use in prediction of supersonic skin friction on a flat plate. To the author's knowledge, no work has been done on the effects of pressure gradients or crossflow on the $I_f(x)$ distributions in either incompressible or compressible flows, although Dhawan and Narasimha speculate that pressure gradients would chiefly influence the manner of spot growth in the initial period near $I_f = 0$. Another point of interest is the distribution of I_f across the boundary layer, viz., normal to the surface. Dhawan and Narasimha state that, although this $I_f(y)$ variation is probably of importance to the detailed structure of the turbulent motion, the value of I_f near the wall is the characteristic property of importance for the transition region and the $I_f(y)$ variation has only a secondary influence in determining the mean velocity profiles in transition. Hence, for the supersonic and hypersonic sharp cone windward streamline flows of interest in the present investigation, Eq. (78) is used for the intermittency factor distribution in order to assess its validity for use in such regimes.

In the present work the intermittency factor multiplies the eddy viscosity in the modified density-viscosity product ratios ℓ^* and ℓ^{**} defined by Eqs. (57) and (58) in the following manner:

$$\ell^* = \frac{\overline{\rho}\mu}{\rho_e \mu_e}\left(1 + I_f \frac{\epsilon}{\mu}\right) \tag{79}$$

$$\ell^{**} = \frac{\overline{\rho}\mu}{\rho_e \mu_e}\left(1 + I_f \frac{\epsilon}{\mu}\frac{Pr}{Pr_t}\right) \tag{80}$$

The physical justification for using the intermittency factor in this manner lies in the basic physical definition of the intermittency factor as representing the fraction of time any point spends in turbulent flow, i.e., the probability of the flow being turbulent at

a given point. If $I_f = 0$, the flow is completely laminar, whereas if $I_f = 1$, the flow is fully turbulent. The present treatment of the intermittency factor-eddy viscosity product in the governing equations simply means that the (fully turbulent) eddy viscosity is multiplied by a damping factor (the intermittency factor) in order to achieve a smooth and continuous variation from laminar to turbulent flow through the transition region. Similar approaches have been reported by Adams (Ref. 11), Harris (Ref. 10), and Martellucci, Rie, and Sontowski (Ref. 6). These references indicate that use of the intermittency factor in the above-defined manner results in very acceptable calculation of transitional heating rates when applied in conjunction with the factor of two transition zone extent criterion discussed previously. Certainly more work remains to be done relative to the definition and application of the intermittency factor concept in three-dimensional flows.

2.9 BOUNDARY-LAYER PARAMETERS

Given the numerical solution to the governing equations of motion (Eqs. (51), (52), and (53)) following the integration procedure of Appendix III, the associated local boundary-layer parameters at a given body station may be determined as follows. The local convective heat flux at the body surface (y = 0) is given by the well-known Fourier law,

$$\dot{q}_w = -k_w\left(\frac{\partial \bar{T}}{\partial y}\right)_w \tag{81}$$

which becomes, in the transformed (ξ,η) coordinates,

$$\dot{q}_w = \frac{-\ell_w \rho_e \mu_e U_e r C_p T_e}{Pr_w \sqrt{2\xi}}\, \theta'(\xi,\eta = 0) \tag{82}$$

where

$$\ell_w = \frac{\bar{\rho}_w \mu_w}{\rho_e \mu_e} \tag{83}$$

In a similar manner, the local wall shearing stress along the windward streamline may be written in terms of the transformed coordinates as

$$\tau_w = \mu_w\left(\frac{\partial \bar{u}}{\partial y}\right)_w = \frac{\ell_w \rho_e \mu_e U_e^2 r}{\sqrt{2\xi}}\, f''(\xi,\eta = 0) \tag{84}$$

The actual height of the boundary layer along the windward streamline is determined from the y-transformation relationship, Eq. (43), as

$$y = \frac{\sqrt{2\xi}}{\rho_e U_e r}\int_0^\eta \theta d\eta \tag{85}$$

The classical definition of the two-dimensional boundary-layer displacement thickness is given by

$$\delta^*_{2\text{-D}} = \int_0^\infty \left(1 - \frac{\overline{\rho}\,\overline{u}}{\rho_e U_e}\right) dy \tag{86}$$

which becomes, in transformed coordinates,

$$\delta^*_{2\text{-D}} = \frac{\sqrt{2\xi}}{\rho_e U_e r} \int_0^{\eta_\infty} (\theta - f')\, d\eta \tag{87}$$

For the case of boundary-layer flow along the windward streamline of a sharp cone at incidence, two lengths characterizing mass-flow defect may be defined in terms of the profiles of the two velocity components tangential to the surface (see Fig. 1 for clarification of nomenclature):

$$\delta^*_x = \int_0^\infty \left(1 - \frac{\overline{\rho}\,\overline{u}}{\rho_e U_e}\right) dy \tag{88}$$

and

$$\delta^*_\phi = \int_0^\infty \left(1 - \frac{\overline{\rho}\,\overline{w}}{\rho_e \overline{W}_e}\right) dy \tag{89}$$

and is is not clear which, if either, defines a displacement thickness properly describing the extent to which the nonviscous flow is deflected by the boundary layer. Moore (Ref. 50) has considered this problem in great detail relative to the proper definition of a three-dimensional displacement surface. For the special case of windward streamline boundary-layer flow on a sharp cone at incidence, Moore's Eq. (14) on page 7 of Ref. 50 shows that

$$\Delta^* = \frac{\frac{3}{2}\delta^*_x + \frac{g'_e}{\sin \delta_v}\delta^*_\phi}{\frac{3}{2} + \frac{g'_e}{\sin \delta_v}} \tag{90}$$

where Δ^* is the three-dimensional plane of symmetry boundary-layer displacement thickness. Note that Δ^* differs from $\delta_x{}^*$ in the plane of symmetry due to the circumferential mass-flow defect. In terms of the transformed (ξ,η) coordinates, the two mass-flow defect lengths may be written as

$$\delta^*_x = \frac{\sqrt{2\xi}}{\rho_e U_e r} \int_0^{\eta_\infty} (\theta - f')\, d\eta \tag{91}$$

and

$$\delta^*_\phi = \frac{\sqrt{2\xi}}{\rho_e U_e r} \int_0^{\eta_\infty} \left(\theta - \frac{g'}{g'_e}\right) d\eta \tag{92}$$

valid along the windward streamline.

Various nondimensional quantities of interest are defined as follows:

LOCAL REYNOLDS NUMBER BASED ON FREE-STREAM CONDITIONS

$$Re_{\infty, x} = \frac{\rho_\infty U_\infty x}{\mu_\infty} \tag{93}$$

LOCAL REYNOLDS NUMBER BASED ON INVISCID EDGE CONDITIONS

$$Re_{e, x} = \frac{\rho_e U_e x}{\mu_e} \tag{94}$$

LOCAL SKIN-FRICTION COEFFICIENT REFERENCED TO FREE-STREAM CONDITIONS

$$C_{f_\infty} = \frac{\tau_w}{\frac{1}{2}\rho_\infty U_\infty^2} \tag{95}$$

LOCAL STANTON NUMBER BASED ON INVISCID EDGE CONDITIONS AND ADIABATIC WALL TEMPERATURE

$$St_{e, aw} = \frac{-\dot{q}_w}{\rho_e U_e C_p (T_{aw} - T_w)} \tag{96}$$

LOCAL STANTON NUMBER BASED ON FREE-STREAM CONDITIONS AND ADIABATIC WALL TEMPERATURE

$$St_{\infty, aw} = \frac{-\dot{q}_w}{\rho_\infty U_\infty C_p (T_{aw} - T_w)} \tag{97}$$

In the above

$$\frac{T_{aw}}{T_{o, \infty}} = r_f + \frac{T_\infty}{T_{o, \infty}} (1 - r_f) \tag{98}$$

with r_f the recovery factor which must be defined relative to the flow under examination, i.e., for laminar boundary layers

$$r_f = \sqrt{Pr} = \sqrt{0.71} = 0.843 \tag{99}$$

and for turbulent boundary layers

$$r_f = \sqrt[3]{Pr} = \sqrt[3]{0.71} = 0.892 \tag{100}$$

where Pr = 0.71, as previously specified in Section 2.1.

2.10 NUMERICAL SOLUTION OF THE GOVERNING BOUNDARY-LAYER EQUATIONS

In the present work (restricted to the windward plane of symmetry of a sharp cone at incidence), numerical solution of the simultaneous, nonlinear, parabolic, partial differential equations (Eqs. (51), (52), and (53)) is performed by obtaining linear finite-difference equivalents of the equations and solving these using an iterative, marching, implicit finite-difference technique involving inversion of tridiagonal matrices. Full details of this numerical approach are given in Appendix III.

The digital computer code is written in FORTRAN 63 for use on a CDC 1604-B digital computer. Solution time including printout is approximately 20 minutes total on the 1604-B machine for a windward streamline divided into 100 stations. No numerical stability problems have been encountered with the present finite-difference approach due to its implicit nature.

2.11 INVISCID FLOW ABOUT A SHARP CONE AT INCIDENCE

A recent investigation by Jones (Ref. 51) has resulted in an accurate and efficient numerical integration procedure for solution of the governing partial differential equations describing the supersonic or hypersonic inviscid flow field around a sharp cone at incidence. Basically, Jones' method uses the condition of conicity to reduce the problem to a set of elliptic nonlinear partial differential equations in two independent variables. A transformation of coordinates is used to fix the boundaries, one of which is the unknown shock wave, between which the elliptic equations are to be satisfied. This transformation also has the effect of including the body shape in the coefficients of the partial differential equations and in the boundary conditions, so that the same method can be used for general conical body shapes simply by changing a few program statements to redefine the equation of the body. In fact the method is, in many cases, only limited by locally supersonic crossflow conditions, by the entropy singularity moving too far away from the surface, or by the shock approaching very close to the Mach wave. In practice, these restrictions limit the allowable angle-of-attack range to $\alpha/\delta_v \lessapprox 1.2$ (see Fig. 1 for clarification of nomenclature).

At the present time the method has been used successfully for circular cones and for bodies that can be obtained by successive perturbations of a circular cone and that do not have curvatures that are too large. Jones (Ref. 51) has reported examples for circular cones at incidence, elliptic cones, and a body whose cross-sectional shape is represented by a fourth order even cosine Fourier series.

The method is efficient in computer time compared with other fully numerical techniques, and one solution takes from about one-half minute to three minutes on an IBM 360/50 computer for the circular cone at incidence - the time increasing as the incidence increases. This is to be compared with a time requirement of approximately one-half hour on an IBM 360/50 computer for the technique developed by Moretti (Ref. 52) in which the flow-field solution is obtained by marching step by step downstream (approximately 400 downstream steps are required) until a conicity condition is sufficiently

well satisfied. Comparison of results between the Jones and Moretti approaches shows excellent agreement, with the Jones digital computer code being a factor of approximately ten faster than the Moretti approach in solution time. An analysis very similar to that of Jones has recently been reported by South and Klunker (Ref. 53), and Holt and Ndefo (Ref. 54) have developed a method of integral relations approach to the problem. The important point to note is that all of the above-referenced analyses report excellent agreement with experiment for sharp circular and elliptic cones at incidence under supersonic and hypersonic flow conditions; therefore, the choice of which analysis is indeed the best remains an open question. The present author's experience with use of the Jones' digital computer code (Ref. 55) has been most favorable from a user's standpoint.

For the present investigation, concerned only with the windward plane of symmetry along a sharp cone at incidence, the important inviscid parameters required for input to the boundary-layer analysis as outer-edge conditions are

$$\frac{\bar{p}}{p_\infty}, \frac{T_e}{T_\infty}, M_e, \text{ and } \chi$$

where recall that

$$\chi = \frac{1}{\gamma \bar{p} M_e^2} \frac{\partial^2 \bar{p}}{\partial \phi^2}$$

and

$$g'_e = \frac{-\left(\beta + G\frac{dr}{dx}\right) + \sqrt{\left(\beta + G\frac{dr}{dx}\right)^2 - 4G^2\chi}}{2G}$$

from Eqs. (60) and (68). respectively, with all quantities evaluated on the windward streamline where $\phi = 0$. All of the above-indicated inviscid parameters may be determined from the Jones digital computer code with numerical differentiation required to evaluate $\partial^2\bar{p}/\partial\phi^2$ on the windward streamline. It should be noted that the so-called "isentropic surface" values of the inviscid parameters (see Ref. 51 for clarification of this terminology) have been used in the present investigation.

It should be pointed out in conclusion that Jones (Ref. 56) has recently published a very complete and thorough set of tables for inviscid supersonic and hypersonic flow about circular cones at incidence in a perfect gas, $\gamma = 1.40$, stream. These tables can be used to provide all of the needed inviscid information for input to the present boundary-layer analysis.

SECTION III
RESULTS AND DISCUSSION

As pointed out by Smith (Ref. 57) in his recent review of boundary-layer research over the past decade, the ultimate test of any theoretical analysis of the turbulent boundary

layer is the end accuracy (and not the intrinsic logic) since empiricism is involved. Hence, with this in mind, comparison of experimental data with the present laminar, transitional, and turbulent windward plane of symmetry boundary-layer analysis is mandatory. Since the current effort is limited solely to sharp cone geometry, the following additional restrictions are imposed at this point in order to clearly define the experimental flow field for comparison with the analytical model:

1. Angle of incidence range $0 \leqq \alpha \lessapprox 1.2\ \delta_v$.

2. Uniform free stream; i.e., no source flow effects.

3. Constant uniform wall temperature.

4. Windward streamline transition zone well defined by heat-transfer data where applicable.

Under the above restrictions, a review of unclassified, published literature on sharp cone at incidence experimental investigations revealed the seven sources (Refs. 58 through 64) listed in Table I, Appendix II. Most published investigations do not meet the rather stringent restrictions imposed above and hence must be eliminated on this basis. For example, Stetson and Rushton (Ref. 65) present no usable heat-transfer data defining the transition zone at angle of attack. By only using experimental data from Table I, meaningful comparisons between theory and experiment can be made with some confidence since the assumptions under which the analytical model is formulated match the restrictions placed on acceptable experimental data.

Table II lists the windward streamline inviscid outer-edge conditions for input to the boundary-layer analysis corresponding to the various flows in Table I for which experimental data are available. The inviscid conditions are determined from numerical solution of the inviscid conical flow equations for a sharp cone at incidence using the Jones' digital computer code (Refs. 51 and 55) described in Section 2.11. Consistent with the gas model adopted in Section 2.1, a perfect gas with $\gamma = 1.40$ is used in the inviscid analysis.

In order to assess the basic applicability of the present windward plane of symmetry boundary-layer analysis for laminar applications, Figs. 2, 3, 4, and 5 present windward ray heat-transfer-rate calculations using the present theory relative to experimental data. Complete flow conditions may be found in Table I with the corresponding inviscid outer-edge conditions given in Table II. Figures 2 and 3 show good agreement between theory and experiment for the heat-transfer ratio $\dot{q}_w(\alpha)/\dot{q}_w$ $(\alpha = 0)$ at a common body location. Figures 4 and 5 present calculated adiabatic wall Stanton numbers relative to experimental measurements. Again, the agreement between theory and experiment is good except for the front half of the distribution presented in Fig. 5. Included in Fig. 5 is a zero-angle-of-attack distribution illustrating the results from an intermittency factor treatment of transition using the present theory relative to experimental data. The favorable heat-transfer results presented above indicate that indeed the present theory is applicable

and accurate under laminar boundary-layer conditions along the windward streamline of a sharp cone. The case of transitional and turbulent boundary layers along the windward plane of symmetry will now be considered.

Of the data in Table I, the investigation by McCauley, Saydah, and Bueche (Ref. 62) is one of the best documented with respect to test conditions and analysis of data. The test was conducted in the Hypersonic Wind Tunnel (C) of the von Kármán Gas Dynamics Facility, Arnold Engineering Development Center, at a nominal Mach number of 10 under cold wall conditions. Complete test conditions are given in Table I. Figure 6 shows a comparison of results from the present theory relative to experimental heat-transfer measurements along the windward streamline under natural transition conditions. In general, the agreement between experimental data and calculated results from the present theory is excellent for both zero and nonzero angles of incidence. The transitional heating rates are well defined by the present theory which, it should be recalled, requires that the location of onset to transition be prescribed as indicated in Fig. 6. All three sets of experimental data presented in Fig. 6 clearly show a factor of about two in the ratio X_T/X_t as previously discussed in Section 2.7 and used in the present analytical model. Note from Fig. 6 that an increase in angle of attack caused the onset of transition location, X_t, to move slightly rearward along the windward streamline which is in agreement with the findings of Stetson and Rushton (Ref. 65). Further note that for this natural transition condition the boundary-layer flow remains transitional over the entire aft half of the cone.

The primary emphasis in the experimental investigation of Ref. 62 was placed on determining the effect of controlled three-dimensional roughness (spherical trips) on hypersonic laminar boundary-layer transition. Presented in Fig. 7 is a comparison of calculated heat transfer relative to experimental measurements for a case in which the laminar boundary layer was "tripped" at the body location x/L = 0.15. For this condition the calculations assumed an instantaneous transition from fully laminar to fully turbulent flow at the above-specified trip location on the body. Also shown for sake of comparison is a zero angle-of-attack calculation using the intermittency factor treatment of transition with onset to transition taken at the body location x/L = 0.25. The important point to observe from Fig. 7 is that the laminar boundary layer is not effectively "tripped" to an immediate fully turbulent state relative to the numerical calculations for the angle-of-attack conditions. Only at the end of the body (x/L = 1.0) has the experimental data for the angle-of-attack conditions reached the level predicted by the present theory. Note especially that the level of the experimental data remains essentially constant from the trip location to the end of the body for the angle-of-attack conditions. For zero angle of attack, the "tripped" boundary-layer response is sufficiently rapid to produce fully turbulent flow over the entire aft half of the cone. Compare Figs. 6 and 7 for clarification of the relative behavior between "untripped" and "tripped" boundary layers.

Turning now to details of the boundary-layer structure along the windward plane of symmetry, Figs. 8 and 9 present calculated boundary-layer profiles (streamwise velocity, crossflow velocity, static temperature, total temperature, Mach number, and pitot pressure) for fully laminar (body location x/L = 0.40) and fully turbulent (body location x/L = 1.0) flow conditions corresponding to Fig. 6. The different character of the laminar and

turbulent profiles is apparent. Note the overshoot in both the laminar and turbulent crossflow velocity profiles. Direct comparison of laminar and turbulent profiles at a common body location will be given in the next paragraph.

In order to present the differences between laminar profiles and fully turbulent profiles at a given common body location along the windward streamline, Fig. 10 shows calculated streamwise velocity. crossflow velocity, and static-temperature distributions for the two types of flow at x/L = 1.0. Note that the streamwise velocity profiles for turbulent flow are much fuller than the laminar profiles, as expected. Further note that the maximum overshoot in the turbulent crossflow velocity profile is less than the corresponding angle-of-attack laminar value which means physically that the outflow influence along the windward streamline of a laminar boundary layer is stronger than a corresponding angle-of-attack turbulent boundary layer. The implications of this finding as it affects surface heat transfer will be discussed in the next paragraph. With respect to the static-temperature distributions, Fig. 10 shows that the peak static temperature in the laminar boundary layer occurs much further from the wall than the peak turbulent static temperature, about a factor of three in distance normal to the surface. This factor of three in location of peak static temperature is somewhat reflected in the thickness of the turbulent boundary layer being approximately twice the thickness of the laminar boundary layer as can be seen by close inspection of Fig. 10.

A concept often used (see Ref. 66, for example) to approximately calculate windward ray heating rates under angle-of-attack conditions is the so-called "effective cone" approach in which a zero angle-of-attack calculation is performed on an "effective cone" which has a cone half-angle equal to the physical cone half-angle plus the physical cone angle of attack. Needless to say, the "effective cone" technique does not properly include the effects of crossflow (outflow) as it affects the windward ray boundary-layer structure. Presented in Fig. 11 are comparisons of "effective cone" calculations relative to the present three-dimensional windward ray analysis for the case of laminar, transitional, and turbulent boundary-layer flow at various angles of attack. Note that the flow conditions are identical with those of Fig. 6 discussed previously. Also, onset to transition locations has been matched between the two analyses for a given angle of attack. As can be seen from Fig. 11, both the heat transfer and skin friction are much more sensitive to three-dimensional crossflow (outflow) effects for a laminar boundary layer than for a turbulent boundary layer. A very informative summary of these results is given in Fig. 12. The important point here is that "effective cone" calculations appear to be acceptable for the present geometry and flow conditions provided the boundary layer is fully turbulent. For a laminar boundary layer, "effective cone" calculations result in a 20- to 30- percent underprediction (based on the x/L = 0.40 laminar results presented in Fig. 12) for both heat transfer and skin friction relative to the present three-dimensional windward streamline analysis. These results confirm the statement of Vaglio-Laurin (Ref. 24) that "due to the larger shearing stresses, smaller three-dimensional effects can be expected for turbulent layers as compared with laminar layers subject to the same boundary conditions." In addition, the recent paper by Widhopf (Ref. 66) concludes that "equivalent cone techniques do not yield uniformly valid approximations but may provide acceptable results in some cases." Indiscriminate use of the "effective cone" approach, especially for laminar boundary layers, is not advised by the present author.

Details of the boundary-layer thickness (based on the normal distance from the surface where $f' = 0.995$) and the three-dimensional displacement thickness defined by Eq. (90) are presented in Fig. 13 for the same flow and angle-of-attack conditions as Fig. 6 previously discussed. The general thinning of the boundary layer as the angle of attack increases is apparent. A comparison of the three-dimensional displacement thickness, Δ^*, relative to the two-dimensional streamwise direction value, δ_x^*, defined by Eq. (91) is given in Fig. 14. The three-dimensional displacement thickness, Δ^*, is slightly smaller than the two-dimensional value at a common body location. Note that the slopes $d\Delta^*/dx$ and $d\delta_x^*/dx$ are very similar at a common body location which is of importance in computing the displacement-induced pressure along the windward streamline using an inviscid tangent-cone technique. Further note that, as the angle of attack is increased, the slope of the displacement thickness decreases for a given body location. This means physically that displacement-induced pressure effects will become of less and less significance on the windward streamline as the angle of attack is increased. For the present flow conditions, Fig. 3 of Ref. 62 shows that the displacement-induced pressure is negligible even at zero angle of attack and hence will not be further considered in the present work. It should be pointed out in passing, however, that the displacement-induced pressure increment may attain its maximum value in the transition region as can be seen from careful examination of the displacement thickness slopes obtained from Figs. 13 and 14.

Turning now to additional comparisons of experimentally obtained transitional and turbulent boundary-layer data, Fig. 15 presents a comparison of a heat-transfer rate parameter calculated using the present windward plane of symmetry theory with the data reported by DiCristina (Ref. 63) for Mach 10.2 hypersonic flow. This test was conducted in the Hypersonic Wind Tunnel (C) of the von Kármán Gas Dynamics Facility, Arnold Engineering Development Center; test conditions are given in Table I with corresponding inviscid-edge conditions in Table II. Agreement of results from the present theory and experiment is excellent with the transitional zone heating well defined by the current intermittency factor analysis. Note the change in recovery factor definition between laminar and transitional flow which is consistent with the manner in which DiCristina presented his data.

One of the most complete and thorough experimental investigations of the turbulent boundary layer on a sharp cone at incidence under supersonic conditions has been reported by Rainbird (Ref. 64). The experiments were performed in the Canadian National Aeronautical Establishment 5-ft intermittent blowdown wind tunnel at Mach numbers of 1.80 and 4.25 for moderate relative incidence ($\alpha/\delta_v \approx 1.2$) under high Reynolds number conditions with a relatively hot wall ($T_w/T_{0,\infty} = 1.0$) on a 12.5-deg semi-vertex-angle sharp cone. Complete flow conditions are given in Table I with the corresponding windward streamline inviscid-edge conditions tabulated in Table II. Presented in Fig. 16 are comparisons of calculated local Mach number profiles across the turbulent boundary layer at the body station $x/L = 0.85$ relative to experimental measurements (via a pitot pressure probe) taken by Rainbird for the 1.80 Mach number condition. In general, the agreement between theory and experiment is reasonably good for both the zero angle of attack and 15.78-deg angle-of-attack conditions. Note that the experimentally determined turbulent boundary-layer thickness is slightly larger than predicted by the present theory. Also shown in Fig. 16 are rough indications of the physical boundaries for the inner and outer regions

of the turbulent boundary layer as discussed by Bradshaw (Ref. 67) in his recent review. The location of the inner-outer boundary at $y/\delta \approx 0.2$ can easily be derived from Eq. (30) by equating the inner and outer mixing lengths to yield

$$\frac{y}{y_{\ell}} = \frac{\lambda}{k_*} = \frac{0.09}{0.435} = 0.206 \tag{101}$$

where y_{ℓ} is the value of y at the point where the velocity in the boundary layer is equal to 0.99 of the velocity at the boundary-layer outer edge, and hence $y_{\ell} \approx \delta$ where δ is the boundary-layer thickness defined as the normal distance from the surface where the boundary-layer velocity equals 0.995 of the outer-edge velocity.

In order to determine the local Mach number distribution, Rainbird measured the pitot pressure across the boundary layer which, when coupled with the assumption that the static pressure remains constant through the boundary layer at a value corresponding to the surface static pressure, yields the local Mach number distribution. Rainbird then assumed the total temperature to remain constant across the boundary layer which allows the distribution of mean velocity to be calculated through the boundary layer. With this information, integrated boundary-layer parameters, such as the displacement thickness, which depend on the actual boundary-layer structure can be determined based on the experimental results. Figure 17 shows a comparison of Rainbird's experimentally determined (in the above-discussed manner) boundary-layer parameters at the body station $x/L = 0.85$ relative to calculated distributions from the present windward ray boundary-layer analysis for both Mach number conditions. Note that the present theory underpredicts the boundary-layer thickness for both Mach numbers at both zero and nonzero angles of attack. However, the calculated two-dimensional boundary-layer displacement thicknesses are in excellent agreement with the experimentally determined values by Rainbird for all cases. It should be noted here that Rainbird used the two-dimensional form of the displacement thickness integral to evaluate his experimentally determined value. As can be seen from Fig. 17, the three-dimensional displacement thickness is slightly smaller than the two-dimensional value which is similar to the results presented previously in Fig. 14 under hypersonic conditions.

A recent note by Copper and Shaw (Ref. 68) was concerned with presentation of a correlation for windward ray turbulent boundary-layer thickness as a function of cone half-angle and angle of attack. Based on examination of a large amount of experimental data, Copper and Shaw recommend the simple expression

$$\ell n\left[\frac{\delta(\alpha)}{\delta(\alpha = 0)}\right] = -2 + 2\exp[-0.3\alpha/\delta_v] \tag{102}$$

as an adequate fit to the data for engineering purposes. The reader is referred to their Note for details of how the above expression is to be modified for surface mass injection effects, if present. Presented in Fig. 18 are selected results comparing the present analytical analysis for fully turbulent boundary layers with the Copper and Shaw correlation. In general, good agreement is observed. For the case of a laminar boundary layer, Fig. 18 shows that the boundary-layer thickness will decrease more rapidly than for a turbulent

boundary layer as the angle of attack increases, which is related to the more severe crossflow influence on laminar boundary layers relative to turbulent boundary layers as discussed previously.

SECTION IV
CONCLUDING SUMMARY

The present investigation was devoted to the formulation and application of a windward plane of symmetry laminar, transitional, and turbulent boundary-layer analysis for sharp cones at incidence in a supersonic or hypersonic flow. The governing boundary-layer equations in the plane of symmetry were numerically integrated on a digital computer using an implicit finite-difference technique which marched along the windward streamline starting at the apex of the cone with a laminar similar solution. A so-called invariant model of turbulence was used in a two-layer eddy viscosity-mixing length approach for calculation of the turbulent boundary layer in conjunction with an intermittency factor treatment of the transition zone. Inviscid edge conditions were input to the boundary-layer analysis from a previously documented inviscid analysis of the conical flow field about a sharp cone at incidence in a supersonic or hypersonic flow.

In general, the agreement between the present theory and experimental data for measured surface heat transfer along the windward streamline was good to excellent for both laminar, transitional, and turbulent boundary layers under a wide range of flow and angle-of-attack conditions. Comparison of calculated and measured local Mach number profiles in a fully turbulent boundary layer revealed reasonable agreement with the turbulent boundary-layer thickness slightly underpredicted by the present theory relative to experimental measurements. Integrated boundary-layer displacement thickness calculations were found to compare quite well with experimentally determined values using a common definition of the displacement thickness.

The effects of three-dimensional crossflow (outflow) along the windward plane of symmetry were shown to be significantly stronger in a laminar boundary layer relative to a turbulent boundary layer. This finding was used in conjunction with an "effective cone" concept to show that windward ray heating distributions for a turbulent boundary layer could be computed satisfactorily (for the geometry and flow conditions under examination) using an "effective cone" of semivertex angle equal to the physical body semivertex angle plus the physical angle of attack in a two-dimensional zero angle-of-attack analysis. Application of this effective cone concept to the windward streamline laminar boundary layer resulted in a 20- to 30-percent underprediction of heat transfer relative to the windward plane of symmetry analysis. In general, smaller crossflow (outflow) effects on the windward streamline boundary layer can be expected for turbulent layers as compared with laminar layers subject to the same boundary conditions. It is important to realize and acknowledge that "equivalent cone" techniques do not yield uniformly valid approximations but may provide acceptable results in some cases (such as the present plane of symmetry turbulent boundary layer). Caution is highly recommended in the use of "equivalent cone" techniques under flow and angle-of-attack conditions where their applicability has not been properly assessed.

REFERENCES

1. Anon. "Analytic Methods in Aircraft Aerodynamics." NASA SP-228, Symposium held at NASA Ames Research Center, Moffett Field, California, October 28-30, 1969.

2. Smith, A.M.O. and Cebeci, T. "Numerical Solution of the Turbulent Boundary-Layer Equations." Douglas Aircraft Division Report 33735, May 1967.

3. Patankar, S. V. and Spalding, D. B. Heat and Mass Transfer in Boundary Layers. CRC Press, Cleveland, Ohio, 1968.

4. Bushnell, D. M. and Beckwith, I. E. "Calculation of Nonequilibrium Hypersonic Turbulent Boundary Layers and Comparisons with Experimental Data." AIAA J., Vol. 8, No. 8, August 1970, pp. 1462-1469.

5. Herring, H. J. and Mellor, G. L. "A Method of Calculating Compressible Turbulent Boundary Layers." NASA CR-1144, September 1968.

6. Martellucci, A., Rie, H., and Sontowski, J. F. "Evaluation of Several Eddy Viscosity Models Through Comparison with Measurements in Hypersonic Flows." AIAA Paper No. 69-688 presented at the AIAA Fluid and Plasma Dynamics Conference, San Francisco, California, June 1969.

7. Mayne, A. W., Jr. and Dyer, D. F. "Comparisons of Theory and Experiment for Turbulent Boundary Layers on Simple Shapes at Hypersonic Conditions." Proceedings of the 1970 Heat Transfer and Fluid Mechanics Institute, Stanford University Press, 1970, pp. 168-188.

8. Cebeci, T. "Calculation of Compressible Turbulent Boundary Layers with Heat and Mass Transfer." AIAA Paper No. 70-741 presented at the AIAA 3rd Fluid and Plasma Dynamics Conference, Los Angeles, California. June 29-July 1, 1970.

9. Pletcher, R. H. "On a Calculation Method for Compressible Turbulent Boundary Layer Flows with Heat Transfer." AIAA Paper No. 71-165 presented at the AIAA 9th Aerospace Sciences Meeting, New York, January 25-27, 1971.

10. Harris, J. E. "Numerical Solution of the Compressible Laminar, Transitional, and Turbulent Boundary Layer Equations with Comparisons to Experimental Data." Ph.D. Dissertation in Aerospace Engineering, Virginia Polytechnic Institute, Blacksburg, Virginia, May 1970. See also NASA TM X-62963, 1970.

11. Adams, J. C., Jr. "Eddy Viscosity-Intermittency Factor Approach to Numerical Calculation of Transitional Heating on Sharp Cones in Hypersonic Flow." AEDC-TR-70-210 (AD714058), November 1970.

12. Masaki, M. and Yakura, J. K. "Transitional Boundary Layer Considerations for the Heating Analysis of Lifting Re-Entry Vehicles." J. Spacecraft and Rockets, Vol. 6, No. 9, September 1969, pp. 1048-1053.

13. Moore, F. K. "Three-Dimensional Compressible Laminar Boundary-Layer Flow." NACA TN 2279. March 1951.

14. Hayes, W. D. "The Three-Dimensional Boundary Layer." NAVORD Report 1313, May 1951.

15. Moore, F. K. "Laminar Boundary Layer on a Circular Cone in Supersonic Flow at a Small Angle of Attack." NACA TN 2521, October 1951.

16. Moore, F. K. "Laminar Boundary Layer on Cone in Supersonic Flow at Large Angle of Attack." NACA TN 2844, November 1952.

17. Reshotko, E. "Laminar Boundary Layer with Heat Transfer on a Cone at Angle of Attack in a Supersonic Stream." NACA TN 4152, December 1957.

18. Brunk, W. E. "Approximate Method for Calculation of Laminar Boundary Layer with Heat Transfer on a Cone at Large Angle of Attack in Supersonic Flow." NACA TN 4380, September 1958.

19. Bodonyi, R. J. and Reshotko, E. "The Compressible Laminar Boundary Layer with Heat Transfer on a Yawed Cone at Small Angle of Attack." NASA CR-109839, January 1970.

20. Libby, P. A., Fox, H., Sanator, R. J., and DeCarlo, J. "Laminar Boundary Layer Near the Plane of Symmetry of a Hypersonic Inlet." AIAA J., Vol. 1, No. 12, December 1963, pp. 2732-2740.

21. Trella, M. and Libby, P. A. "Similar Solutions for the Hypersonic Laminar Boundary Layer Near a Plane of Symmetry." AIAA J., Vol. 3, No. 1, January 1965, pp. 75-83.

22. Libby, P. A. and Liu, T. M. "Some Similar Laminar Flows Obtained by Quasilinearization." AIAA J., Vol. 6, No. 8, August 1968, pp. 1541-1548.

23. Libby, P. A. "Three-Dimensional Boundary Layer with Uniform Mass Transfer." Phys. Fluids, Vol. 12, No. 2, February 1969, pp. 408-417.

24. Vaglio-Laurin, R. "Turbulent Heat Transfer on Blunt-Nosed Bodies in Two-Dimensional and General Three-Dimensional Hypersonic Flow." WADC Technical Note 58-301, September 1958. See also J. Aero. Sci., Vol. 27, No. 1, January 1960, pp. 27-36.

25. Braun, W. H. "Turbulent Boundary Layer on a Yawed Cone in a Supersonic Stream." NASA TR R-7, 1959.

26. Johnston, J. P. "The Turbulent Boundary Layer at a Plane of Symmetry in a Three-Dimensional Flow." J. of Basic Engineering, Series D, Trans. ASME, Vol. 82, September 1960, pp. 622-628.

27. Mellor, G. L. "Incompressible, Turbulent Boundary Layers with Arbitrary Pressure Gradients and Divergent or Convergent Cross Flows." AIAA J., Vol. 5, No. 9, September 1967, pp. 1570-1579.

28. Zakkay, V. and Calarese, W. "Theoretical Investigation of Crossflow Effects on Compressible Turbulent Boundary Layer Over Bodies of Revolution." New York University School of Engineering and Science Report No. F-69-5, December 1969. See also Israel J. of Technology, Vol. 8, No. 1-2, 1970, pp. 127-138.

29. Hunt, J. L., Bushnell, D. M., and Beckwith, I. E. "Finite-Difference Analysis of the Compressible Turbulent Boundary Layer on a Blunt Swept Slab with Leading-Edge Blowing." Paper 19 in "Analytic Methods in Aircraft Aerodynamics." NASA SP-228, Symposium held at NASA Ames Research Center, Moffett Field, California, October 28-30, 1969, pp. 417-472. See also NASA TN D-6203, March 1971.

30. Prandtl, L. "On a New Representation of Fully Developed Turbulence." Jet Propulsion Lab. Publ. No. 13, California Inst. Technology, August 1952.

31. Glushko, G. S. "Turbulent Boundary Layer on a Flat Plate in an Incompressible Fluid." NASA TT F-10,080, April 1966.

32. Nash, J. F. "The Calculation of Three-Dimensional Turbulent Boundary Layers in Incompressible Flow." J. Fluid Mech., Vol. 37, Pt. 4, July 1969, pp. 625-642.

33. Bradshaw, P. "Calculation of Boundary-Layer Development Using the Turbulent Energy Equation. VII. Three-Dimensional Flow." National Physical Lab. Report 1286, January 1969.

34. Cooper, P. "Turbulent Boundary Layer on a Rotating Disk Calculated with an Effective Viscosity." AIAA J., Vol. 9, No. 2, February 1971, pp. 255-261.

35. Escudier, M. P. "The Distribution of the Mixing Length in Turbulent Flows Near Walls." Mechanical Eng. Dept. Report TWF/TN/1, Imperial College, London, March 1965.

36. Maise, G. and McDonald, H. "Mixing Length and Kinematic Eddy Viscosity in a Compressible Boundary Layer." AIAA J., Vol. 6, No. 1, January 1968, pp. 73-80.

37. van Driest, E. R. "On Turbulent Flow Near a Wall." J. Aero Sci., Vol. 23, No. 11, November 1956, pp. 1007-1011, 1036.

38. Rotta, J. C. "Heat Transfer and Temperature Distribution in Turbulent Boundary Layers at Supersonic and Hypersonic Flow." AGARDograph 97, Pt. I, May 1965, pp. 35-63.

39. Rotta, J. C. "Recent Developments in Calculation Methods for Turbulent Boundary Layers with Pressure Gradients and Heat Transfer." J. Applied Mech., Vol. 33, No. 2, June 1966, pp. 429-437.

40. Meier, H. U. and Rotta, J. C. "Experimental and Theoretical Investigation of Temperature Distributions in Supersonic Boundary Layers." AIAA Paper No. 70-744 presented at the AIAA 3rd Fluid and Plasma Dynamics Conference, Los Angeles, California, June 29-July 1, 1970.

41. Dorrance, W. H. Viscous Hypersonic Flow. McGraw-Hill, Inc.. New York, 1962.

42. Blottner, F. G. "Finite Difference Methods of Solution of the Boundary Layer Equations." AIAA J., Vol. 8, No. 2, February 1970, pp. 193-205.

43. Potter, J. L. and Whitfield, J. D. "Effects of Slight Nose Bluntness and Roughness on Boundary-Layer Transition in Supersonic Flows." J. Fluid Mech., Vol. 12, No. 4, April 1962, pp. 501-535.

44. Murphy, J. D. and Rubesin, M. W. "Re-Evaluation of Heat Transfer Data Obtained in Flight Tests of Heat-Sink Shielded Re-Entry Vehicles." J. Spacecraft and Rockets, Vol. 3, No. 1, January 1966, pp. 53-60.

45. Young, C. H., Reda, D. C., and Roberge, A. M. "Hypersonic Transitional and Turbulent Flow Studies on a Lifting Entry Vehicle." AIAA Paper No. 71-100 presented at the AIAA 9th Aerospace Sciences Meeting, New York, January 25-27, 1971. .

46. Kipp, H. W. and Masek, R. V. "Aerodynamic Heating Constraints on Space Shuttle Vehicle Design." ASME Paper No. 70-HT/SpT-45 presented at the ASME Space Technology and Heat Transfer Conference, Los Angeles, California, June 21-24, 1970.

47. Emmons, H. W. "The Laminar-Turbulent Transition in a Boundary Layer-Part I." J. Aero. Sci., Vol. 18, No. 7, July 1951, pp. 490-498.

48. Emmons, H. W. and Bryson, A. E. "The Laminar-Turbulent Transition in a Boundary Layer-Part II." Proceedings of the First U. S. National Congress of Theoretical and Applied Mechanics, ASME, New York, 1951, pp. 859-868.

49. Dhawan, S. and Narasimha, R. "Some Properties of Boundary Layer Flow during the Transition from Laminar to Turbulent Motion." J. Fluid Mech., Vol. 3, No. 4, April 1958, pp. 418-436.

50. Moore, F. K. "Displacement Effect of a Three-Dimensional Boundary Layer." NACA TN 2722, June 1952.

51. Jones, D. J. "Numerical Solutions of the Flow Field for Conical Bodies in a Supersonic Stream." National Research Council of Canada Aeronautical Report LR-507, July 1968. See also C.A.S.I. Transactions, Vol. 3, No. 1, March 1970, pp. 62-71.

52. Moretti, G. "Inviscid Flow Field Past a Pointed Cone at Angle of Attack. Part I-Analysis." GASL TR-577, December 1965. See also AIAA J., Vol. 5, No. 4, April 1967, pp. 789-791.

53. South, J. C., Jr. and Klunker, E. B. "Methods for Calculating Nonlinear Conical Flows." Paper 8 in "Analytic Methods in Aircraft Aerodynamics." NASA SP-228, Symposium held at NASA Ames Research Center, Moffett Field, California, October 28-30, 1969, pp. 131-158.

54. Holt, M. and Ndefo, D. E. "A Numerical Method for Calculating Steady Unsymmetrical Supersonic Flow Past Cones." J. Computational Physics, Vol. 5, 1970, pp. 463-486.

55. Jones, D. J. "Use of the Jones Computer Programme to Determine the Flow Field for Conical Flow Situations. Part I: The Circular Cone at Incidence." National Research Council of Canada NAE LTR-HA-1, June 1969.

56. Jones, D. J. "Tables of Inviscid Supersonic Flow About Circular Cones at Incidence $\gamma = 1.4$, Parts I and II." AGARDograph 137, November 1969.

57. Smith, A.M.O. "A Decade of Boundary-Layer Research." Applied Mechanics Reviews, Vol. 23, No. 1, January 1970, pp. 1-9.

58. Wittliff, C. E. and Wilson, M. R. "Heat Transfer to Slender Cones in Hypersonic Air Flow, Including Effects of Yaw and Nose Bluntness." J. Aero Sci., Vol. 29, No. 7, July 1962, pp. 761-774.

59. Tracy, R. R. "Hypersonic Flow Over a Yawed Circular Cone." GALCIT Hypersonic Research Project Memorandum No. 69, August 1963.

60. Chan, Y. Y. "An Experimental Study of a Yawed Circular Cone in Hypersonic Flows." AIAA J., Vol. 7, No. 10, October 1969, pp. 2035-2037.

61. Fischer, M. C. "An Experimental Investigation of Boundary-Layer Transition on a 10° Half-Angle Cone at Mach 6.9." NASA TN D-5766, April 1970.

62. McCauley, W. D., Saydah, A., and Bueche, J. "The Effect of Controlled Three Dimensional Roughness on Hypersonic Laminar Boundary Layer Transition." AIAA Paper No. 66-26 presented at the AIAA 3rd Aerospace Sciences Meeting, New York, January 24-26, 1966.

63. DiCristina, V. "Three-Dimensional Laminar Boundary-Layer Transition on a Sharp 8° Cone at Mach 10." AIAA J., Vol. 8, No. 5, May 1970, pp. 852-856.

64. Rainbird, W. J. "Turbulent Boundary-Layer Growth and Separation on a Yawed Cone." AIAA J., Vol. 6, No. 12, December 1968. pp. 2410-2416.

65. Stetson, K. F. and Rushton, G. H. "Shock Tunnel Investigation of Boundary Layer Transition at M = 5.5." AIAA J., Vol. 5, No. 5, May 1967, pp. 899-906.

66. Widhopf, G. F. "Turbulent Heat Transfer Measurements on a Blunt Cone at Angle of Attack." AIAA Paper No. 71-38 presented at the AIAA 9th Aerospace Sciences Meeting, New York. January 25-27, 1971.

67. Bradshaw, P. "Turbulent Boundary Layers." The Aeronautical Journal of the Royal Aeronautical Society, Vol. 72, May 1968, pp. 451-459.

68. Copper, J. A. and Shaw, W. J., Jr. "Turbulent Boundary-Layer Thicknesses on Yawed Cones." AIAA J., Vol. 8, No. 6, June 1970, pp. 1138-1140.

69. Davis, R. T. "Numerical Solution of the Hypersonic Viscous Shock-Layer Equations." AIAA J., Vol. 8, No. 5, May 1970, pp. 843-851.

70. Richtmyer, R. D. and Morton, K. W. Difference Methods for Initial-Value Problems, Second Edition. Interscience Publishers, 1967.

71. Flugge-Lotz, I. and Blottner, F. G. "Computation of the Compressible Laminar Boundary-Layer Flow Including Displacement Thickness Interaction Using Finite-Difference Methods." Stanford University Division of Engineering Mechanics Report No. 131, Stanford, California, January 1962.

72. Conte, S. D. Elementary Numerical Analysis. McGraw-Hill, Inc., New York, 1965.

73. Adams, J. C., Jr. "Thin Viscous Shock Layer Analysis of Blunt Body Stagnation-Point Air Ionization." AIAA J., Vol. 7, No. 7, July 1969, pp. 1396-1398.

74. Adams, J. C., Jr. "Shock Slip Analysis of Merged Layer Stagnation Point Air Ionization." AIAA J., Vol. 8, No. 5, May 1970, pp. 971-973.

APPENDIXES

I. ILLUSTRATIONS
II. TABLES
III. IMPLICIT FINITE-DIFFERENCE SOLUTION OF GOVERNING BOUNDARY-LAYER EQUATIONS
IV. VARIABLE GRID DIFFERENTIATION FORMULAS

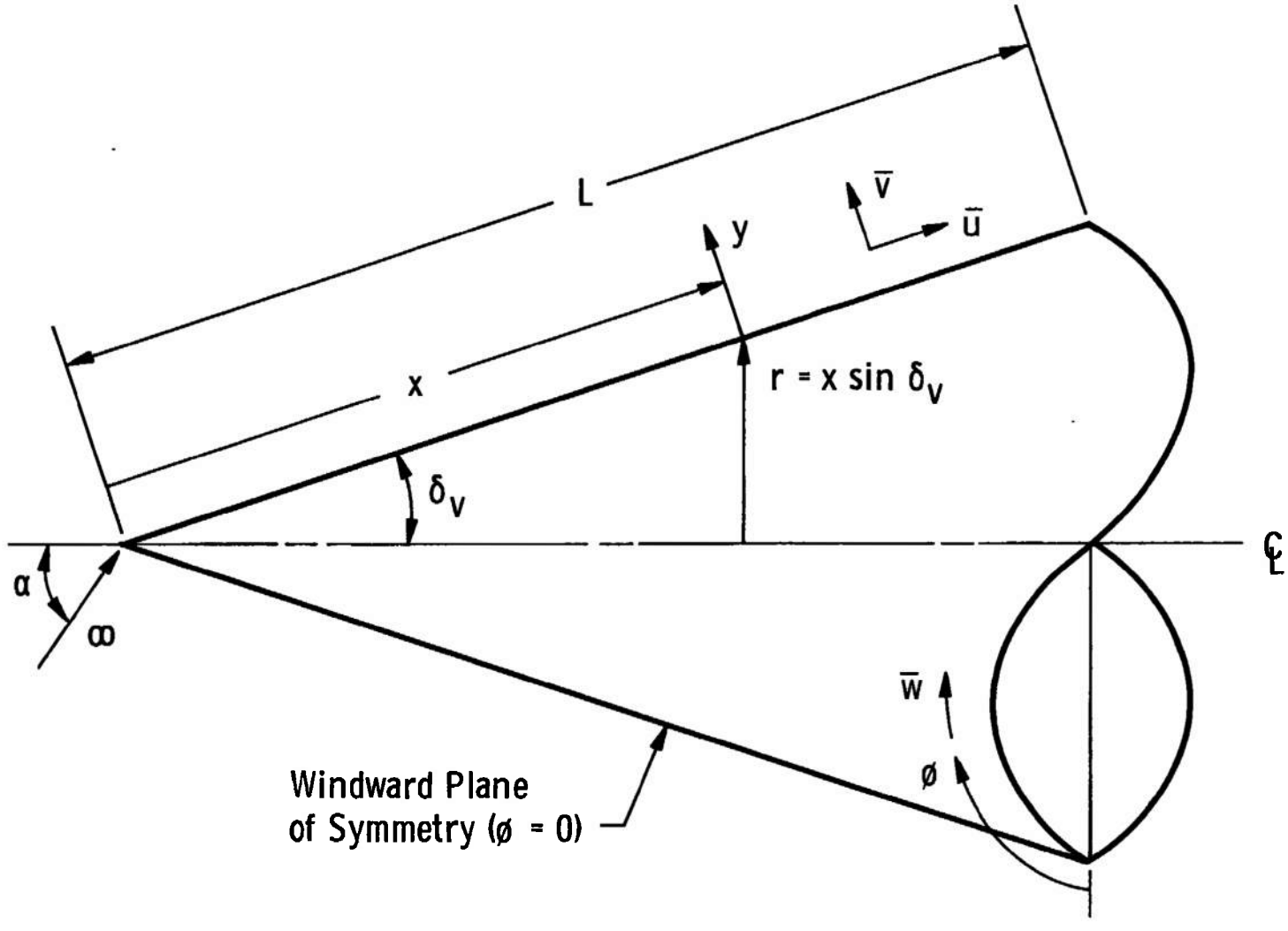

Fig. 1 Sharp Cone at Angle-of-Attack Geometry and Nomenclature

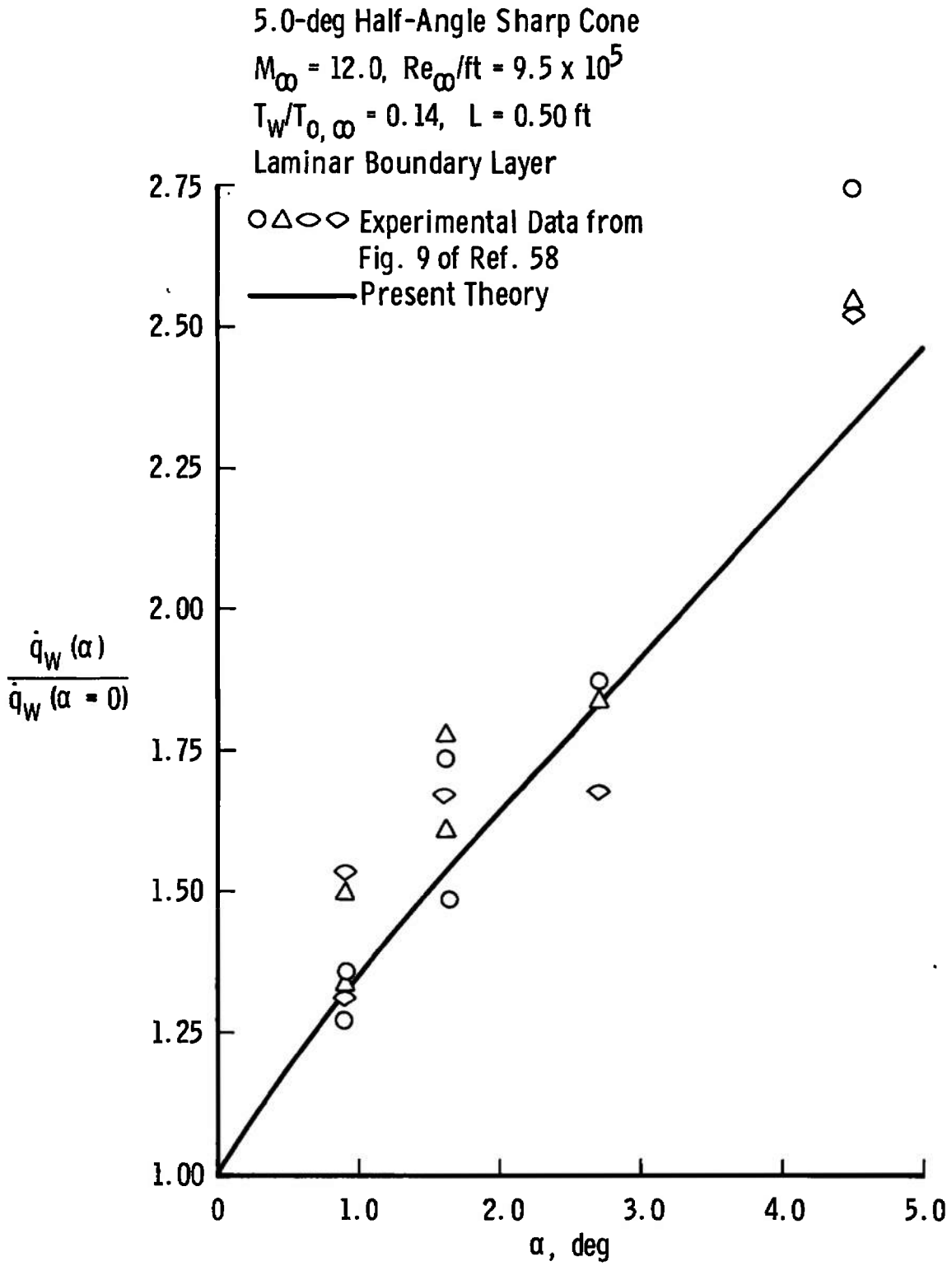

Fig. 2 Comparison of Present Results with Experimental Data from Wittliff and Wilson (Ref. 58)

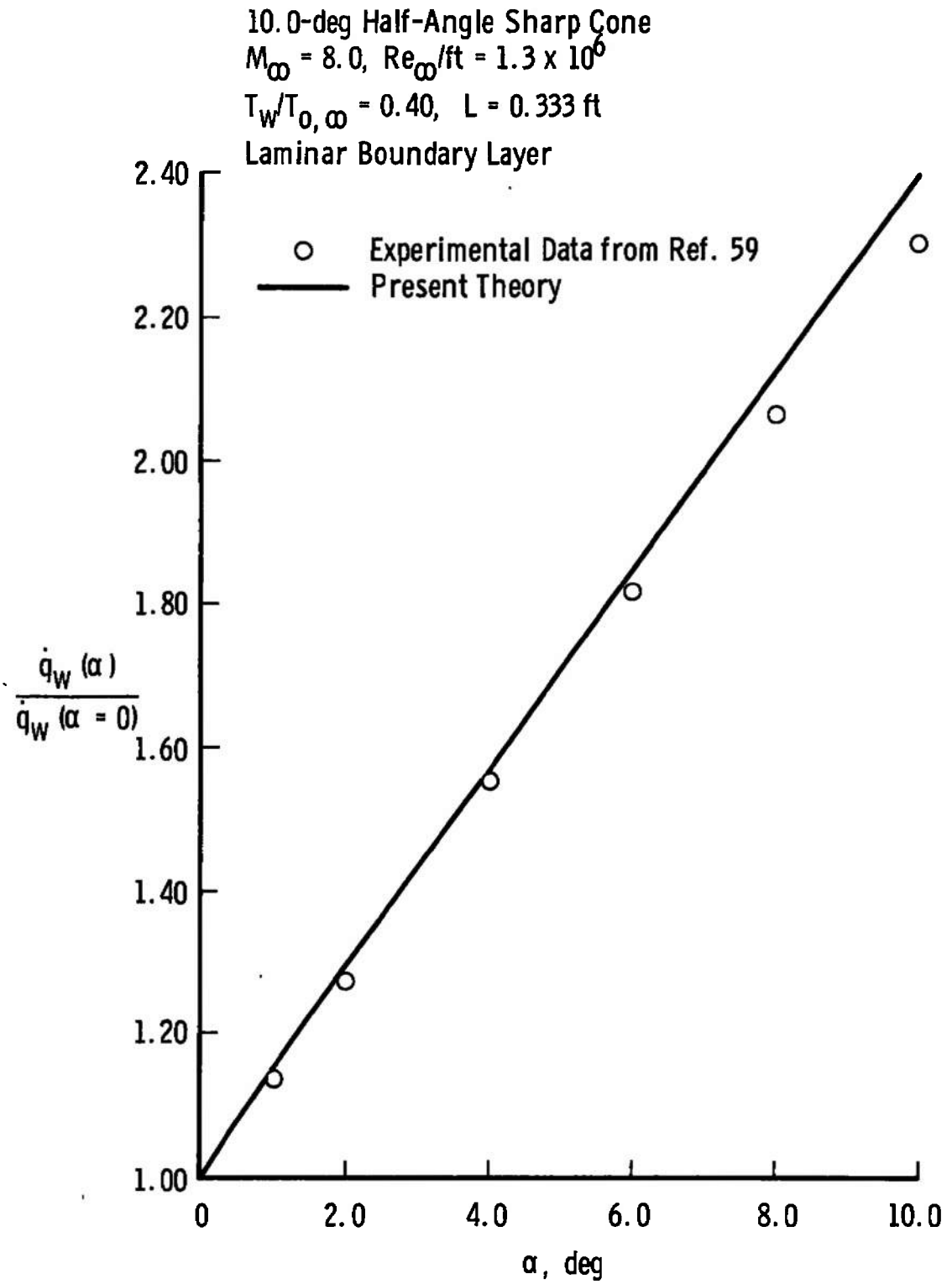

Fig. 3 Comparison of Present Results with Experimental Data from Tracy (Ref. 59)

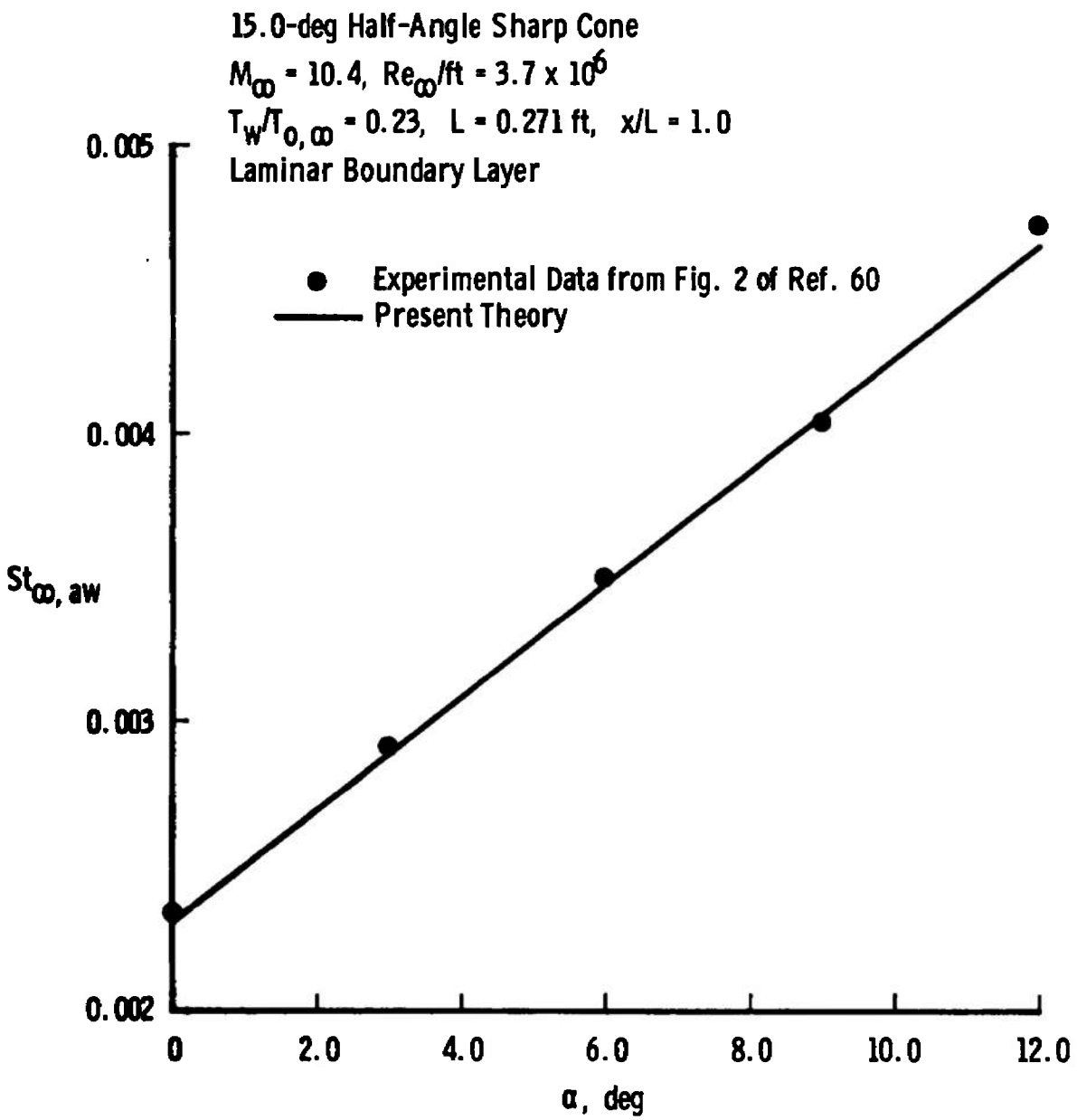

Fig. 4 Comparison of Present Results with Experimental Data from Chan (Ref. 60)

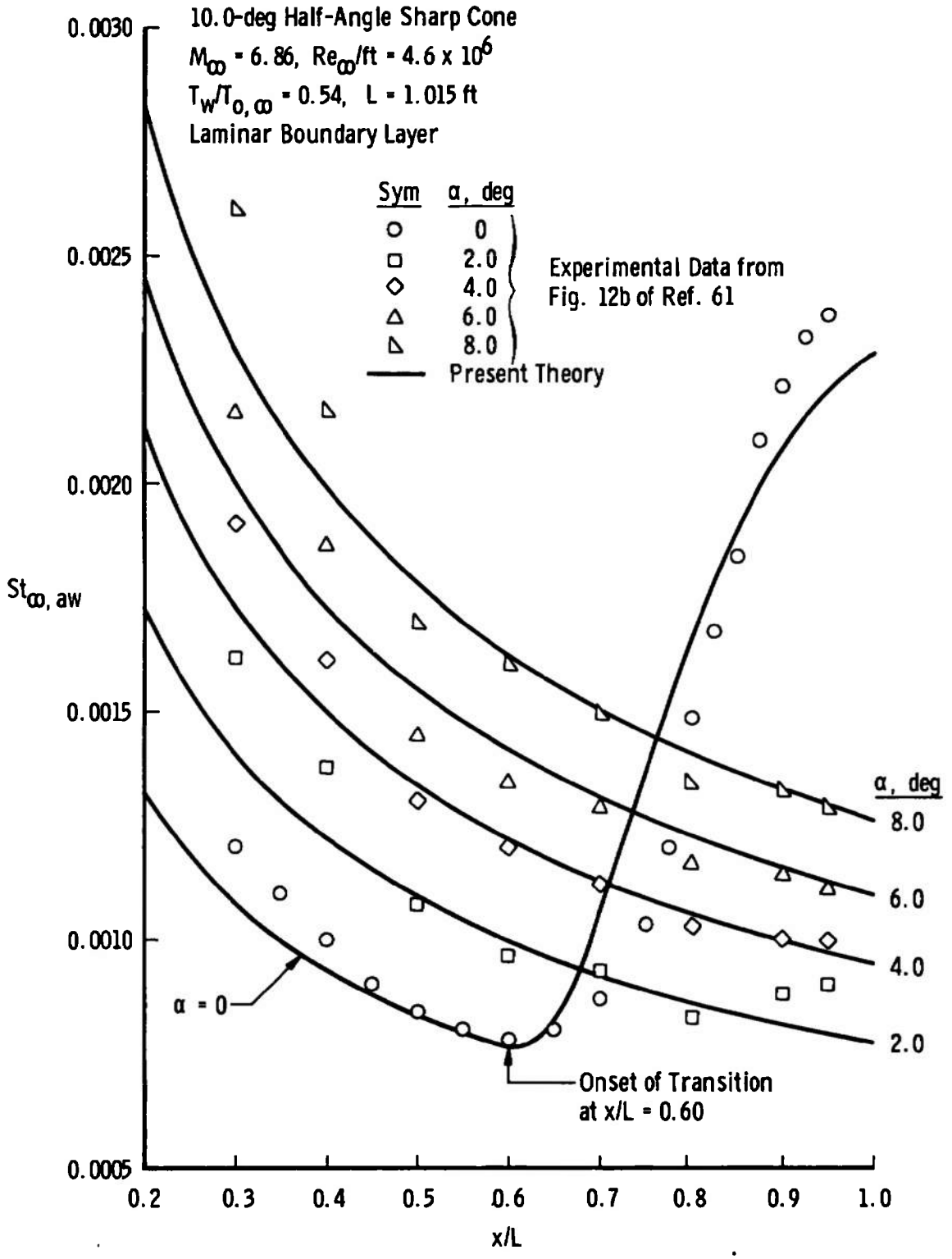

Fig. 5 Comparison of Present Results with Experimental Data from Fischer (Ref. 61)

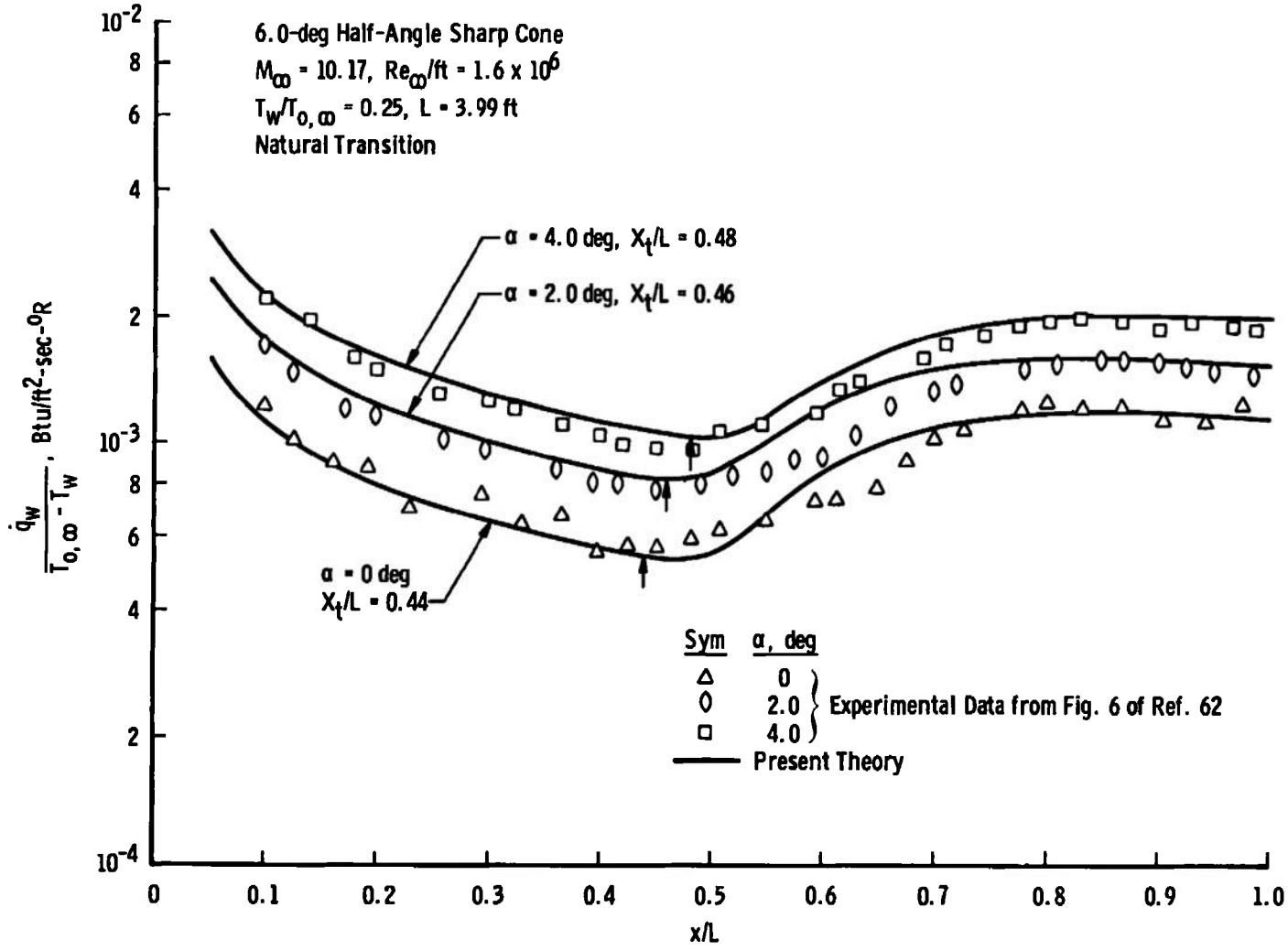

Fig. 6 Comparison of Present Results for Natural Transition with Experimental Data from McCauley, Saydah, and Bueche (Ref. 62)

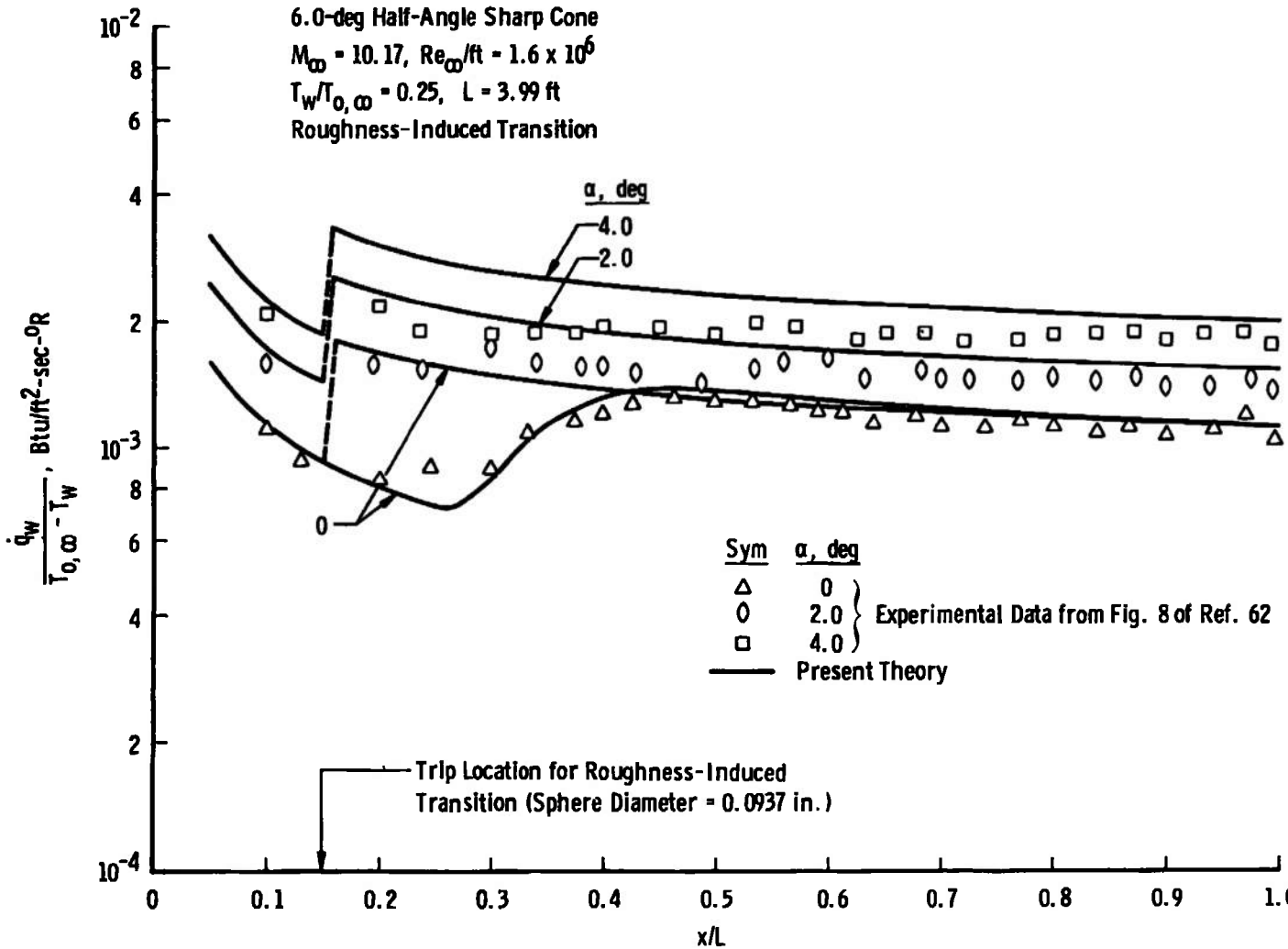

Fig. 7 Comparison of Present Results for Roughness-Induced Transition with Experimental Data from McCauley, Saydah, and Bueche (Ref. 62)

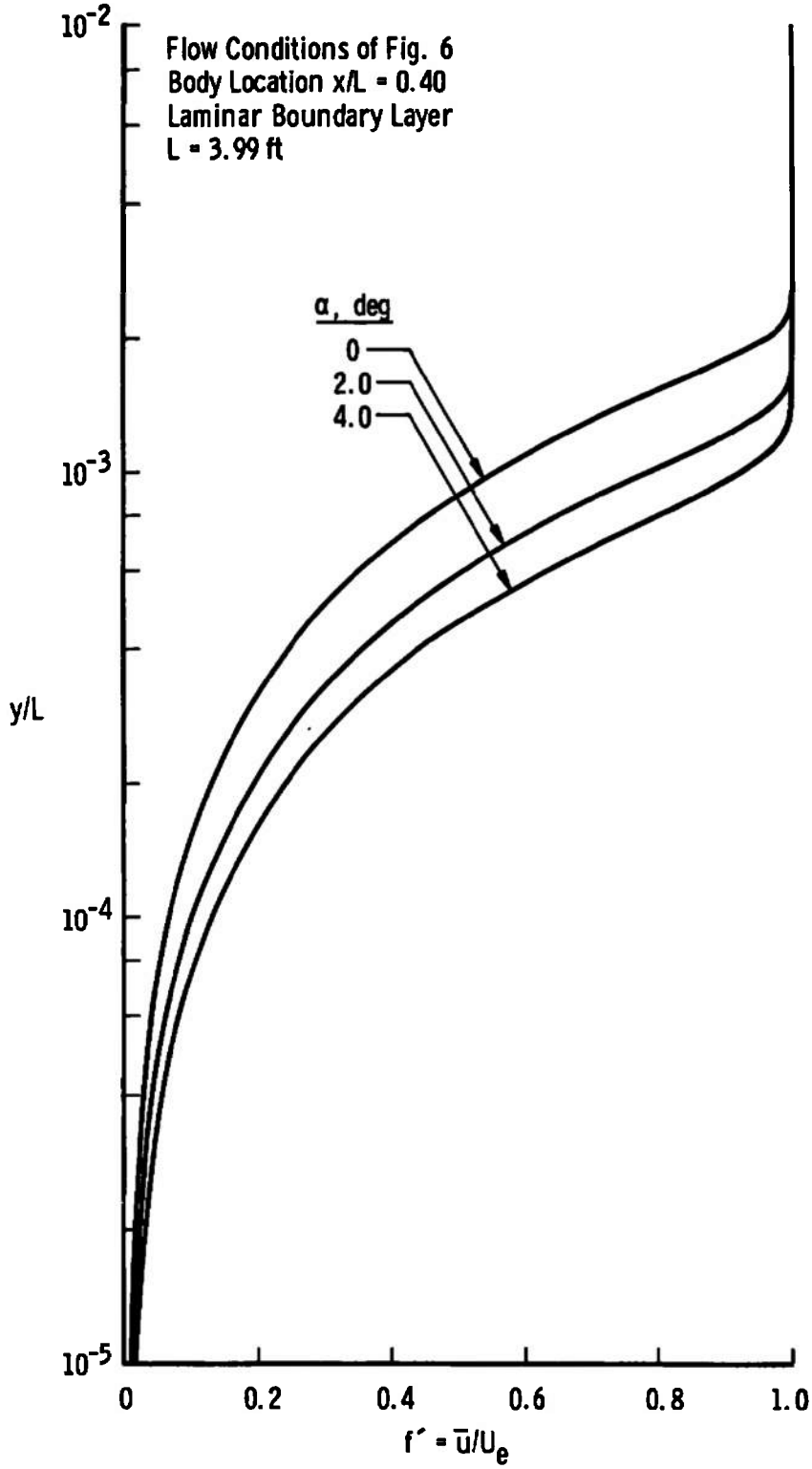

a. Streamwise Velocity Ratio

Fig. 8 Calculated Laminar Boundary-Layer Profiles

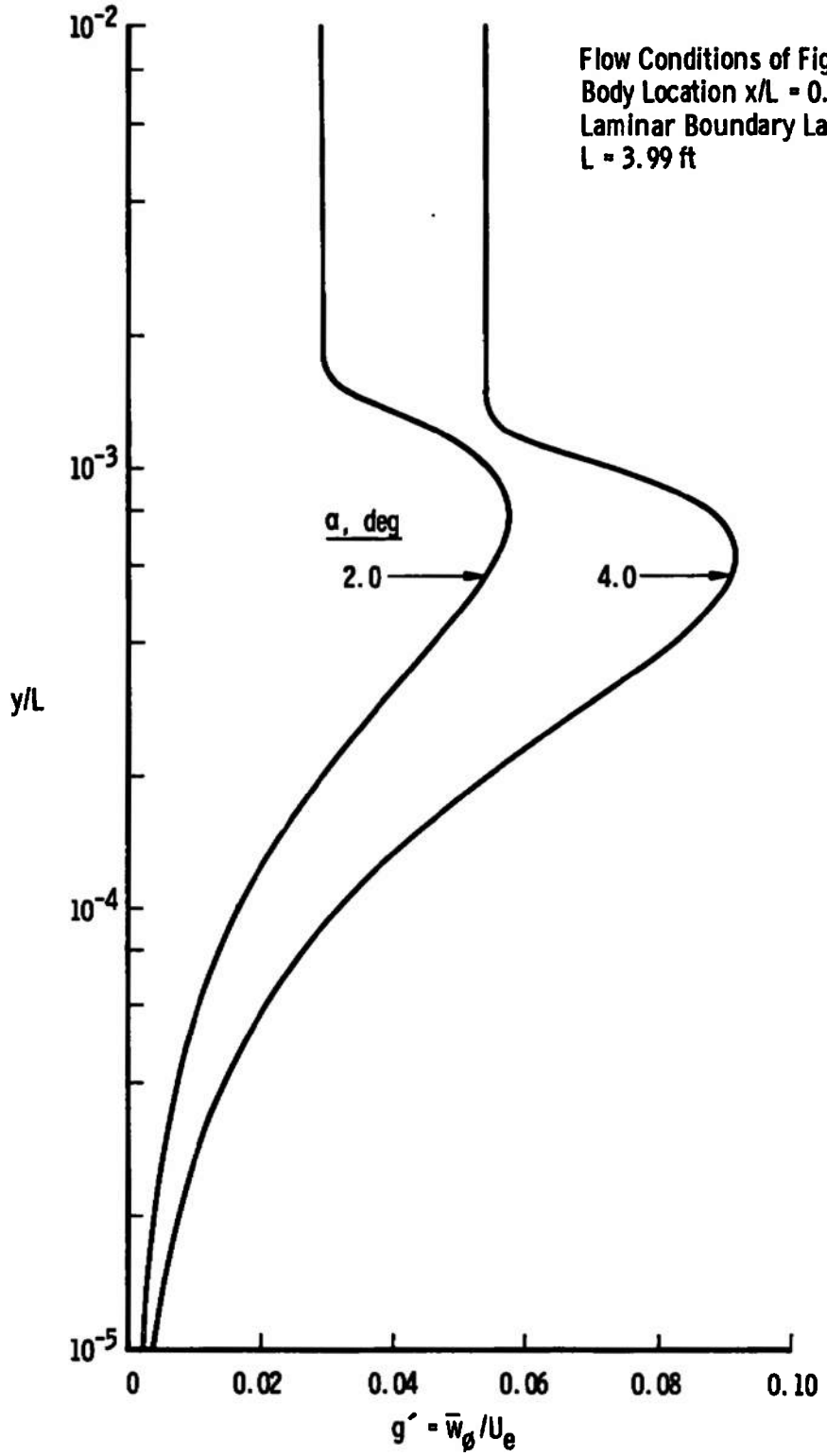

b. Crossflow Velocity Ratio
Fig. 8 Continued

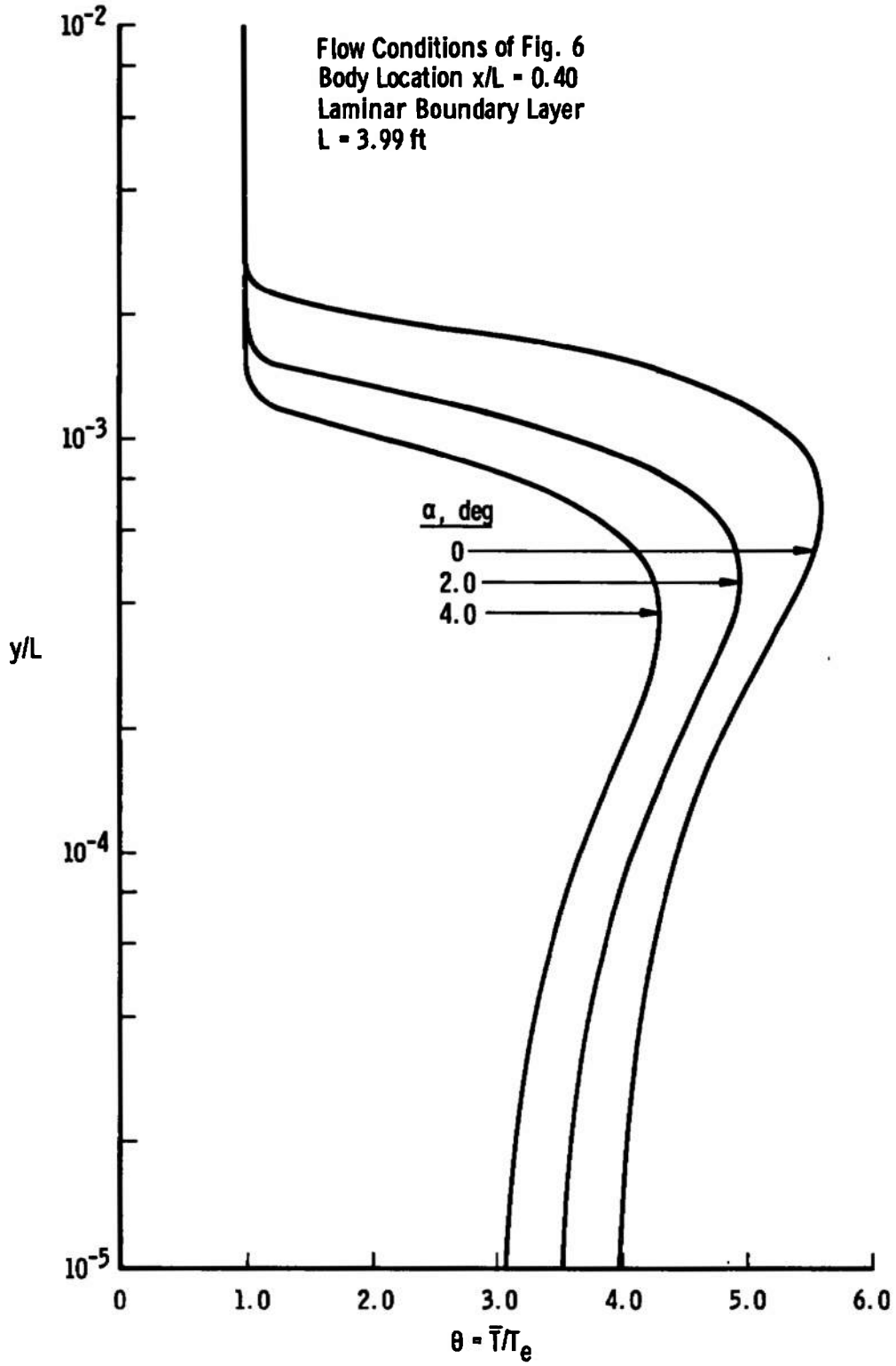

c. Static Temperature Ratio
Fig. 8 Continued

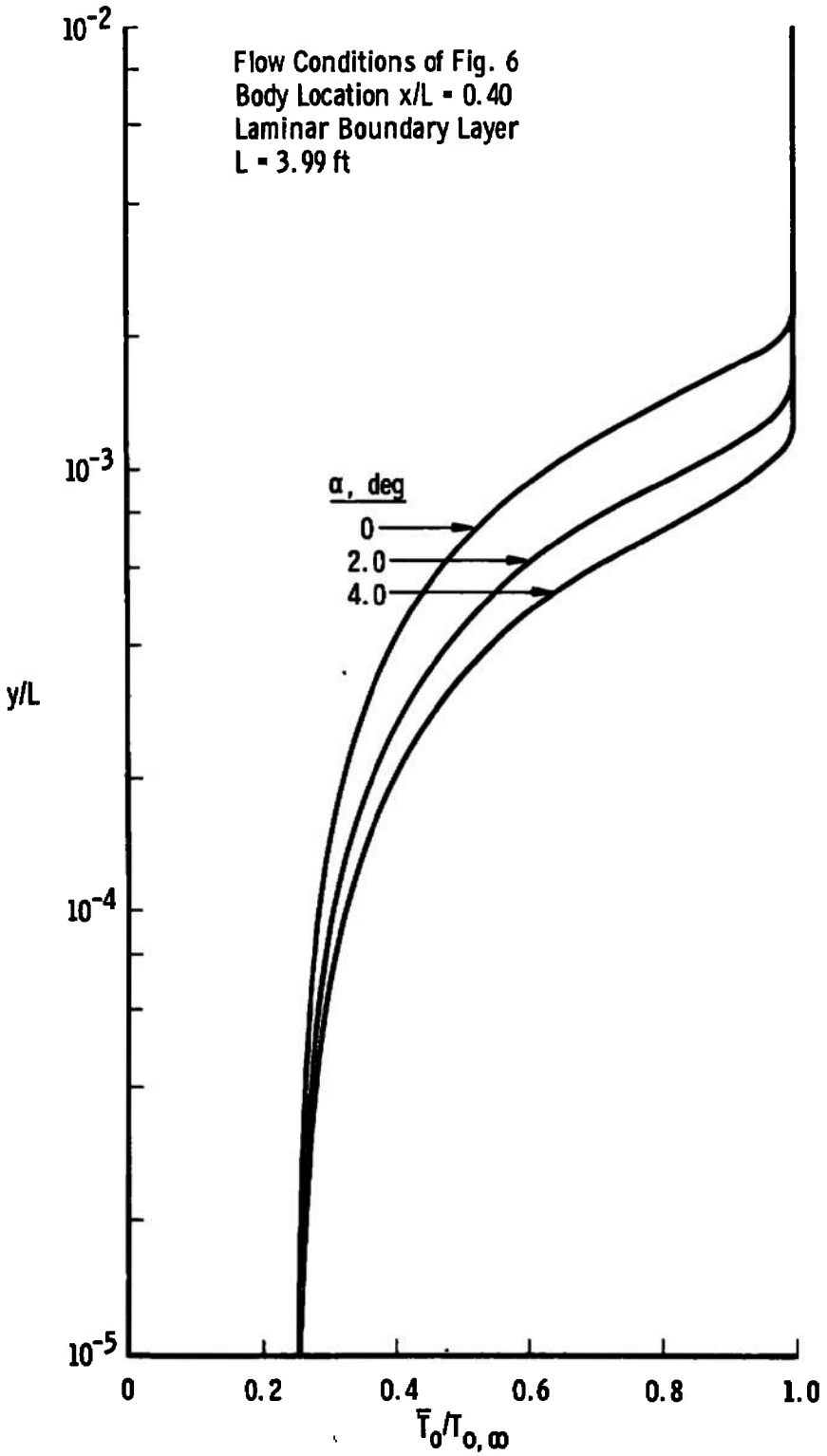

d. Total Temperature Ratio

Fig. 8 Continued

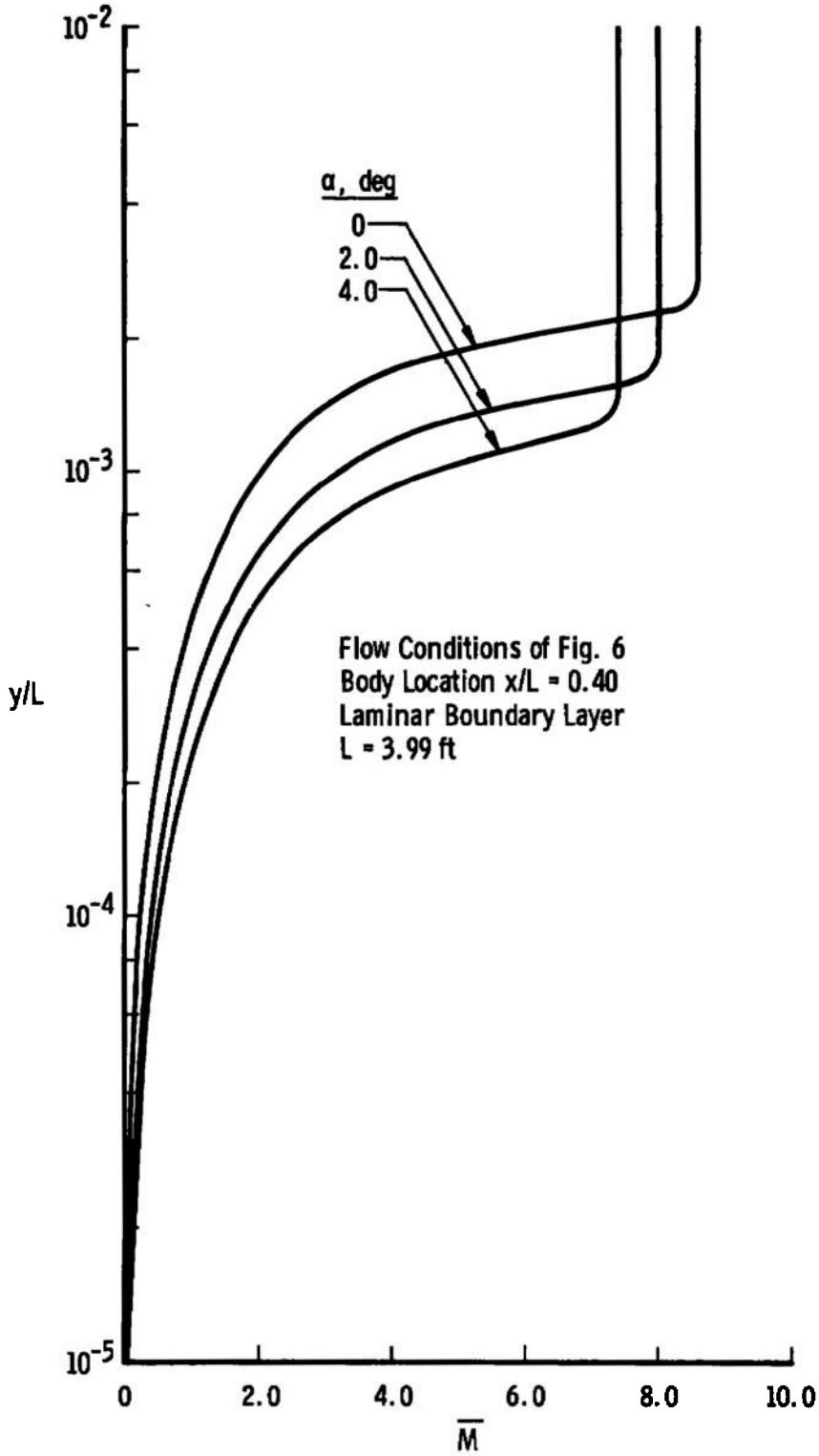

e. Local Mach Number
Fig. 8 Continued

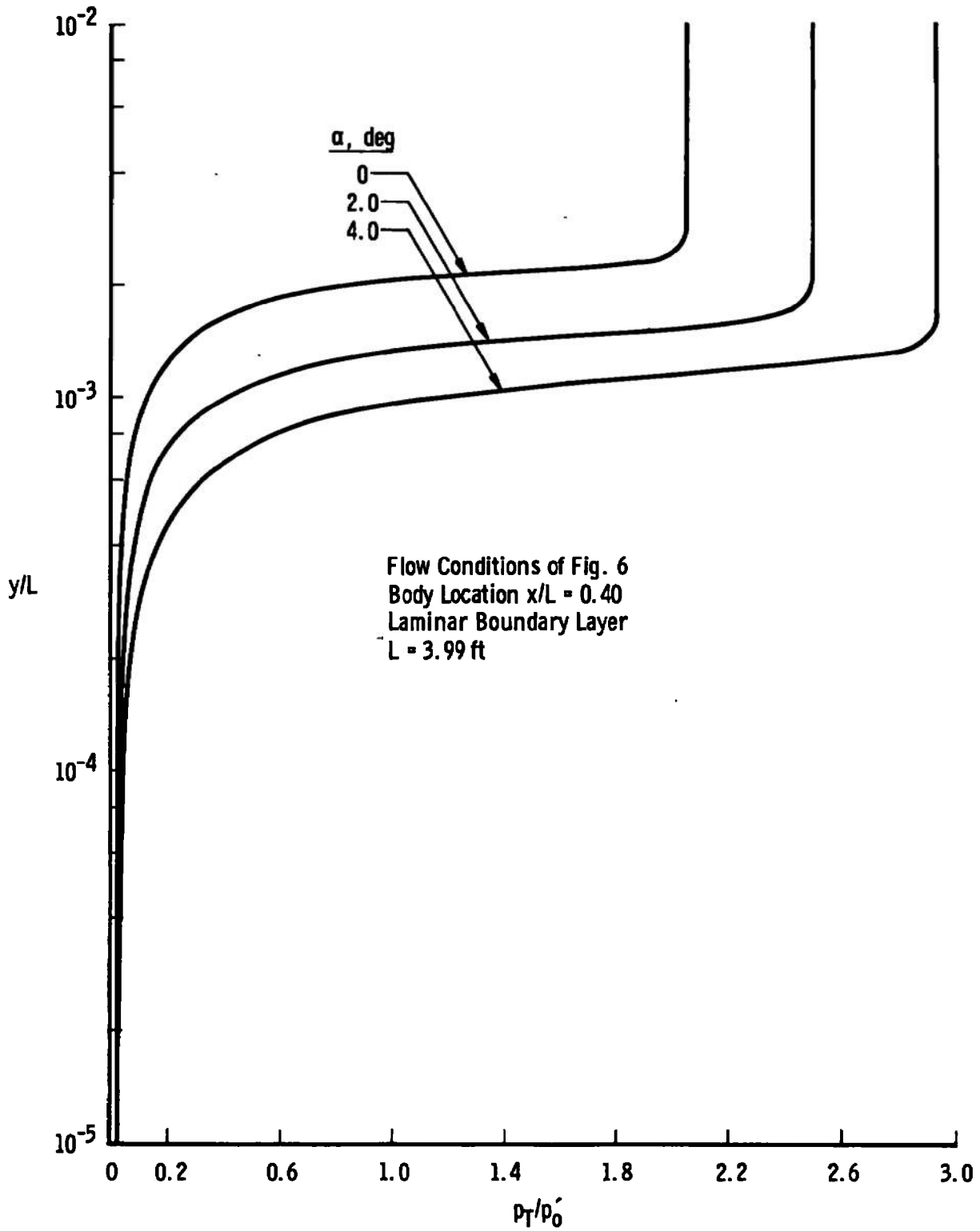

f. Pitot Pressure Ratio
Fig. 8 Concluded

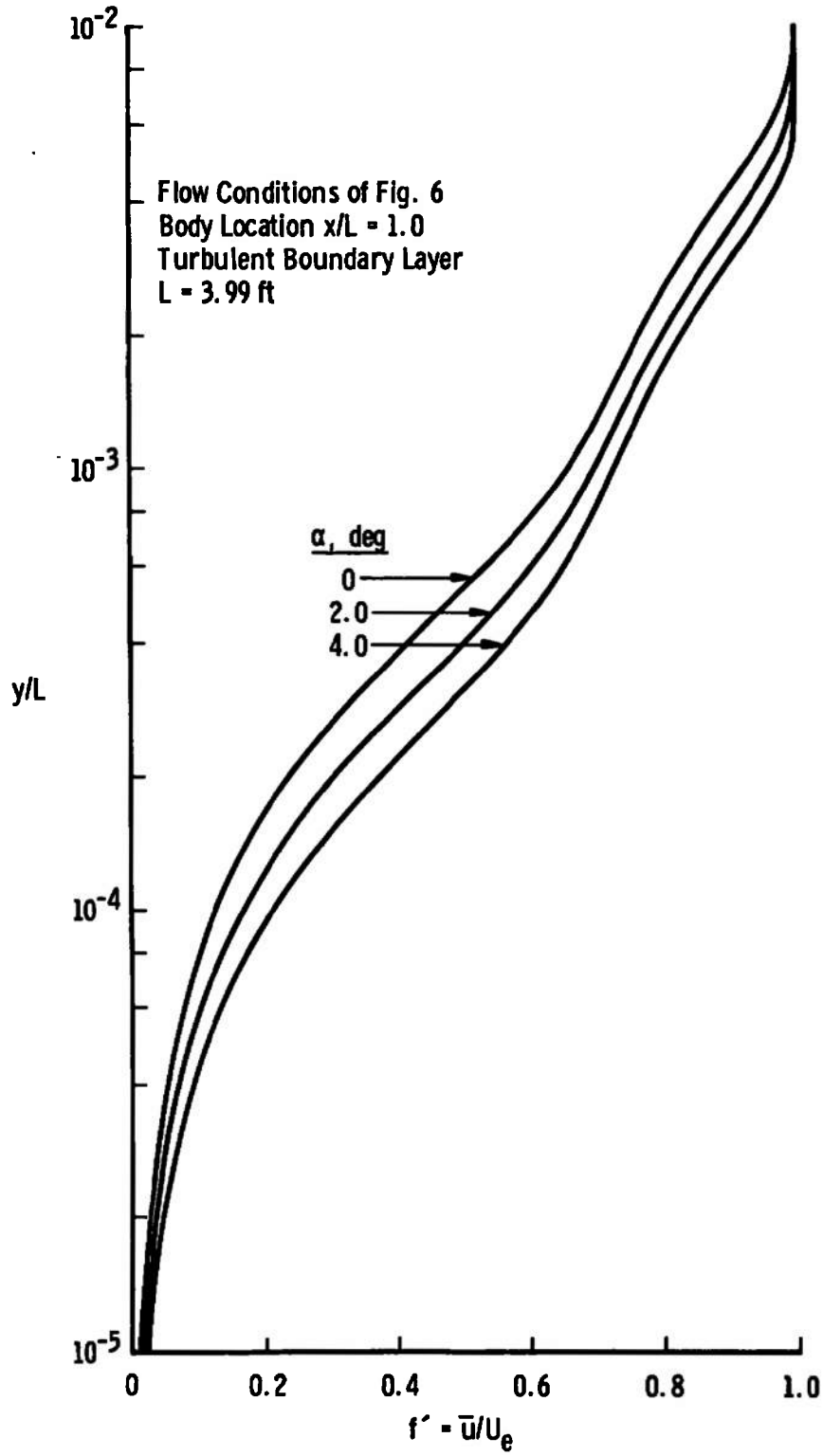

a. Streamwise Velocity Ratio

Fig. 9 Calculated Turbulent Boundary-Layer Profiles

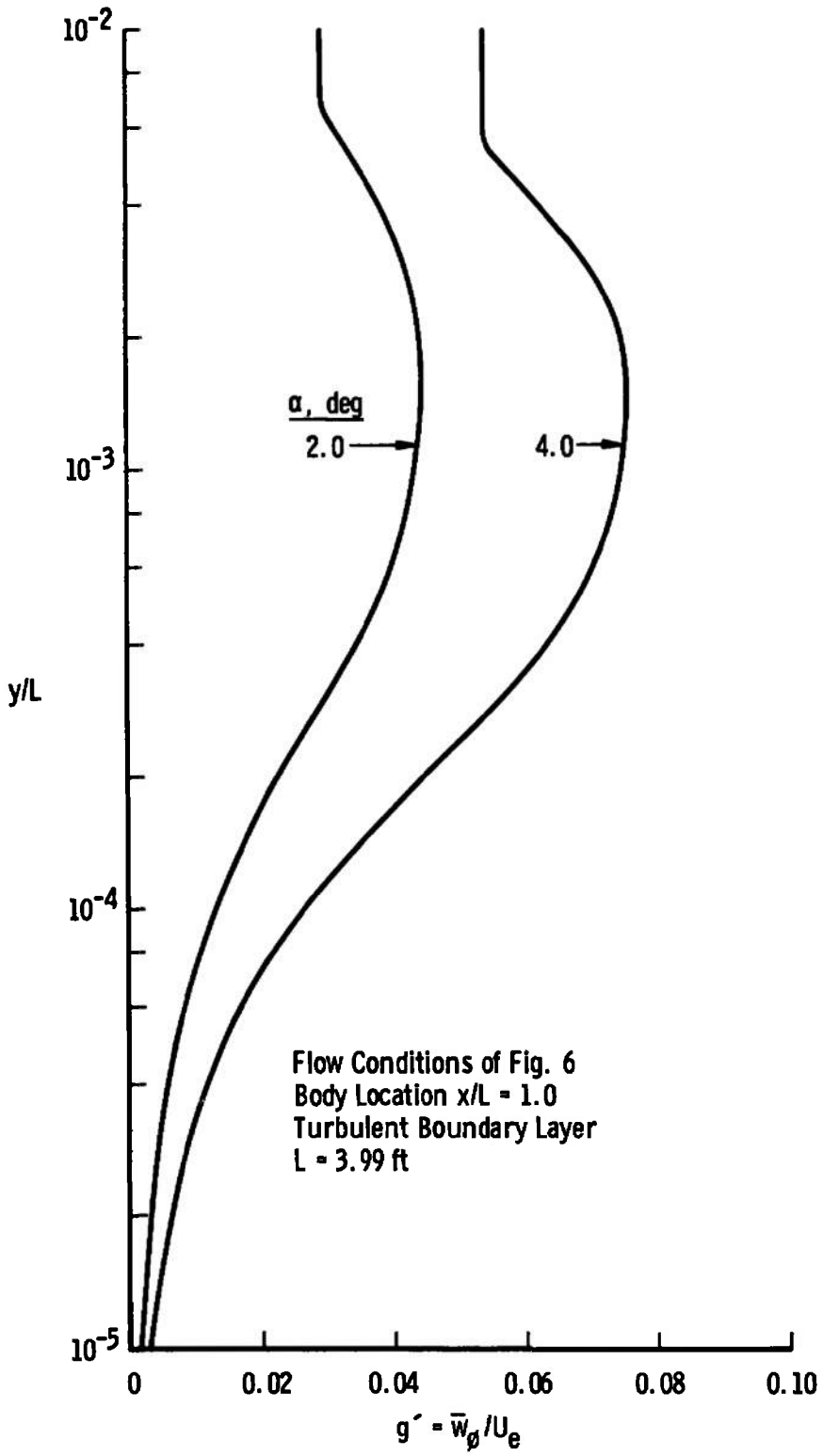

b. Crossflow Velocity Ratio
Fig. 9 Continued

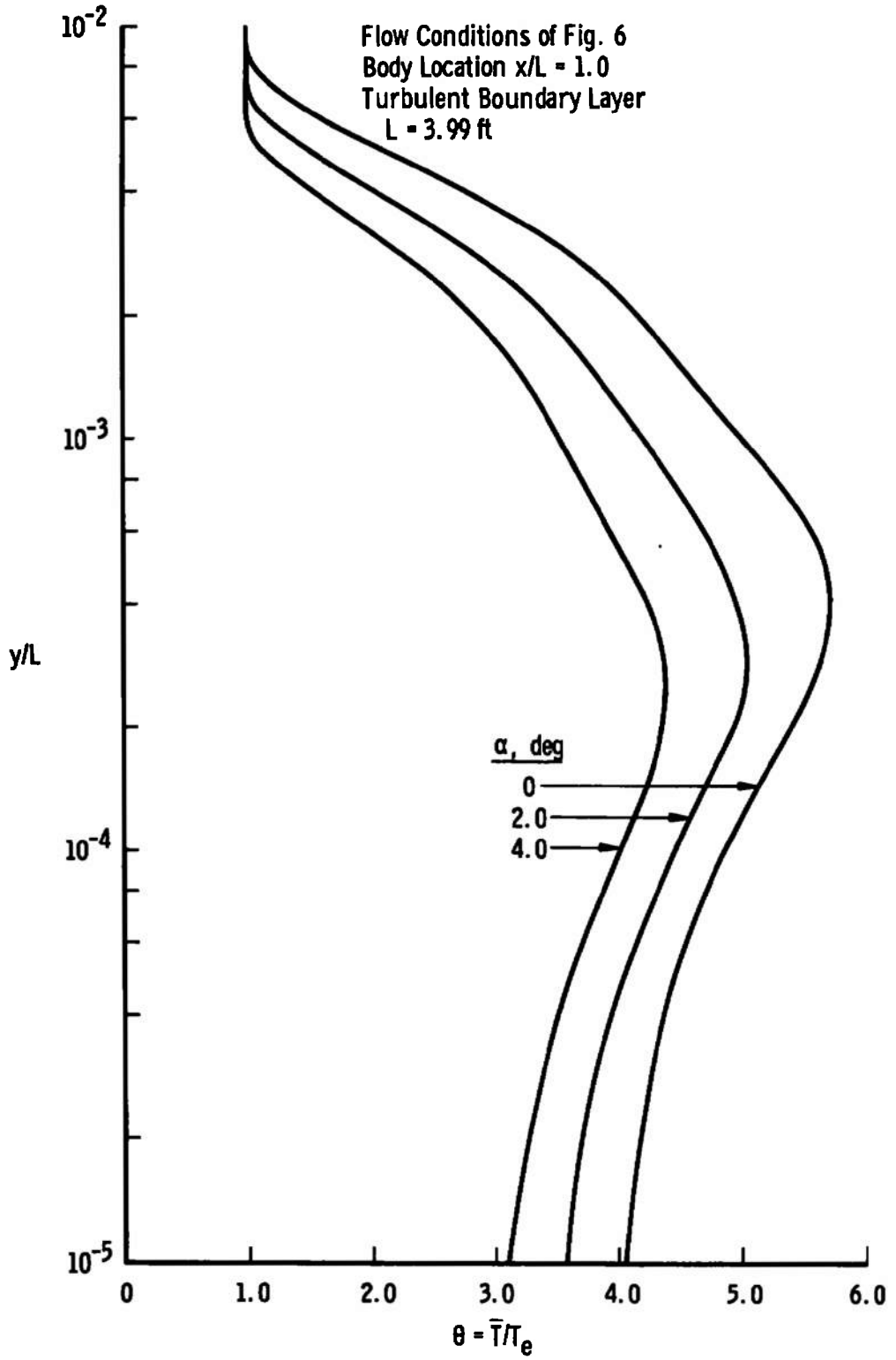

c. Static Temperature Ratio
Fig. 9 Continued

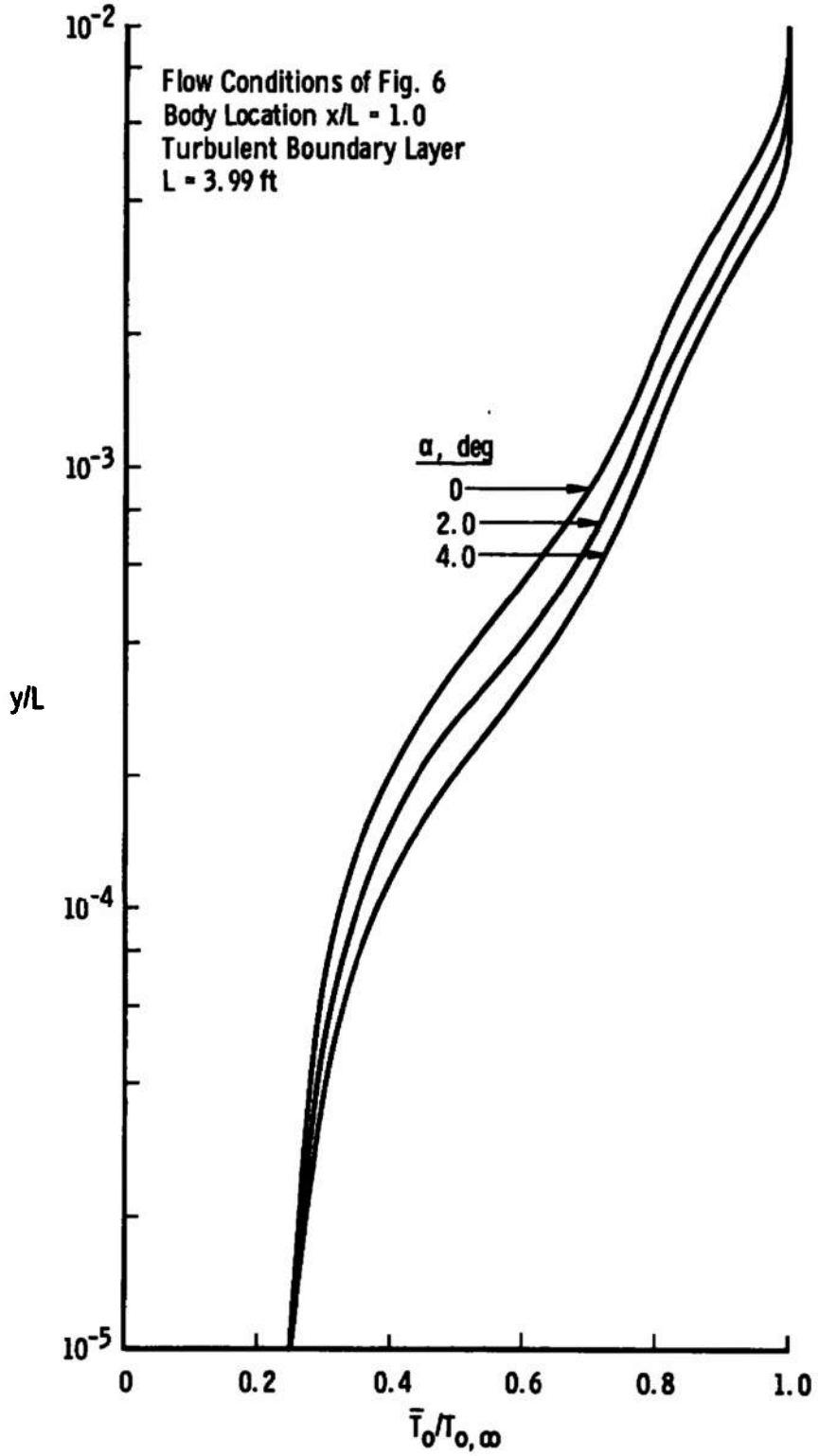

d. Total Temperature Ratio
Fig. 9 Continued

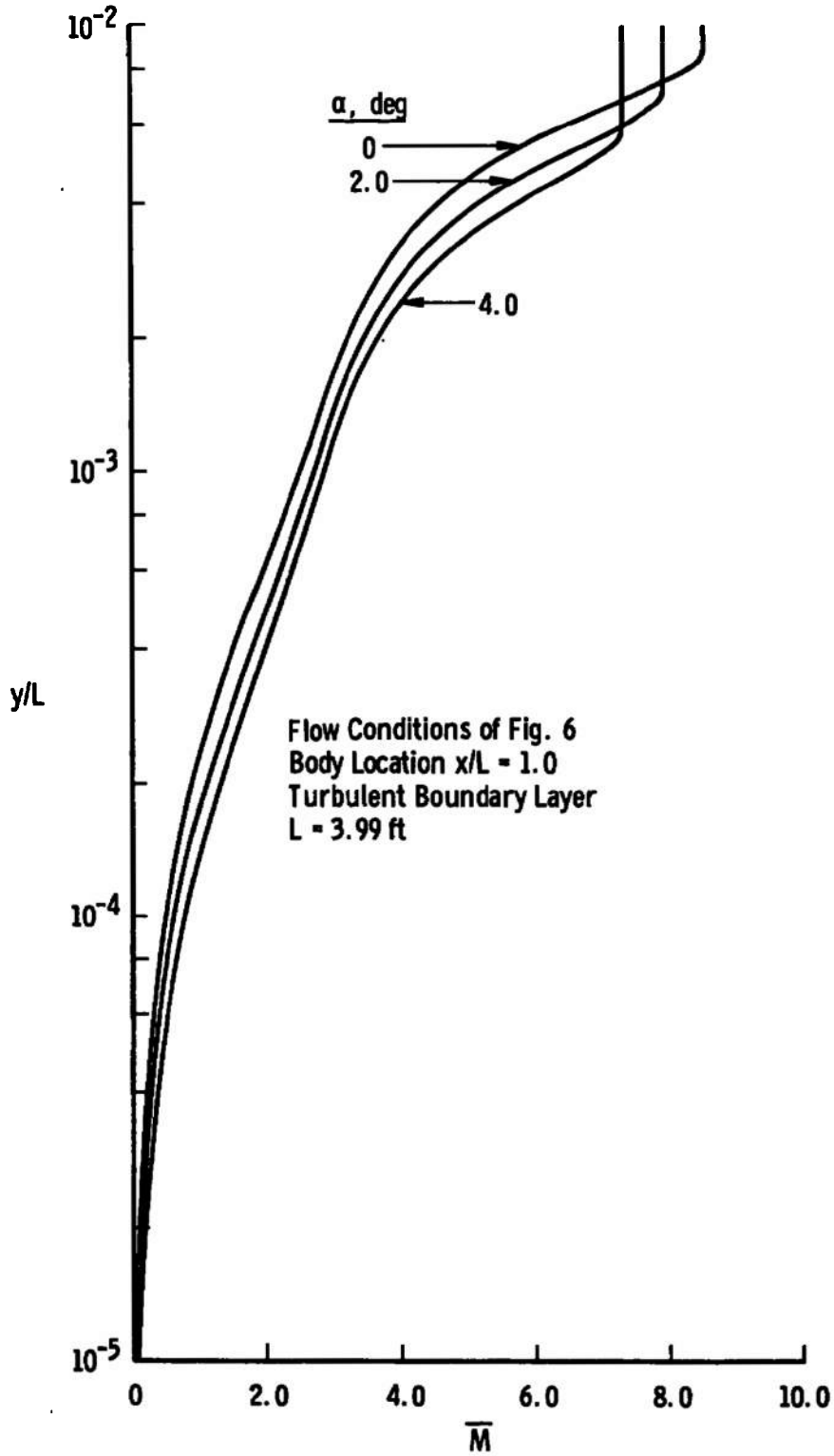

e. Local Mach Number
Fig. 9 Continued

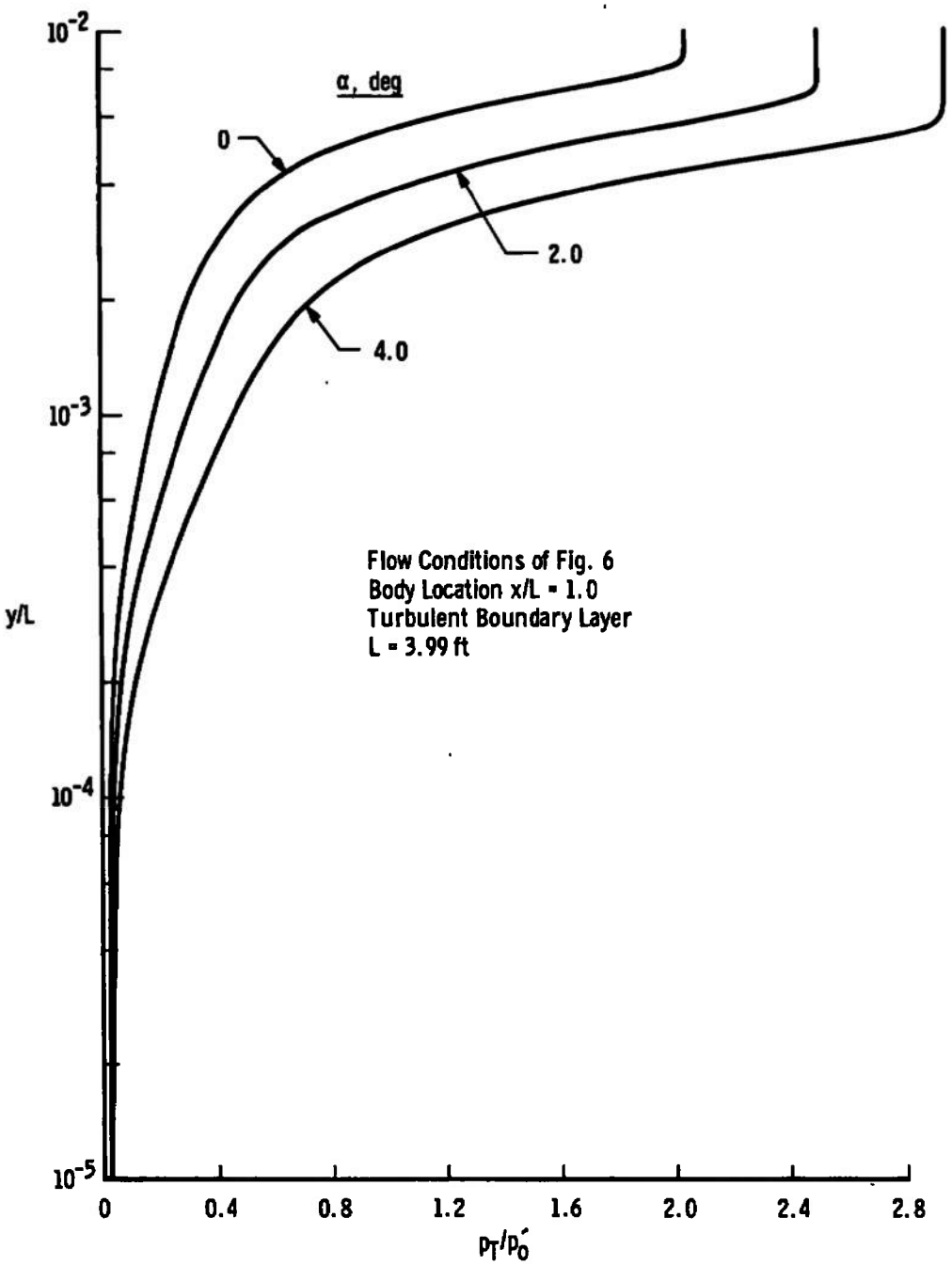

f. Pitot Pressure Ratio
Fig. 9 Concluded

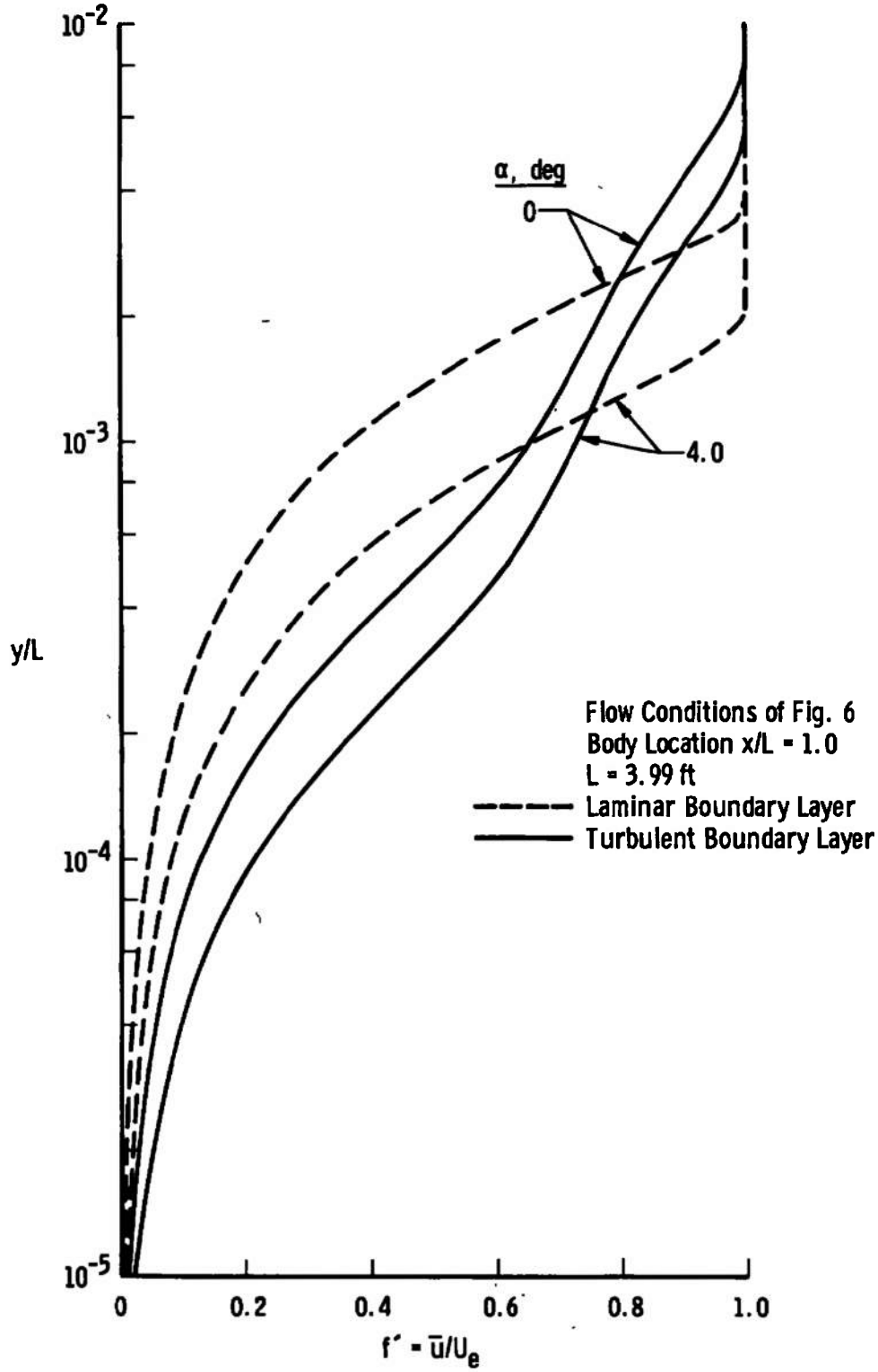

a. Streamwise Velocity Ratio

Fig. 10 Comparison of Laminar and Turbulent Boundary-Layer Profiles

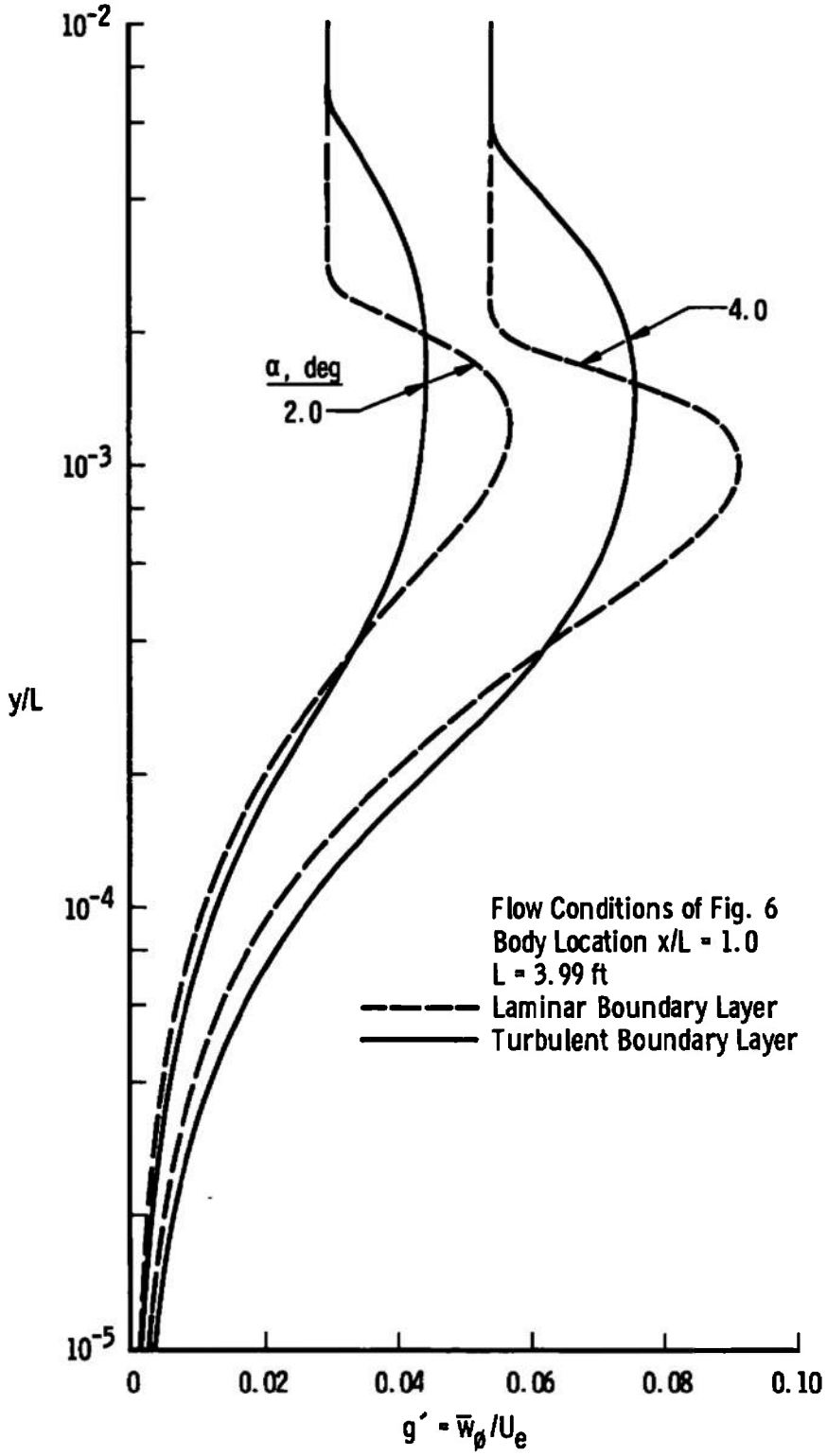

b. Crossflow Velocity Ratio
Fig. 10 Continued

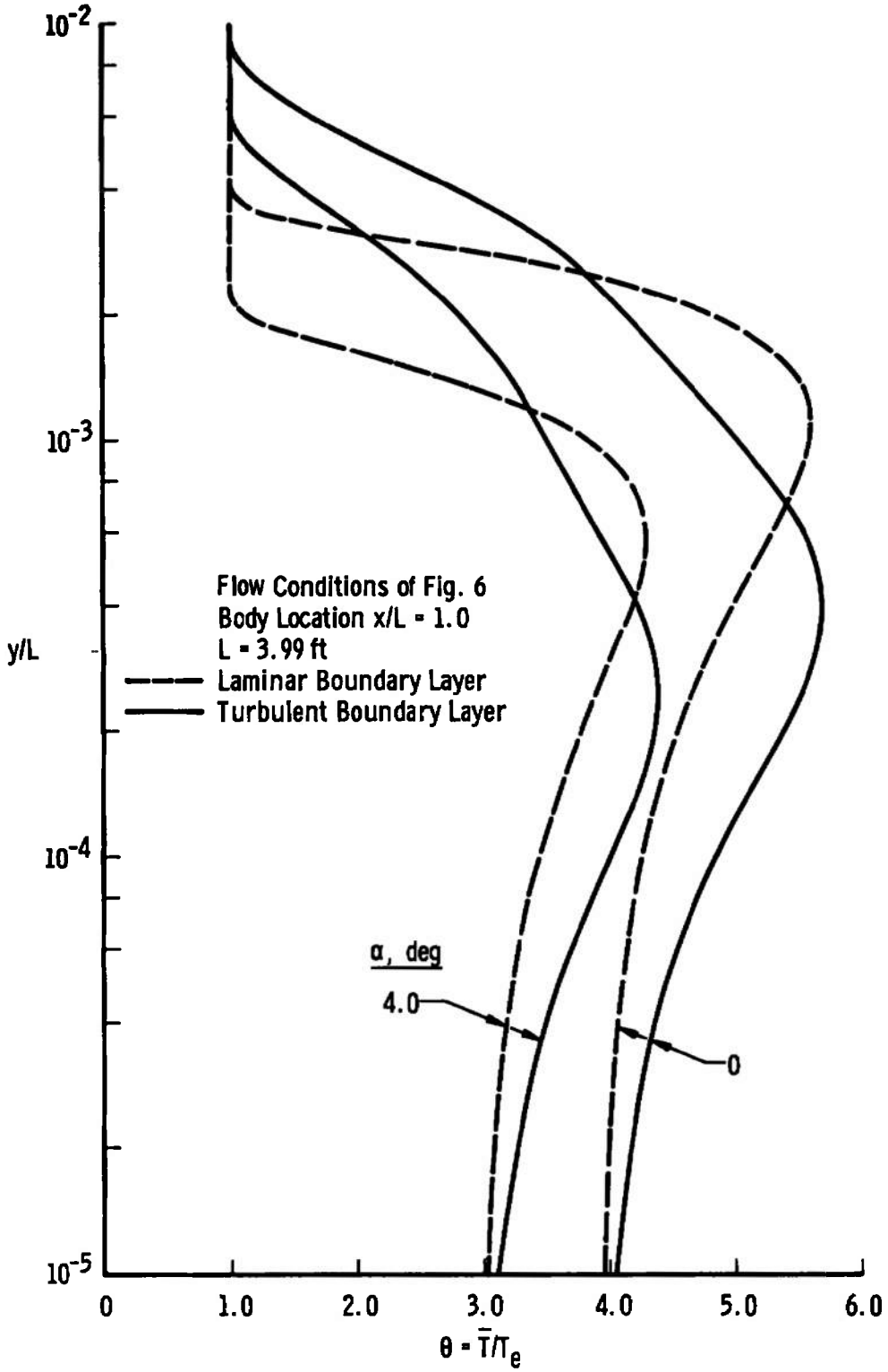

c. Static Temperature Ratio
Fig. 10 Concluded

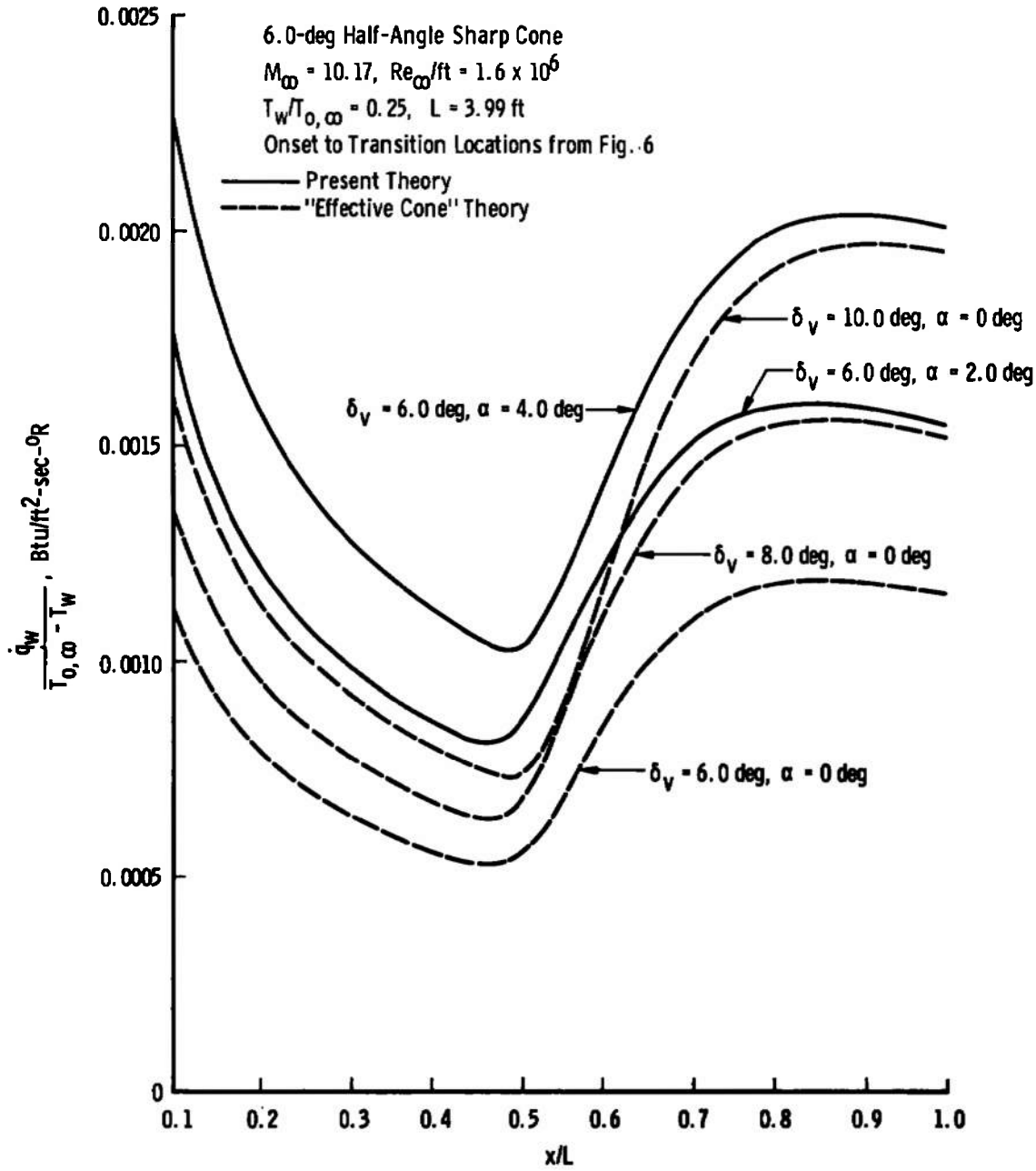

a. Local Heat Transfer

Fig. 11 Comparison of Present Results with "Effective Cone" Calculations

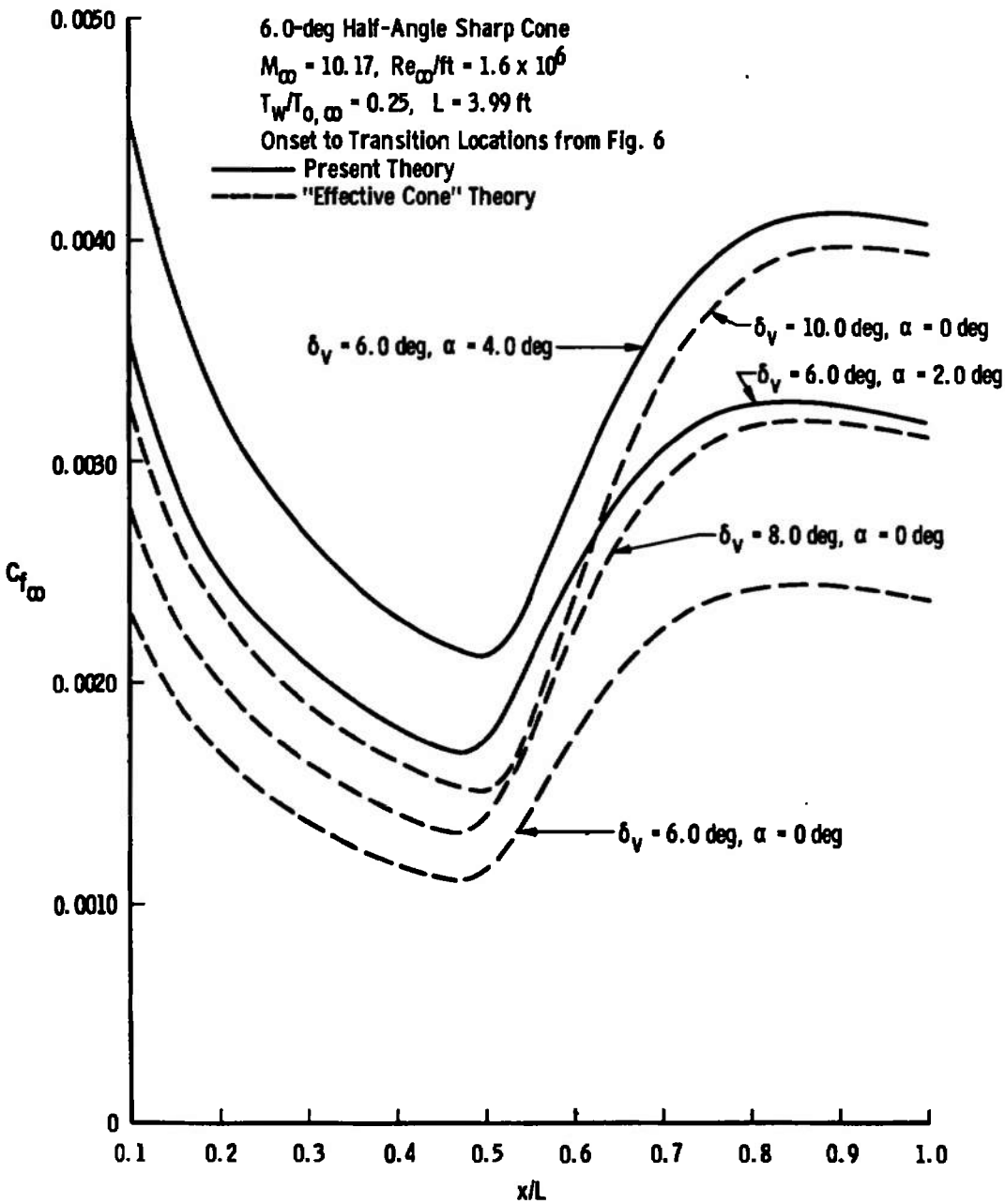

b. Local Skin Friction
Fig. 11 Concluded

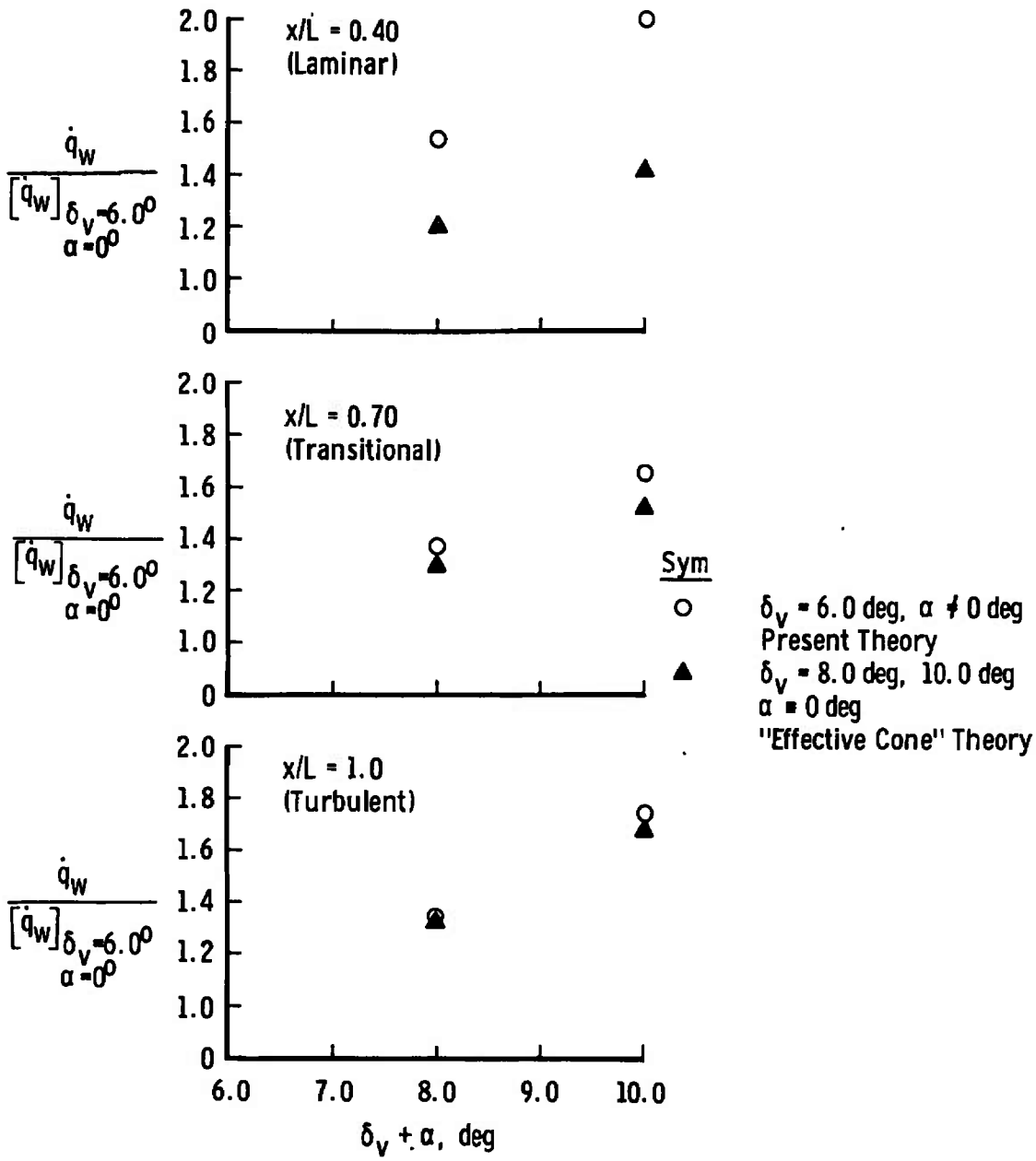

a. Local Heat Transfer

Fig. 12 Summary of "Effective Cone" Results Based on Fig. 11

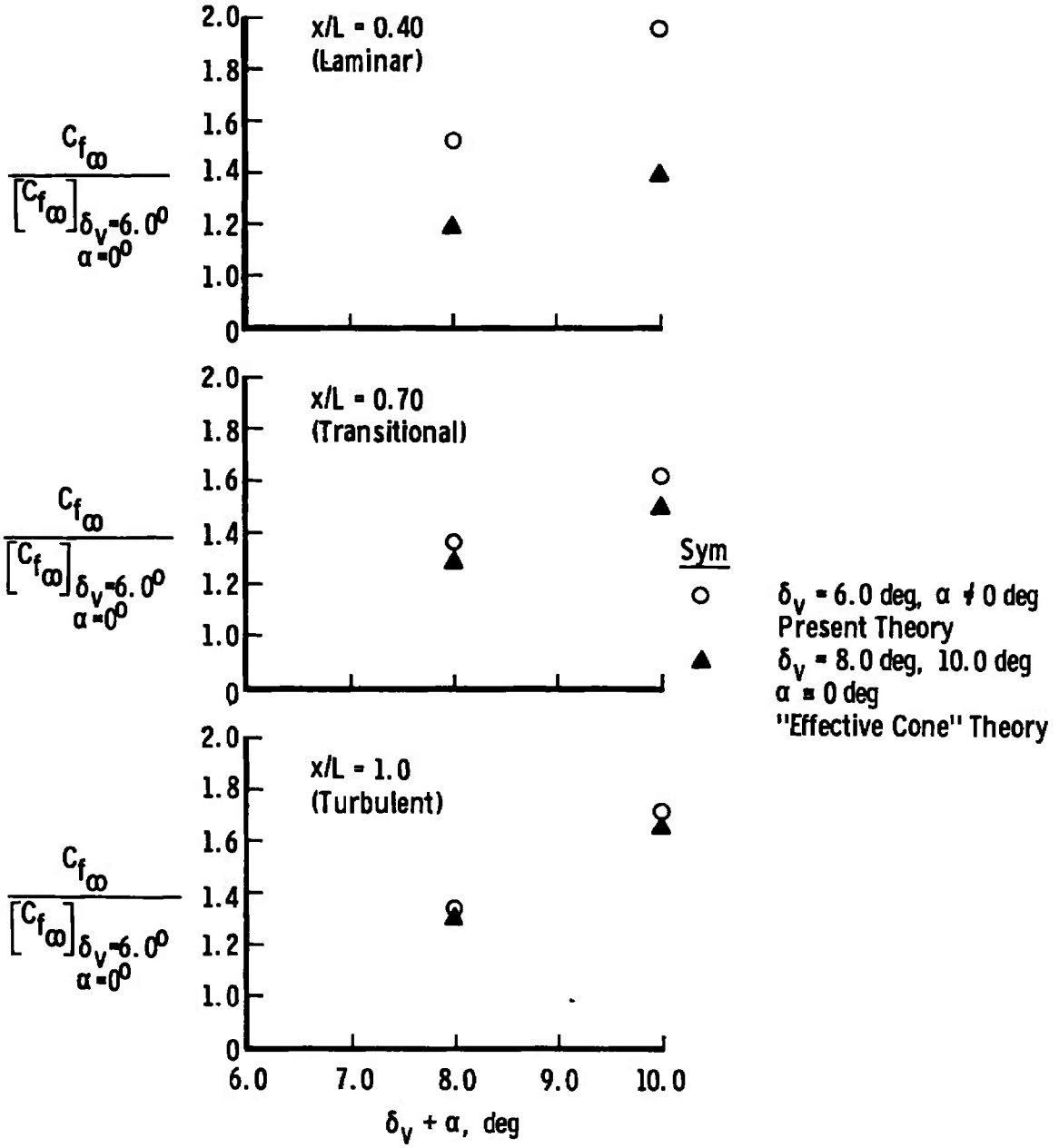

b. Local Skin Friction
Fig. 12 Concluded

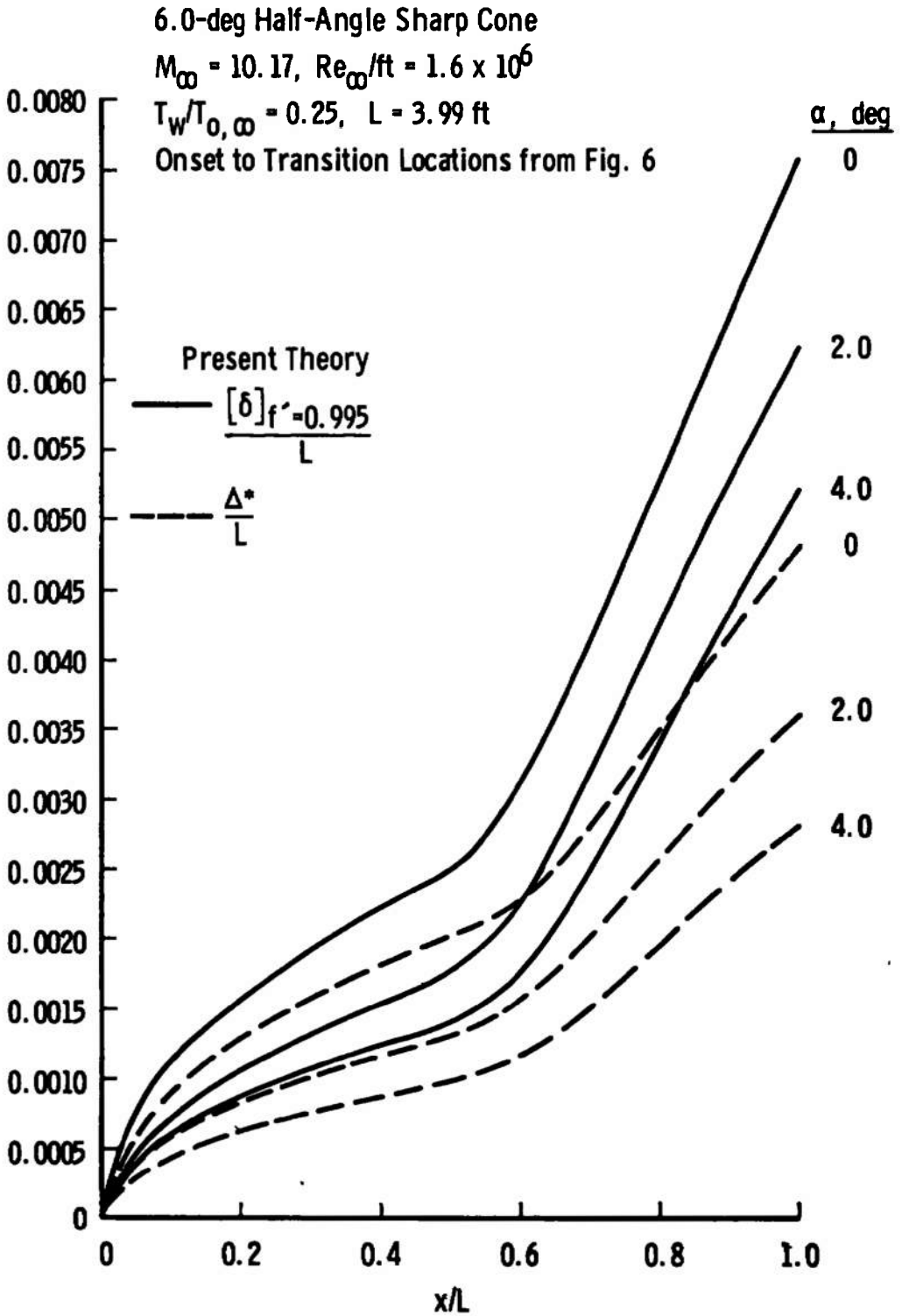

Fig. 13 Calculated Boundary-Layer Thickness and Displacement Thickness Distributions

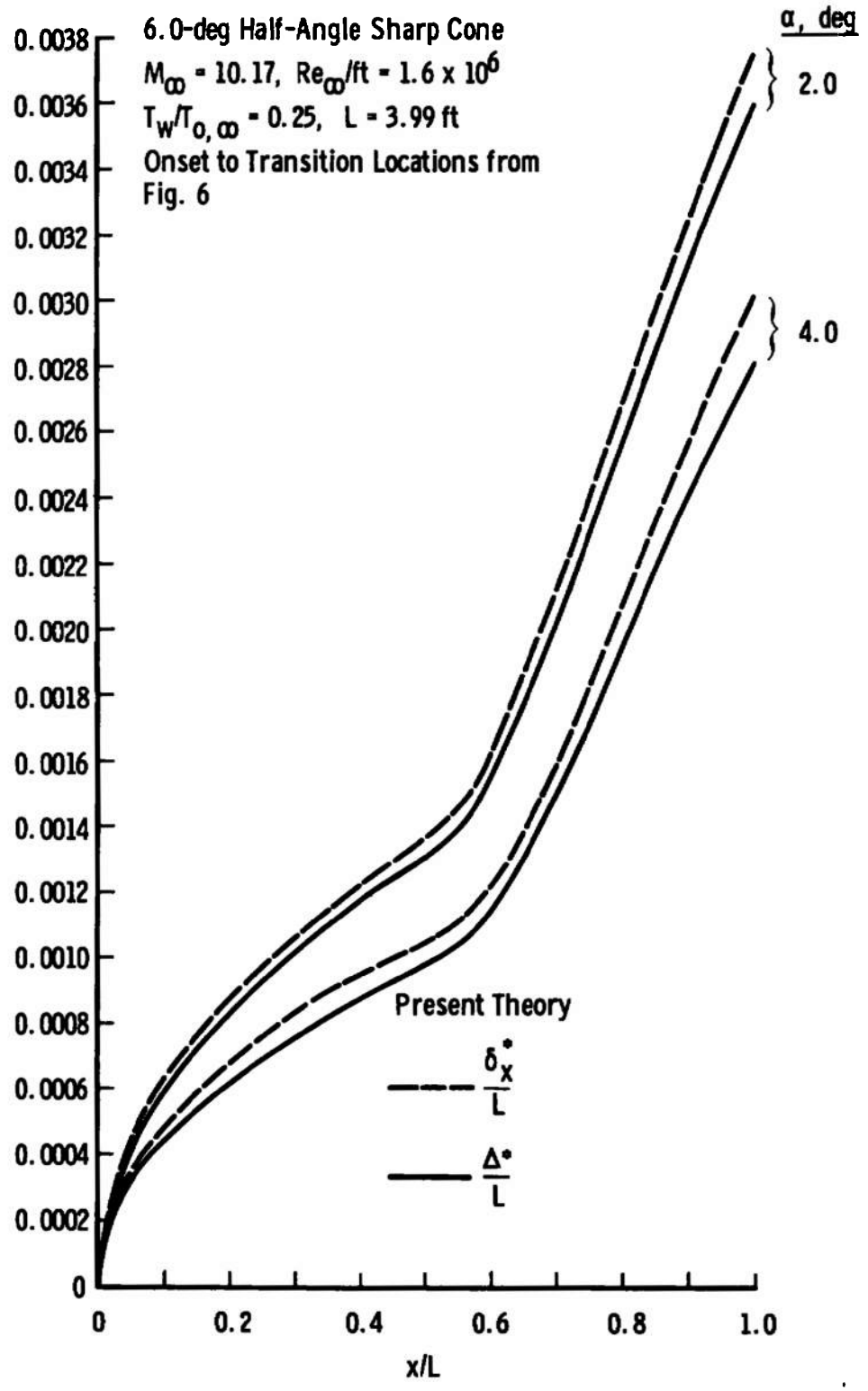

Fig. 14 Comparison of Two- and Three-Dimensional Displacement Thickness Distributions

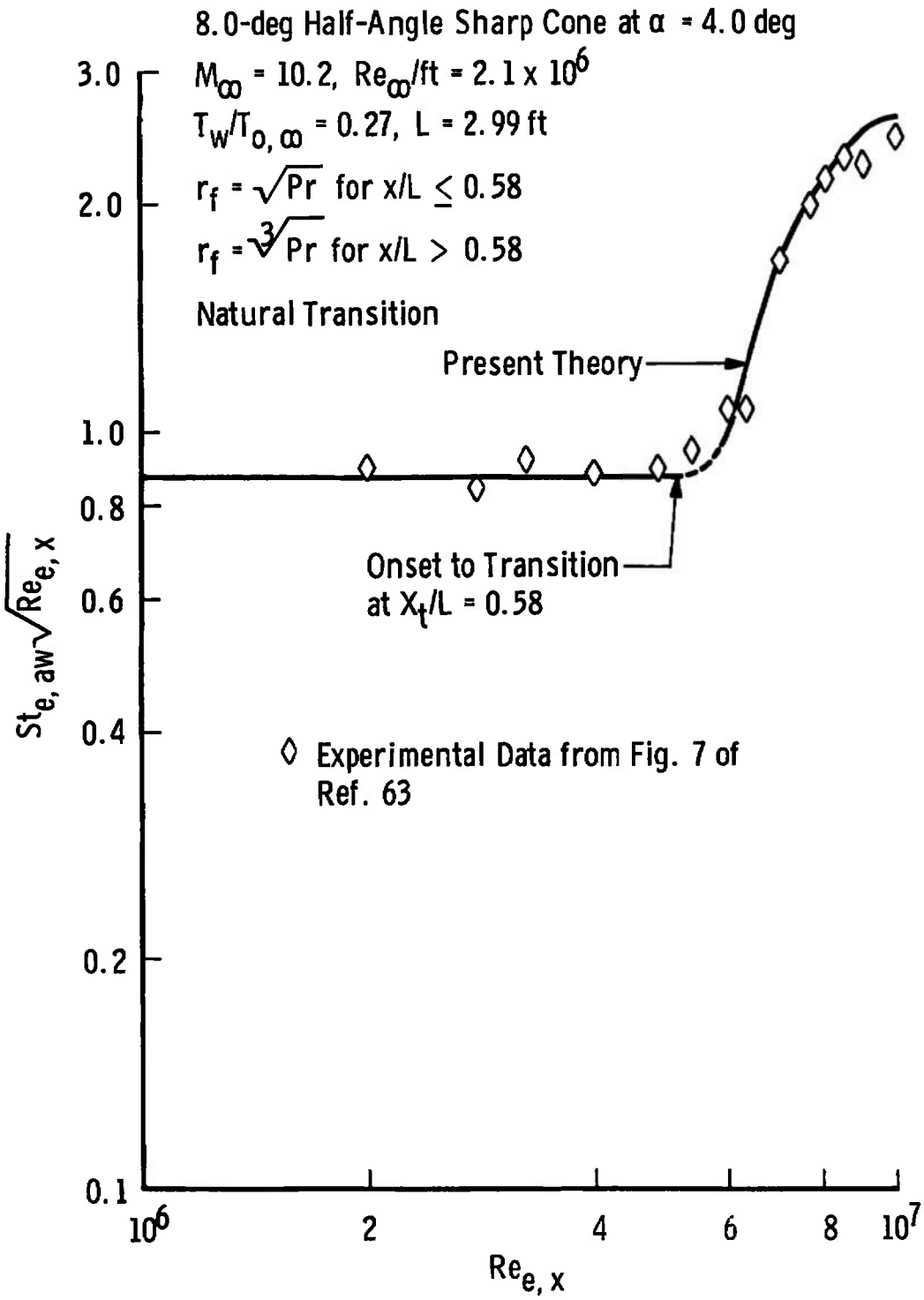

Fig. 15 Comparison of Present Results with Experimental Data from DiCristina (Ref. 63)

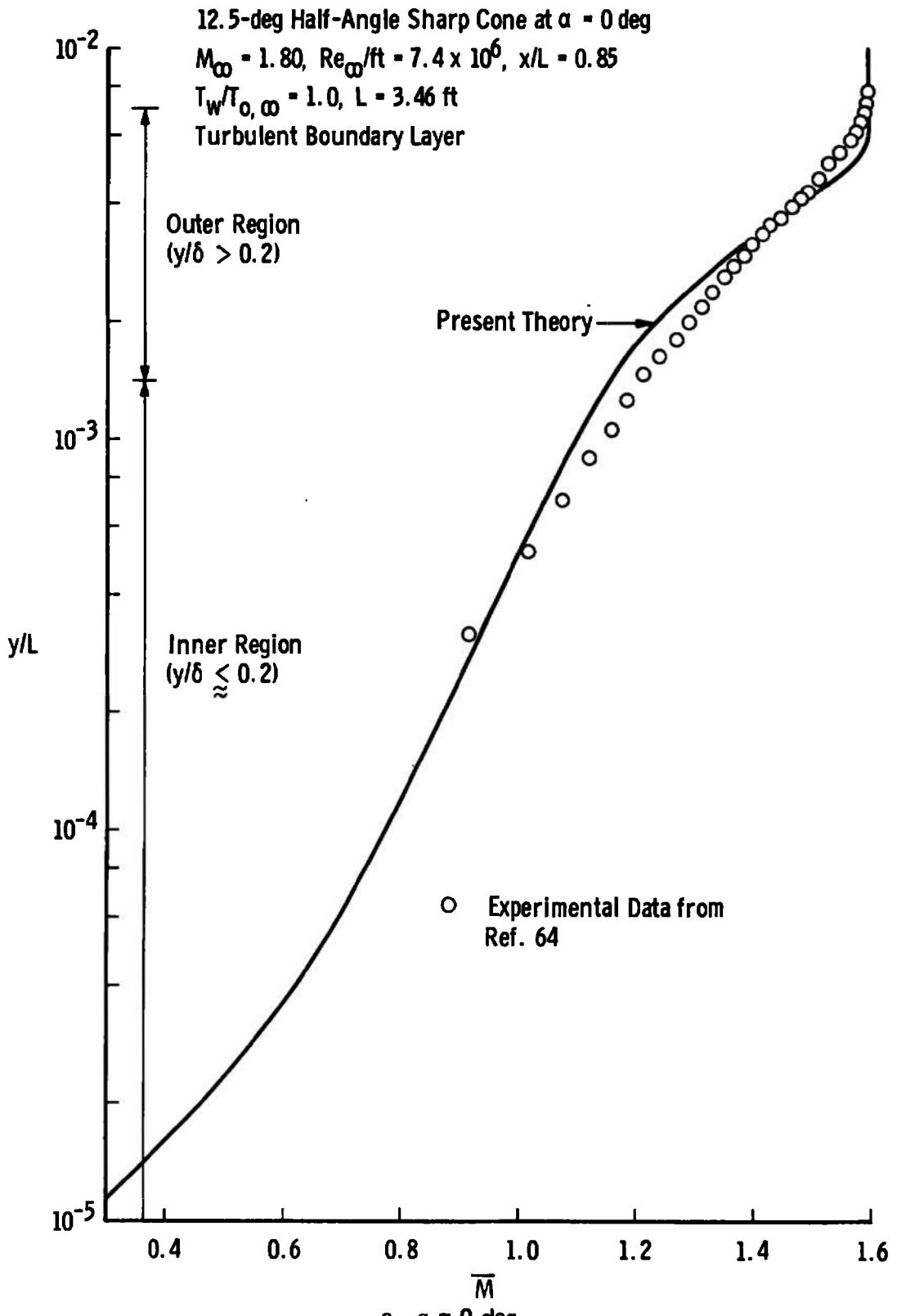

a. α = 0 deg

Fig. 16 Comparison of Calculated Local Mach Number Profiles with Experimental Measurements from Rainbird (Ref. 64)

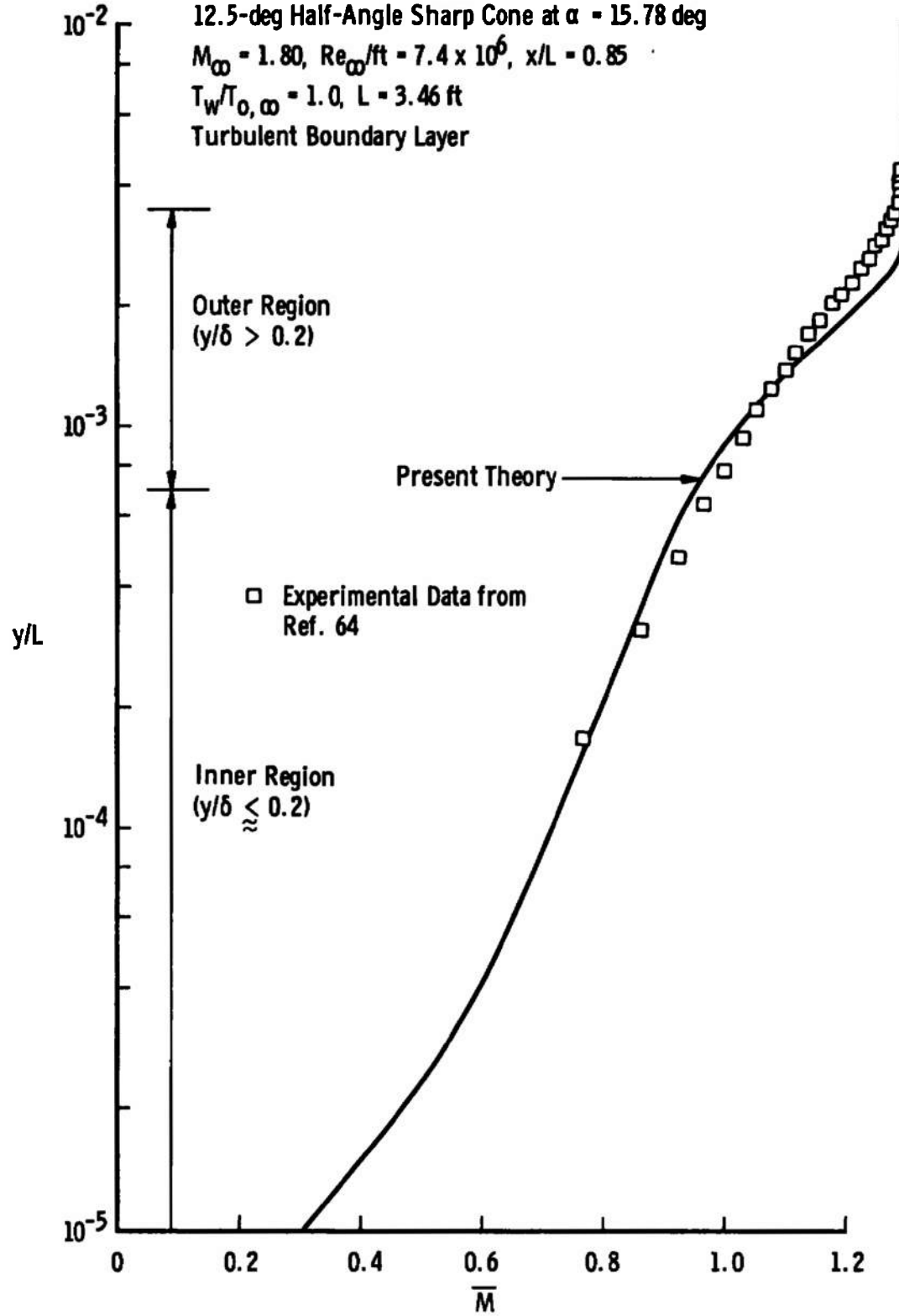

b. α = 15.78 deg
Fig. 16 Concluded

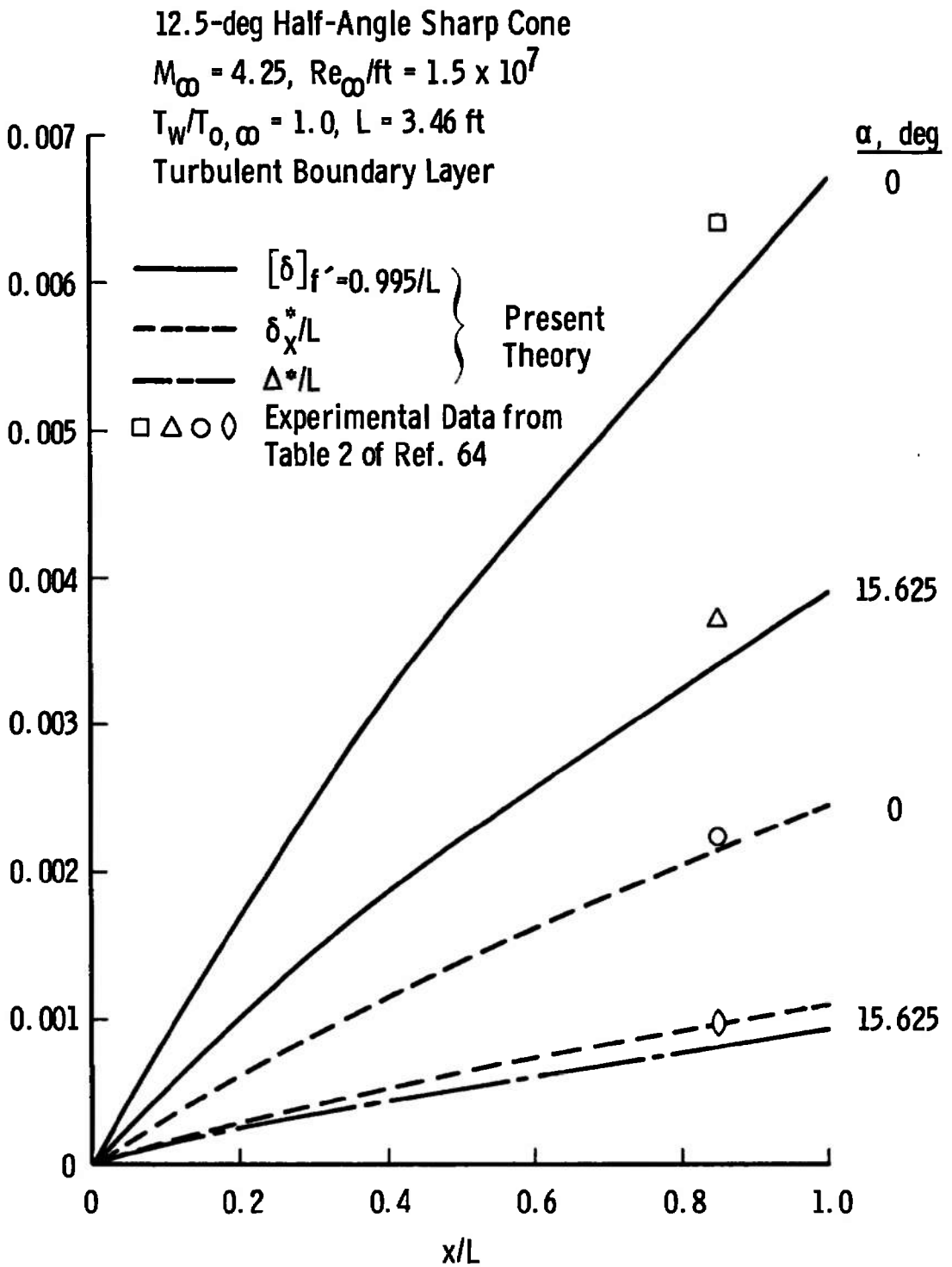

a. M_∞ = 4.25

Fig. 17 Comparison of Calculated Boundary-Layer Parameters with Experimental Measurements from Rainbird (Ref. 64)

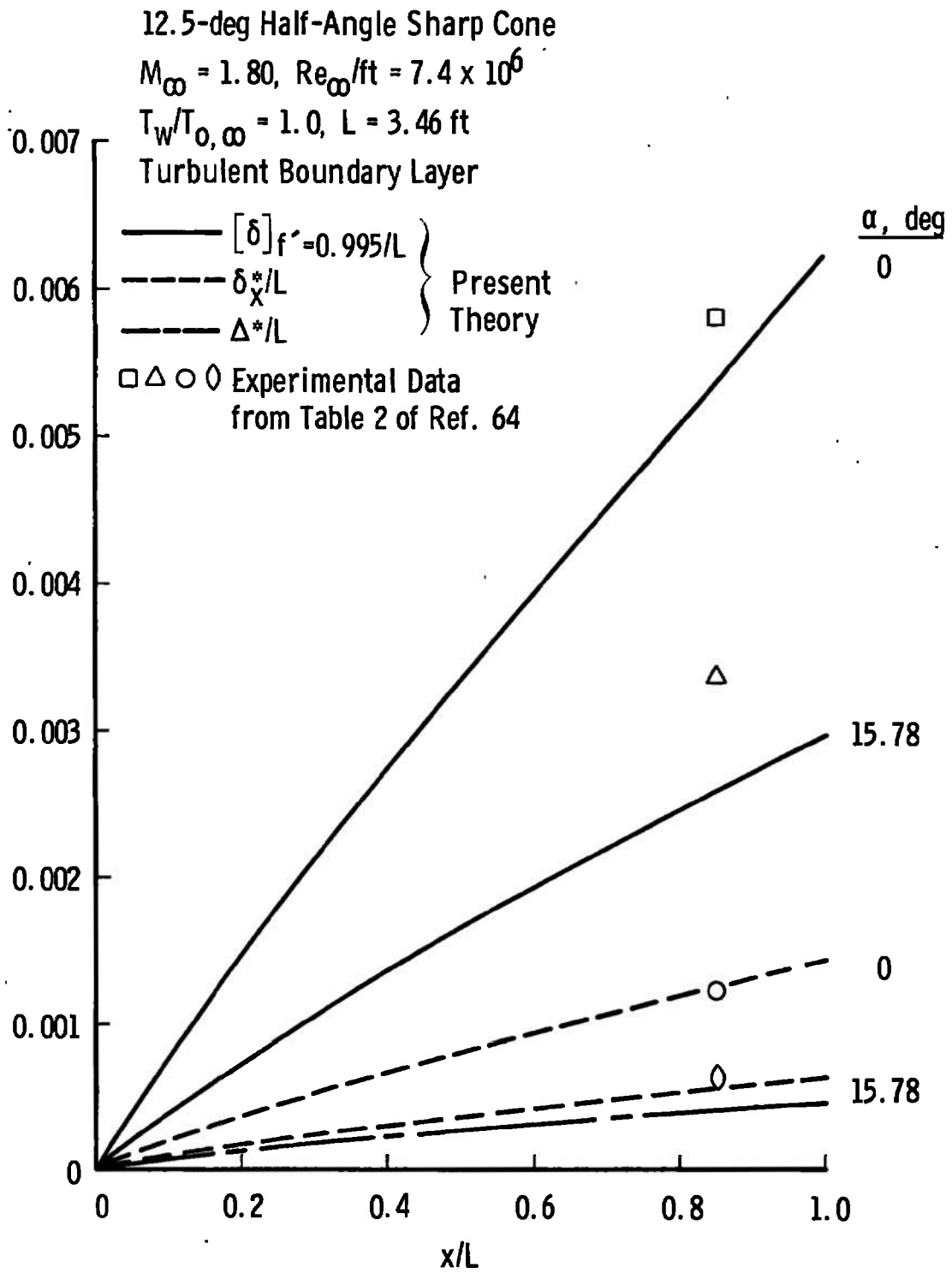

b. M_∞ = 1.80

Fig. 17 Concluded

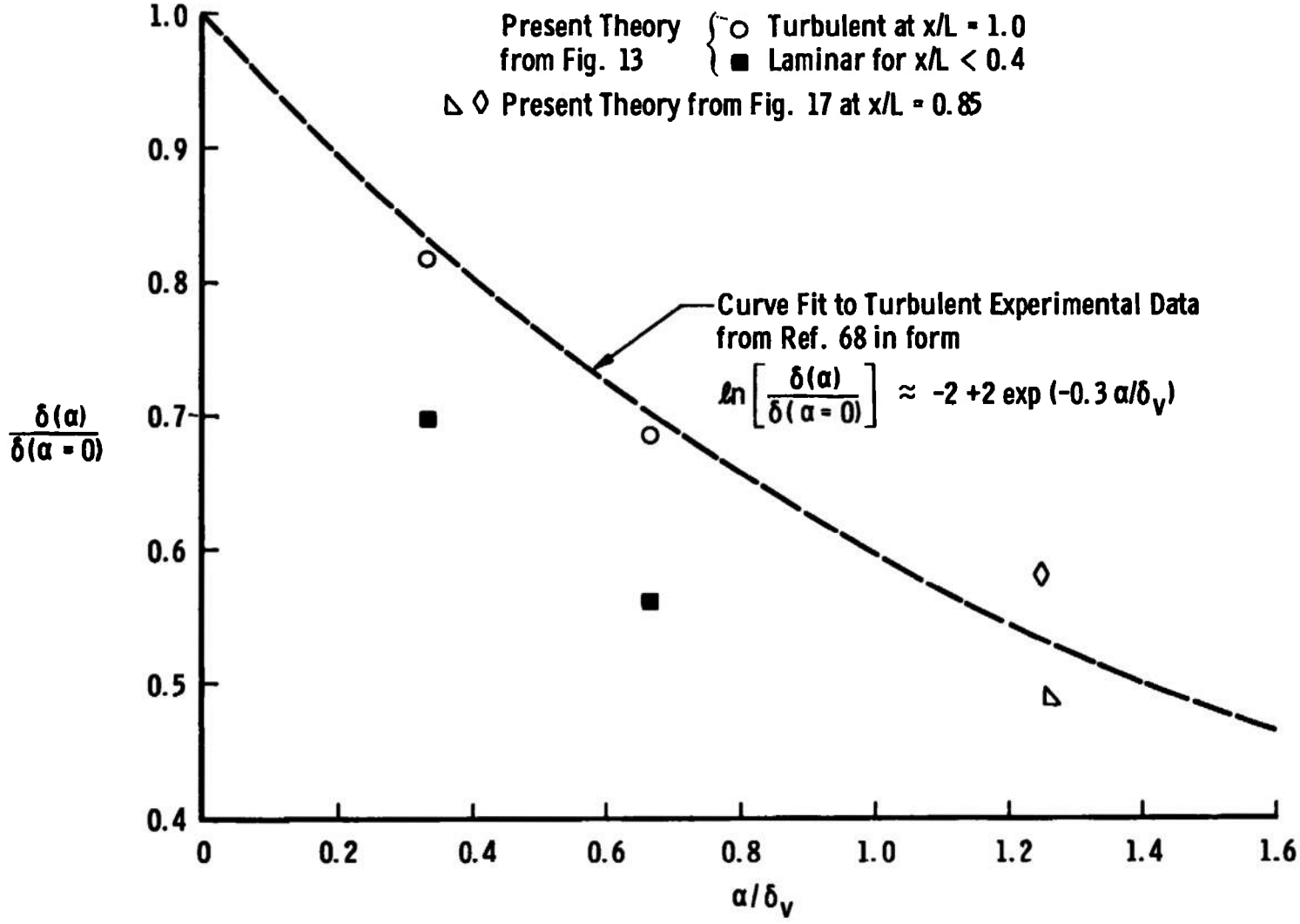

Fig. 18 Comparison of Calculated Boundary-Layer Thicknesses with Correlation to Experimental Data as Proposed by Copper and Shad (Ref. 68)

TABLE I
FLOW CONDITIONS

Ref.	δ_v,deg	M_∞	Re_∞/ft	$T_w/T_{o,\infty}$	$p_{o,\infty}$,psia	$T_{o,\infty}$,°R	L,in.
58	5.0	12.0	9.5×10^5	0.14	4200.0	3600.0	6.0
59	10.0	8.0	1.3×10^6	0.40	259.0	1360.0	4.0
60	15.0	10.4	3.7×10^6	0.23	3830.0	2260.0	3.25
61	10.0	6.86	4.6×10^6	0.54	452.0	1020.0	12.2
62	6.0	10.17	1.6×10^6	0.25	1310.0	1875.0	47.8
63	8.0	10.2	2.1×10^6	0.27	1710.0	1890.0	35.9
64	12.50	4.25	1.5×10^7	1.0	166.0	530.0	41.6
64	12.50	1.80	7.4×10^6	1.0	25.0	530.0	41.6

TABLE II
WINDWARD STREAMLINE INVISCID EDGE CONDITIONS

Ref.	δ_v, deg	α, deg	M_∞	$\bar{p}/p_\infty$	T_e/T_∞	M_e	$-\chi$
58	5.0	0.0	12.0	2.817	1.371	10.180	0.0
58	5.0	1.0	12.0	3.467	1.481	9.777	1.556×10^{-3}
58	5.0	2.0	12.0	4.232	1.608	9.364	3.283×10^{-3}
58	5.0	3.0	12.0	5.114	1.751	8.950	5.124×10^{-3}
58	5.0	4.0	12.0	6.109	1.911	8.543	7.080×10^{-3}
58	5.0	5.0	12.0	7.220	2.089	8.145	9.191×10^{-3}
59	10.0	0.0	8.0	4.068	1.584	6.210	0.0
59	10.0	2.0	8.0	5.216	1.771	5.827	5.143×10^{-3}
59	10.0	4.0	8.0	6.557	1.987	5.452	1.104×10^{-2}
59	10.0	6.0	8.0	8.084	2.231	5.092	1.768×10^{-2}
59	10.0	8.0	8.0	9.789	2.503	4.751	2.521×10^{-2}
59	10.0	10.0	8.0	11.668	2.801	4.431	3.384×10^{-2}
60	15.0	0.0	10.4	11.886	2.858	5.882	0.0
60	15.0	3.0	10.4	16.203	3.546	5.187	7.935×10^{-3}
60	15.0	6.0	10.4	21.164	4.335	4.594	1.829×10^{-2}
60	15.0	9.0	10.4	26.706	5.214	4.087	3.145×10^{-2}
60	15.0	12.0	10.4	32.759	6.172	3.652	4.790×10^{-2}
61	10.0	0.0	6.86	3.309	1.456	5.546	0.0
61	10.0	2.0	6.86	4.147	1.595	5.258	5.803×10^{-3}
61	10.0	4.0	6.86	5.125	1.754	4.968	1.241×10^{-2}
61	10.0	6.0	6.86	6.241	1.934	4.682	1.973×10^{-2}
61	10.0	8.0	6.86	7.488	2.133	4.405	2.789×10^{-2}
62	6.0	0.0	10.17	2.872	1.381	8.575	0.0
62	6.0	2.0	10.17	4.056	1.579	7.980	3.934×10^{-3}
62	6.0	4.0	10.17	5.567	1.824	7.378	8.512×10^{-3}
63	8.0	4.0	10.20	7.599	2.155	6.753	9.003×10^{-3}
64	12.50	0.0	4.25	2.454	1.307	3.556	0.0
64	12.50	15.625	4.25	6.686	2.000	2.556	1.036×10^{-1}
64	12.50	0.0	1.80	1.360	1.092	1.596	0.0
64	12.50	15.78	1.80	2.066	1.234	1.295	2.558×10^{-1}

APPENDIX III
IMPLICIT FINITE-DIFFERENCE SOLUTION OF GOVERNING BOUNDARY-LAYER EQUATIONS

For the special case of a sharp cone at zero to moderate angle of attack ($0 \leqq \alpha \lessapprox 1.2\ \delta_v$) in a supersonic or hypersonic flow, the inviscid flow field is conical in character so that all the inviscid flow parameters ($\bar{p}$, T_e, ρ_e, U_e, M_e, $\partial W_e/\partial\phi$, $\partial^2\bar{p}/\partial\phi^2$) remain constant along rays from the apex of the cone. Under this restriction the relationship between ξ and x is found by integration of Eq. (42) with $r = x \sin\delta_v$ from geometry which results in

$$\xi = \frac{1}{3}\rho_e\mu_e U_e \sin^2\delta_v\, x^3 \tag{III-1}$$

This definition of ξ leads to a simple expression for the G function defined by Eq. (62), namely

$$G = \frac{2}{3\sin\delta_v} \tag{III-2}$$

Noting that $dr/dx = \sin\delta_v$ geometry and $\beta \equiv 0$ due to the inviscid conical flow, the governing plane of symmetry boundary-layer equations (51), (52), and (53) in transformed coordinates reduce to the following simpler set:

x-MOMENTUM

$$\ell^* f''' + \left[\frac{\partial\ell^*}{\partial\eta} + f + Gg\right]f'' = 2\xi\left[f'\frac{\partial f'}{\partial\xi} - f''\frac{\partial f}{\partial\xi}\right] \tag{III-3}$$

ϕ-MOMENTUM

$$\ell^* g''' - \left[\frac{\partial\ell^*}{\partial\eta} + f + Gg\right]g'' - G[(g')^2 + f'g'\sin\delta_v + \chi\theta] = 2\xi\left[f'\frac{\partial g'}{\partial\xi} - g''\frac{\partial f}{\partial\xi}\right] \tag{III-4}$$

ENERGY

$$\left(\frac{\ell^*}{Pr}\right)\theta'' + \left[\frac{\partial}{\partial\eta}\left(\frac{\ell^*}{Pr}\right) + f + Gg\right]\theta' + (\gamma-1)M_e^2\,\ell^*(f'')^2 = 2\xi\left[f'\frac{\partial\theta}{\partial\xi} - \theta'\frac{\partial f}{\partial\xi}\right] \tag{III-5}$$

The boundary conditions remain unchanged from Eqs. (65) through (68) which are repeated below for completeness.

MOMENTUM

$$f(\xi, \eta = 0) = 0 \tag{III-6}$$

$$f'(\xi, \eta = 0) = 0 \tag{III-7}$$

$$\lim_{\eta \to \infty}{}' \; f'(\xi, \eta) = 1 \tag{III-8}$$

$$g(\xi, \eta = 0) = 0 \tag{III-9}$$

$$g'(\xi, \eta = 0) = 0 \tag{III-10}$$

$$\lim_{\eta \to \infty} g'(\xi, \eta) = g'_e \tag{III-11}$$

ENERGY

$$\theta(\xi, \eta = 0) = \theta_w(\xi) \tag{III-12}$$

$$\lim_{\eta \to \infty} \theta(\xi, \eta) = 1 \tag{III-13}$$

Following the approach by Blottner (Ref. 42) and Davis (Ref. 69) the momentum and energy equations (III-3, -4, -5) are rewritten in "standard" form for a parabolic partial differential equation as

$$\frac{\partial^2 W}{\partial \eta^2} + a_1 \frac{\partial W}{\partial \eta} + a_2 W + a_3 + a_4 \frac{\partial W}{\partial \xi} = 0 \tag{III-14}$$

where W = f' for the x-momentum equation, W = g' for the ϕ-momentum equation, and W = θ for the energy equation. Using Eqs. (III-3, -4, -5), one finds the coefficients a_1 through a_4 in linearized form:

x-MOMENTUM

$$a_1 = \frac{\frac{\partial \ell^*}{\partial \eta} - f + Gg + 2\xi \frac{\partial f}{\partial \xi}}{\ell^*} \tag{III-15}$$

$$a_2 = 0 \tag{III-16}$$

$$a_3 = 0 \tag{III-17}$$

$$a_4 = \frac{-2\xi f'}{\ell^*} \tag{III-18}$$

ϕ-MOMENTUM

$$a_1 = \frac{\frac{\partial \ell^*}{\partial \eta} + f + Gg + 2\xi \frac{\partial f}{\partial \xi}}{\ell^*} \tag{III-19}$$

$$a_2 = \frac{-Gg' - \frac{2f'}{3}}{\ell^*} \tag{III-20}$$

$$a_3 = \frac{-G\chi\theta}{\ell^*} \tag{III-21}$$

$$a_4 = \frac{-2\xi f'}{\ell^*} \tag{III-22}$$

ENERGY

$$a_1 = \frac{\frac{\partial}{\partial\eta}\left(\frac{\ell^{**}}{Pr}\right) + f + Gg - 2\xi\frac{\partial f}{\partial\xi}}{\left(\frac{\ell^{**}}{Pr}\right)} \tag{III-23}$$

$$a_2 = 0 \tag{III-24}$$

$$a_3 = \frac{(\gamma-1)M_e^2\,\ell^*(f'')^2}{\left(\frac{\ell^{**}}{Pr}\right)} \tag{III-25}$$

$$a_4 = \frac{-2\xi f'}{\left(\frac{\ell^{**}}{Pr}\right)} \tag{III-26}$$

The η derivatives in Eq. (III-14) are replaced with finite-difference quotients which allow variable grid spacing in the η direction so as to concentrate grid points in the region near the body surface where the dependent variables change most rapidly. The derivative in the ξ direction in Eq. (III-14) is handled in the usual manner as a two-point backward difference between points (m+1,n) and (m,n), whereas all η derivatives are evaluated at point (m+1,n) according to the grid mesh shown below.

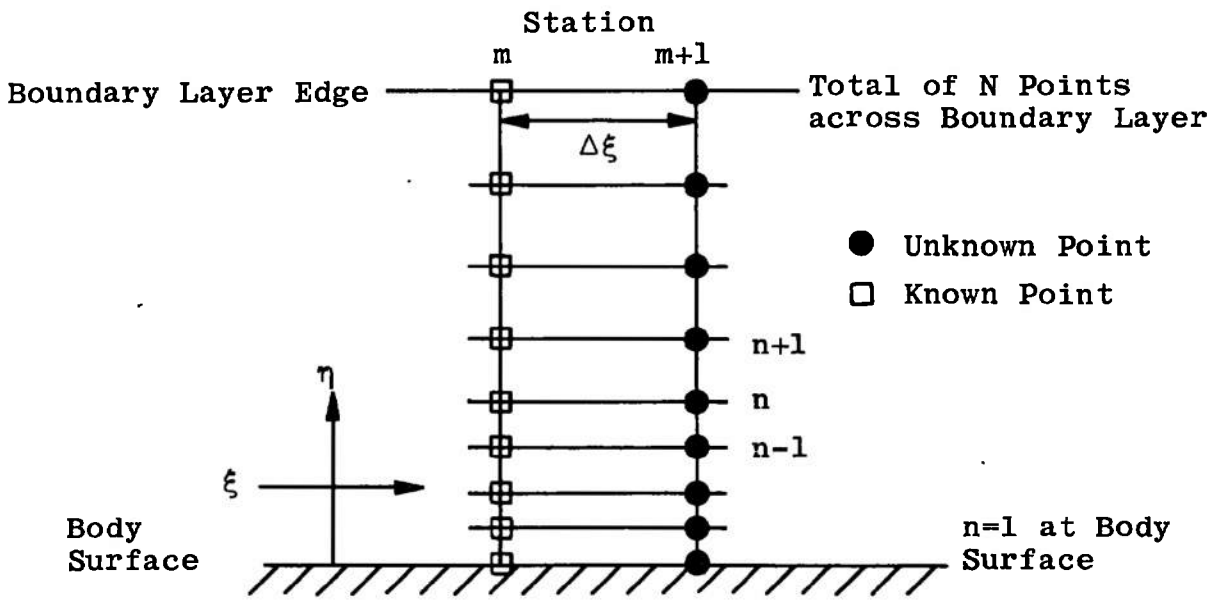

The solution is assumed to be known at point (m,n) and unknown at point (m+1,n) so that the finite-difference scheme to be constructed will be implicit in nature. The finite-difference replacements for the derivatives are as follows (see Appendix IV for derivation):

$$\left[\frac{\partial^2 W}{\partial \eta^2}\right]_{m+1,\,n} = \frac{2[W_{n+1} + KW_{n-1} - (1+K)W_n]_{m+1}}{D_2} \tag{III-27}$$

$$\left[\frac{\partial W}{\partial \eta}\right]_{m+1,\,n} = \frac{[W_{n+1} - K^2 W_{n-1} - (1-K^2)W_n]_{m+1}}{D_1} \tag{III-28}$$

$$\left[\frac{\partial W}{\partial \xi}\right]_{m+1,\,n} = \frac{W_{m+1,\,n} - W_{m,\,n}}{\Delta\xi} \tag{III-29}$$

where

$$D_1 = (\eta_{n+1} - \eta_n) + K^2(\eta_n - \eta_{n-1}) \tag{III-30}$$

$$D_2 = (\eta_{n+1} - \eta_n)^2 + K(\eta_n - \eta_{n-1})^2 \tag{III-31}$$

$$K = \frac{\eta_{n+1} - \eta_n}{\eta_n - \eta_{n-1}} \quad \text{(constant)} \tag{III-32}$$

$$\Omega = \eta_2 - \eta_1 \quad \text{(constant)} \tag{III-33}$$

The finite-difference form of Eq. (III-14) becomes, upon substitution of Eqs. (III-27, -28, -29),

$$A_n W_{m+1,\,n+1} + B_n W_{m+1,\,n} + C_n W_{m+1,\,n-1} = R_n \tag{III-34}$$

where

$$A_n = \frac{2}{D_2} + \frac{a_1}{D_1} \tag{III-35}$$

$$B_n = \frac{-2(1+K)}{D_2} - \frac{a_1(1-K^2)}{D_1} + a_2 + \frac{a_4}{\Delta\xi} \tag{III-36}$$

$$C_n = \frac{2K}{D_2} - \frac{K^2 a_1}{D_1} \tag{III-37}$$

$$R_n = -a_3 + \frac{a_4 W_{m,\,n}}{\Delta\xi} \tag{III-38}$$

In order for Eq. (III-34) to be linear, the coefficients A_n, B_n, C_n, and R_n must be treated as known quantities at point n; more will follow on this subject later. The important point is that Eq. (III-34) represents a set of simultaneous linear algebraic equations under this restriction.

Since the simultaneous linear algebraic equations resulting from Eq. (III-34) are of a special form (tridiagonal), an efficient method of solution on a digital computer is available from Richtmyer and Morton (Ref. 70, pp. 198-201, 274-282). For this procedure the boundary conditions at the wall (n=1) and the outer edge (n=N) must have specified values $W_{m+1,1}$ and $W_{m+1,N}$. Due to the special form of the Eq. (III-34), the relation

$$W_{m+1,\,n} = E_n\, W_{m+1,\,n+1} + e_n, \quad 2 \leqq n \leqq N-1 \tag{III-39}$$

exists where

$$E_2 = \frac{-A_2}{B_2} \tag{III-40}$$

$$e_2 = \frac{R_2 - C_2\, W_{m+1,\,1}}{B_2} \tag{III-41}$$

$$\left.\begin{aligned} E_n &= \frac{-A_n}{B_n + C_n E_{n-1}} \qquad \text{(III-42)} \\ e_n &= \frac{R_n - C_n\, e_{n-1}}{B_n + C_n E_{n-1}} \qquad \text{(III-43)} \end{aligned}\right\} \quad 3 \leqq n \leqq N-1$$

The quantities E_n and e_n are computed from Eqs. (III-40) through (III-43) starting with n = 2 and progressing to n = N-1. The solution $W_{m+1,n}$ is then obtained by evaluating Eq. (III-39) from n = N-1 to n=2. Knowing the distribution of f' and θ across the boundary layer from the above procedure, the transformed stream function f is evaluated from

$$f(\xi,\eta) = \int_0^{\eta} f'(\xi,\eta)\, d\eta \tag{III-44}$$

where the integral is numerically integrated using the well-known trapezoidal rule, viz.,

$$f(\xi,\eta=\eta_n) = \sum_{i=2}^{n} [f'(\xi,\, \eta=\eta_i) + f'(\xi,\, \eta=\eta_{i-1})]\, D_i \tag{III-45}$$

with

$$D_i = \frac{\eta_i - \eta_{i-1}}{2} \tag{III-46}$$

The transformed stream function, g, is evaluated in a similar manner. Inversion from the transformed (ξ,η) plane to the physical (x,y) plane is, from Eq. (85),

$$y = \frac{\sqrt{2\xi}}{\rho_e U_e r} \int_0^{\eta} \frac{\rho_e}{\bar{\rho}}\, d\eta \tag{III-47}$$

where

$$\frac{\rho_e}{\overline{\rho}} = \frac{T}{T_e} = 0 \tag{III-48}$$

due to the constancy of static pressure across the boundary layer. Again using the trapezoidal rule method of numerical integration yields

$$y_n = \frac{\sqrt{2\xi}}{\rho_e U_{e^r}} \sum_{i=2}^{n} [\theta(\xi, \eta = \eta_i) + \theta(\xi, \eta = \eta_{i-1})] D_i \tag{III-49}$$

with D_i given by Eq. (III-46). The relationship between ξ and x for sharp cone flows is given by Eq. (III-1) which results in

$$2\xi \frac{\partial}{\partial \xi} = \frac{2}{3} x \frac{\partial}{\partial x} \tag{III-50}$$

For the present sharp cone study, Eq. (III-50) was used in conjunction with an x-step size division $\Delta x = 0.01$ L, i.e., 100 stations spaced equally along the physical body.

The mathematical basis of the above tridiagonal matrix procedure applied to the solution of boundary-layer problems is due to Flügge-Lotz and Blottner (Ref. 71). The present application differs from their original work in one important aspect, the linearized difference equations herein are uncoupled and solved separately. In Flügge-Lotz and Blottner's approach, the difference equations remain coupled and require additional machine storage and manipulations for solution. With the present uncoupled approach, the difference equations are iterated to convergence at each station along the body so that one must pay the price of iteration: this procedure is how the linearizing coefficients a_1 through a_4 are evaluated at each station using the results of the previous iteration. Iteration at a given station is continued until successive values of f', g', and θ differ by less than 0.10 percent from the corresponding value of the preceding cycle. Typically about three iterations per station are required for fully turbulent flow; only one to two iterations per station are necessary for laminar flow. By use of the above procedure the final solution obtained at each station is exact in the sense that it represents a converged iterated solution to the governing nonlinear partial differential equations written in finite-difference form.

The variable grid mesh used in the present work is taken from Smith and Cebeci (Ref. 2). The various constants used herein are as follows:

$$N = 85$$
$$K = 1.063$$
$$\Omega = 0.010$$

Experience with varying these constants and observing their influence on the resultant numerical solution has indicated that the above choices are adequate under the present

flow conditions. These values may not be satisfactory, however, for other body geometries and flow conditions so that the influence of the variable grid mesh constants should be ascertained for each new investigation. Provisions are included in the present program for addition of points (if necessary) to the solution as the body is traversed. This may be required in order to prevent numerical supression of boundary-layer growth, especially in the case of transitional and turbulent boundary layers.

Evaluation of heat-transfer rate and shear stress at the cone surface requires numerical determination of the wall derivatives $\theta'(\xi,\eta=0)$ and $f''(\xi,\eta=0)$ since

$$\dot{q}_w \propto \theta'(\xi, \eta = 0)$$

$$\tau_w \propto f''(\xi, \eta = 0)$$

from Eqs. (82) and (84). Due to the variable grid spacing in the η-direction discussed previously, the wall derivatives are evaluated in the present work by application of the three-point Lagrangian interpolation formula (Ref. 72, pp. 71-77) evaluated according to the following diagram

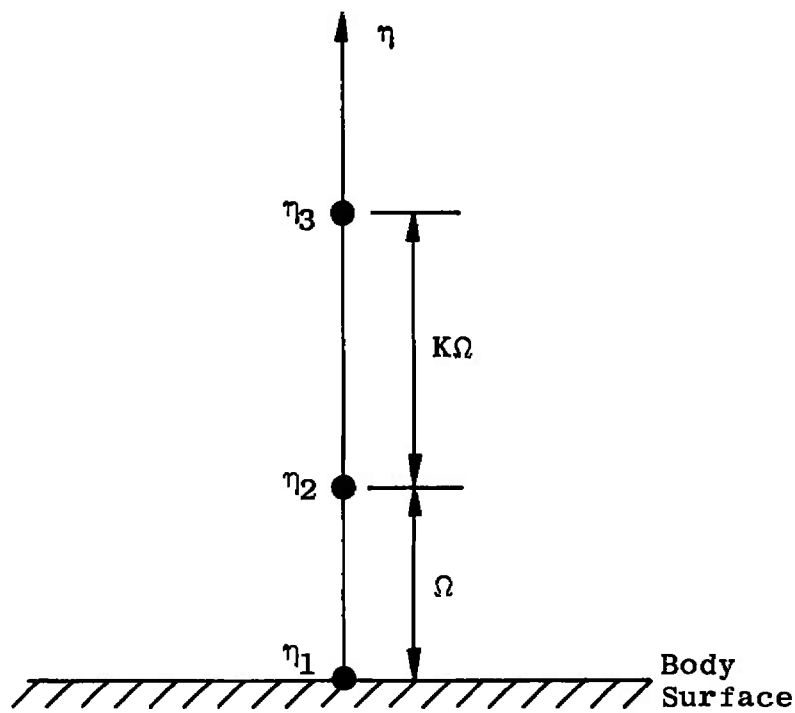

which yields, at station m+1,

$$f''(\eta = 0) = \Omega [B_1(2+K)f'_{\eta_1} + B_2(1+K)f'_{\eta_2} + B_3 f'_{\eta_3}] \qquad \text{(III-51)}$$

$$\theta'(\eta=0) = \Omega[B_1(2+K)\theta_{\eta_1} - B_2(1+K)\theta_{\eta_2} - B_3\theta_{\eta_3}] \qquad \text{(III-52)}$$

where

$$B_1 = \frac{-1}{\Omega^2(1+K)} \tag{III-53}$$

$$B_2 = \frac{+1}{K\Omega^2} \tag{III-54}$$

$$B_3 = \frac{-1}{\Omega^2 K(1+K)} \tag{III-55}$$

and

$$f'_{\eta_i} = f'(\eta=\eta_i) \tag{III-56}$$

$$\theta_{\eta_i} = \theta(\eta=\eta_i) \tag{III-57}$$

with i = 1, 2, 3. The parameters K and Ω are defined by Eqs. (III-32) and (III-33), respectively. The use of the three-point Lagrangian interpolation formula for the wall derivatives is consistent with the formulation of the variable grid spacing derivatives discussed in Appendix IV and follows the work of Smith and Cebeci (Ref. 2, Appendix C).

At the apex of a sharp cone where $\xi = 0$, the governing boundary-layer equations (III-3), (III-4), and (III-5) reduce to the following ordinary, nonlinear, differential equations:

x-MOMENTUM

$$\ell^* f''' + \left[\frac{\partial \ell^*}{\partial \eta} + f + Gg\right] f'' = 0 \tag{III-58}$$

ϕ-MOMENTUM

$$\ell^* g''' + \left[\frac{\partial \ell^*}{\partial \eta} + f + Gg\right] g'' - G[(g')^2 + f'g' \sin \delta_v + \chi\theta] = 0 \tag{III-59}$$

ENERGY

$$\left(\frac{\ell^*}{Pr}\right)\theta'' + \left[\frac{\partial}{\partial \eta}\left(\frac{\ell^*}{Pr}\right) + f - Gg\right]\theta' + (\gamma-1)\, M_e^2 \ell^* (f'')^2 = 0 \tag{III-60}$$

with the boundary conditions (III-6) through (III-13). In order to obtain starting profiles for the finite-difference scheme to march downstream, Eqs. (III-58), (III-59), and (III-60) are solved by using the tridiagonal matrix procedure described previously in the following manner. At the apex of the sharp cone, $\xi = 0$ so that $a_4 = 0$ in both of the momentum equations as well as the energy equation; in addition, the term containing ξ in a_1 of

both the momentum and energy equations vanishes. Initial guesses for f', g', and θ are input to the program as

$$f'_I = 1 - \exp(-\eta) \tag{III-61}$$

$$g'_I = g'_e f'_I \tag{III-62}$$

$$\theta_I = \theta_w + (1-\theta_w) f'_I \tag{III-63}$$

where the subscript I denotes the initial approximation. The equations are then iterated to convergence in the same manner described previously; an averaging scheme is used to speed convergence. Typically about 20 to 25 iterations are required to generate a converged initial solution.

By use of the above procedures, the numerical solution of any two-point boundary-value problem governed by either linear or nonlinear ordinary differential equations as well as sets of coupled parabolic partial differential equations, either linear or nonlinear, is reduced to subroutine status on a digital computer in that only the coefficients a_1 through a_4 must be defined in conjunction with the required boundary conditions for each new problem. Much application of these procedures has been found in the von Kármán Facility of the Arnold Engineering Development Center on many different problems involving both nonlinear ordinary differential equations as well as parabolic partial differential equations. The thin viscous shock layer analyses by Adams (Refs. 73 and 74) are good examples. In these works eight simultaneous, nonlinear, ordinary differential equations governing momentum, energy, and species conservation were solved using the iterative tridiagonal matrix method presented above. The problem was made even more difficult in that chemical nonequilibrium effects were included in the analysis. Based on experience with analyses of this type, the author highly recommends use of the iterative tridiagonal matrix approach where applicable.

APPENDIX IV
VARIABLE GRID DIFFERENTIATION FORMULAS

The first and second derivative formulas for the variable grid system discussed in Appendix III can be most easily derived from consideration of the three-point Lagrangian interpolation polynomial (Ref. 72, pp. 71-77) evaluated according to the following diagram:

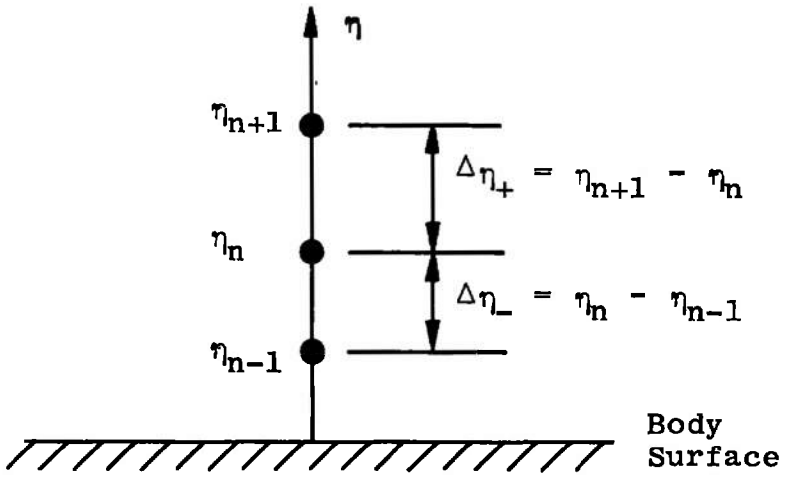

which yields, for the function $W(\eta)$ in the range $\eta_{n-1} < \eta < \eta_{n+1}$,

$$W(\eta) = \sum_{i=n-1}^{n+1} L_i(\eta)\, W_i(\eta_i) + E(\eta) \tag{IV-1}$$

where

$$L_k(\eta) = \frac{\prod_{\substack{j=n-1 \\ j\neq k}}^{n+1} (\eta - \eta_j)}{\prod_{\substack{j=n-1 \\ j\neq k}}^{n+1} (\eta_k - \eta_j)} \tag{IV-2}$$

and $E(\eta)$ represents the error of the interpolating polynomial as discussed in Section 3.2 of Ref. 72. Differentiating Eq. (IV-1) yields

$$\frac{dW(\eta)}{d\eta} = \sum_{i=n-1}^{n+1} \frac{dL_i(\eta)}{d\eta} W_i(\eta_i) + \frac{dE(\eta)}{d\eta} \tag{IV-3}$$

$$\frac{d^2W(\eta)}{d\eta^2} = \sum_{i=n-1}^{n+1} \frac{d^2L_i(\eta)}{d\eta^2} W_i(\eta_i) + \frac{d^2E(\eta)}{d\eta^2} \tag{IV-4}$$

where $[dL_i(\eta)]/d\eta$ and $[d^2L_i(\eta)]/d\eta^2$ are to be evaluated from differentiation of Eq. (IV-2).

The present application is concerned with evaluation of the above derivatives at the location $\eta = \eta_n$. Under this restriction, Eq. (IV-3) can be expanded to read

$$\frac{dW(\eta_n)}{d\eta} = \frac{(\eta_n - \eta_{n+1})}{(\eta_{n-1} - \eta_n)(\eta_{n-1} - \eta_{n-1})} W(\eta_{n-1}) + \frac{(\eta_n - \eta_{n-1}) + (\eta_n - \eta_{n+1})}{(\eta_n - \eta_{n-1})(\eta_n - \eta_{n+1})} W(\eta_n)$$

$$+ \frac{(\eta_n - \eta_{n-1})}{(\eta_{n+1} - \eta_{n-1})(\eta_{n+1} - \eta_n)} W(\eta_{n+1}) + \frac{dE(\eta_n)}{d\eta} \tag{IV-5}$$

Introducing the nomenclature

$$\Delta\eta_+ = \eta_{n+1} - \eta_n \tag{IV-6}$$

and

$$\Delta\eta_- = \eta_n - \eta_{n-1} \tag{IV-7}$$

Equation (IV-5) can be written as, by forming a common denominator for the first three terms on the right-hand side,

$$\frac{dW(\eta_n)}{d\eta} = \frac{-(\Delta\eta_+)^2 W(\eta_{n-1}) - [(\Delta\eta_-)^2 - (\Delta\eta_+)^2] W(\eta_n) + (\Delta\eta_-)^2 W(\eta_{n+1})}{[\Delta\eta_+(\Delta\eta_-)^2] + [\Delta\eta_-(\Delta\eta_+)^2]} + \frac{dE(\eta_n)}{d\eta} \tag{IV-8}$$

or, upon division of both numerator and denominator of the first term on the right-hand side by $(\Delta\eta\text{-})^2$,

$$\frac{dW(\eta_n)}{d\eta} = \frac{-\left(\frac{\Delta\eta_+}{\Delta\eta_-}\right)^2 W(\eta_{n-1}) - \left[1 - \left(\frac{\Delta\eta_+}{\Delta\eta_-}\right)^2\right] W(\eta_n) + W(\eta_{n+1})}{\Delta\eta_+ + \Delta\eta_-\left(\frac{\Delta\eta_+}{\Delta\eta_-}\right)^2} + \frac{dE(\eta_n)}{d\eta} \tag{IV-9}$$

Smith and Cebeci (Ref. 2) have proposed a variable grid system such that the ratio of lengths of any two adjacent intervals is a constant, i.e.,

$$\Delta\eta_+ = K\Delta\eta_- \tag{IV-10}$$

where the value of K must be specified. The distance from the body surface to the i-th grid point is given by the following formula

$$\eta_i = \Omega\left[\frac{K^i - 1}{K - 1}\right] \tag{IV-11}$$

where Ω is the length of the first step, i.e.,

$$\Omega = \eta_2 - \eta_1 \tag{IV-12}$$

In Eq. (IV-12), η_1 corresponds to the grid point on the body surface ($\eta_1 = 0$) and η_2 is the first grid point away from the wall. Adopting the Smith and Cebeci grid system for the present work permits Eq. (IV-9) to be written as

$$\frac{dW(\eta_n)}{d\eta} = \frac{-K^2 W(\eta_{n-1}) - [1 - K^2]\, W(\eta_n) + W(\eta_{n+1})}{D_1} + \frac{dE(\eta_n)}{d\eta} \tag{IV-13}$$

with

$$D_1 = \Delta\eta_+ + K^2\Delta\eta_- = (\eta_{n-1} - \eta_n) + K^2(\eta_n - \eta_{n-1}) \tag{IV-14}$$

In a similar manner, Eq. (IV-4) can be expanded to read

$$\frac{d^2W(\eta_n)}{d\eta^2} = \frac{2\Delta\eta_- W(\eta_{n-1}) - 2(\Delta\eta_+ + \Delta\eta_-)W(\eta_n) + 2\Delta\eta_- W(\eta_{n+1})}{\Delta\eta_+\Delta\eta_-(\Delta\eta_+ + \Delta\eta_-)} + \frac{d^2E(\eta_n)}{d\eta^2} \tag{IV-15}$$

which becomes, upon division of the numerator and denominator of the first term on the right-hand side by $\Delta\eta_-$,

$$\frac{d^2W(\eta_n)}{d\eta^2} = \frac{2\left[\left(\frac{\Delta\eta_+}{\Delta\eta_-}\right)W(\eta_{n-1}) - \left(1 + \frac{\Delta\eta_+}{\Delta\eta_-}\right)W(\eta_n) + W(\eta_{n+1})\right]}{(\Delta\eta_+)^2 - \left(\frac{\Delta\eta_+}{\Delta\eta_-}\right)(\Delta\eta_-)^2} + \frac{d^2E(\eta_n)}{d\eta^2} \tag{IV-16}$$

Introducing K according to Eq. (IV-10) into Eq. (IV-16) gives

$$\frac{d^2W(\eta_n)}{d\eta^2} = \frac{2[KW(\eta_{n-1}) - (1 + K)W(\eta_n) + W(\eta_{n+1})]}{D_2} + \frac{d^2E(\eta_n)}{d\eta^2} \tag{IV-17}$$

with

$$D_2 = (\Delta\eta_+)^2 + K(\Delta\eta_-)^2 = (\eta_{n+1} - \eta_n)^2 + K(\eta_n - \eta_{n-1})^2 \tag{IV-18}$$

The error terms can be shown to be (see Ref. 72, pp. 108-113)

$$\frac{dE(\eta_n)}{d\eta} = -\frac{1}{6}\frac{d^3W(\eta_*)}{d\eta^3}\Delta\eta_+\Delta\eta_- \qquad \text{(IV-19)}$$

$$\frac{d^2E(\eta_n)}{d\eta^2} = -\frac{1}{12}\frac{d^4W(\eta_*)}{d\eta^4}\Delta\eta_+\Delta\eta_- \qquad \text{(IV-20)}$$

where η_* is some η-point in the interval $\eta_{n-1} \leqq \eta_* \leqq \eta_{n+1}$ so that theoretically, by letting $\Delta\eta_+$ and $\Delta\eta_-$ approach zero, the discretization error also approaches zero. It is implicitly assumed in all of the foregoing analyses that the function W and its derivatives are single-valued, finite, and continuous functions of the independent variable η.

UNCLASSIFIED

Security Classification

DOCUMENT CONTROL DATA - R & D

(Security classification of title, body of abstract and indexing annotation must be entered when the overall report is classified)

1. ORIGINATING ACTIVITY (Corporate author)	2a. REPORT SECURITY CLASSIFICATION
Arnold Engineering Development Center Arnold Air Force Station, Tennessee	UNCLASSIFIED
	2b. GROUP N/A

3 REPORT TITLE

IMPLICIT FINITE-DIFFERENCE ANALYSIS OF COMPRESSIBLE LAMINAR, TRANSITIONAL, AND TURBULENT BOUNDARY LAYERS ALONG THE WINDWARD STREAMLINE OF A SHARP CONE AT INCIDENCE

4 DESCRIPTIVE NOTES (Type of report and inclusive dates)

Final Report - July 1970 to June 1971

5 AUTHOR(S) (First name, middle initial, last name)

John C. Adams, Jr., ARO, Inc.

6. REPORT DATE	7a. TOTAL NO. OF PAGES	7b. NO. OF REFS
December 1971	100	74

8a. CONTRACT OR GRANT NO.	9a. ORIGINATOR'S REPORT NUMBER(S)
b. PROJECT NO.	AEDC-TR-71-235
c. Program Element 64719F	9b. OTHER REPORT NO(S) (Any other numbers that may be assigned this report)
d.	ARO-VKF-TR-71-148

10 DISTRIBUTION STATEMENT

Approved for public release; distribution unlimited.

11 SUPPLEMENTARY NOTES	12. SPONSORING MILITARY ACTIVITY
Available in DDC	Arnold Engineering Development Center, Air Force Systems Command, Arnold AF Station, Tenn. 37389

13. ABSTRACT

Formulation and application of a windward plane of symmetry laminar, transitional, and turbulent boundary-layer analysis is presented for sharp cones at incidence in a supersonic or hypersonic flow. The governing boundary-layer equations in the plane of symmetry are numerically integrated on a digital computer using a marching implicit finite-difference technique. A so-called invariant model of turbulence is used in a two-layer eddy viscosity-mixing length approach for calculation of the turbulent boundary layer in conjunction with an intermittency factor treatment of the transition zone. Comparison of the present theory with experimental data (surface heat transfer, boundary-layer parameters such as displacement thickness, and boundary-layer profiles) under supersonic and hypersonic flow conditions over sharp cones at incidence reveals good agreement. In general, smaller cross-flow (outflow) effects on the windward plane of symmetry boundary layer can be expected for turbulent layers as compared with laminar layers subject to the same boundary conditions.

DD FORM 1 NOV 68 1473

UNCLASSIFIED

Security Classification

14. KEY WORDS	LINK A		LINK B		LINK C	
	ROLE	WT	ROLE	WT	ROLE	WT
boundary layer						
analyzing						
compressible flow						
conical bodies						
supersonic flow						
hypersonic flow						